DATING DELTAS

AN ABSTRACT

SUBMITTED ON THE FIFTEENTH DAY OF AUGUST 2017

TO THE DEPARTMENT OF EARTH AND ENVIRONMENTAL SCIENCES

IN PARTIAL FULFILLMENT OF THE REQUIREMENTS

OF THE SCHOOL OF SCIENCE AND ENGINEERING

OF TULANE UNIVERSITY

FOR THE DEGREE

OF

DOCTOR OF PHILOSOPHY

BY

Elizabeth L. Chamberlain

APPROVED:

Torbjörn E. Törnqvist, Ph.D.
Director

Mead Allison, Ph.D.

Steven Goodbred Jr., Ph.D.

Zhixiong Shen, Ph.D.

Jakob Wallinga, Ph.D.

ABSTRACT

Deltas are highly complex landscapes characterized by dynamic processes of growth and decline that may be driven by a multitude of factors. A greater level of understanding of deltaic processes is now possible through luminescence dating approaches, which enable the direct dating of clastic deposits. This dissertation applies luminescence dating to identify fundamental mechanisms of delta evolution in a pre-anthropogenic system over centennial to millennial timescales. Topics explored here include the rates and patterns of land-building, and the primary drivers, rates, and spatial variability of subsidence. In addition to applications, this dissertation makes contributions to the science of luminescence dating through the development of new techniques and assessments of luminescence characteristics of sediment in two megadeltas, the Mississippi and Ganges-Brahmaputra-Meghna deltas. The results herein show that river-dominated deltas operating under natural conditions grow in a radial pattern where sediment resources are directed by avulsions that occur over a broad spatial zone extending well landward of the delta, and decline in elevation due largely to compaction induced by sediment loading. Zeroing (or bleaching) of the luminescence clock is tested through a new "Bleaching Index" that compares multiple signals obtained from polymineral sediment, and through measurements of modern analogues. These tests show that quartz silt is likely to be well-bleached in large river-delta systems, a finding which extends the prospects and geographic range of luminescence dating.

DATING DELTAS

A DISSERTATION

SUBMITTED ON THE FIFTEENTH DAY OF AUGUST 2017

TO THE DEPARTMENT OF EARTH AND ENVIRONMENTAL SCIENCES

IN PARTIAL FULFILLMENT OF THE REQUIREMENTS

OF THE SCHOOL OF SCIENCE AND ENGINEERING

OF TULANE UNIVERSITY

FOR THE DEGREE

OF

DOCTOR OF PHILOSOPHY

BY

Elizabeth L. Chamberlain

APPROVED:

Torbjörn E. Törnqvist, Ph.D.
Director

Mead Allison, Ph.D.

Steven Goodbred Jr., Ph.D.

Zhixiong Shen, Ph.D.

Jakob Wallinga, Ph.D.

ACKNOWLEDGEMENTS

This dissertation was possible through the innovation and guidance of my doctoral advisor, Torbjörn Törnqvist. I have a deep respect for the integrity, perspective, and skill with which Tor conducts and communicates scientific research. I especially want to thank Tor for encouraging me to pursue research beyond our original plans. I acknowledge Zhixiong Shen for taking me under his wing and teaching me about luminescence dating and hand coring: the two essential tools used herein. Many advancements presented in this dissertation were possible through the mentorship of researchers at the Netherlands Centre for Luminescence Dating, including Jakob Wallinga and Tony Reimann. I acknowledge Mead Allison and Steve Goodbred for serving on my dissertation committee and providing research and writing insights. A big thank you to Michael Steckler for introducing me to Bangladesh and for supporting subsequent work there. Cheers to my student cohort (plus or minus a year): Jordan Adams, Chris Esposito, Emily Eidam, and Jeff Obelcz, and to long-departed M.S. student Ciara Chambers, for fun times and solidarity. Thanks to my friend Jayur Mehta, an archaeologist who provided a fresh perspective on the Mississippi Delta, and to Jon Bridgeman, who hand-cored through many meters of Lafourche sand. I am grateful to Dr. Hanor, my M.S. advisor, for investing in me. Ultimately, this research is the product of many collaborators and friends too numerous to list. I acknowledge members of the luminescence laboratory at the University of Liverpool, leaders and participants of the BanglaPIRE program, colleagues at Dhaka University, and fellow students. I thank all land-owners who permitted us to work. Finally, I acknowledge my family, especially my mother for supporting field campaigns by babysitting. This dissertation is dedicated to my son, Frederick, who possesses a great enthusiasm for sediment and for many other things in nature.

TABLE OF CONTENTS

LIST OF TABLES

A.D.4 Brightness and overdispersion of T_N

LIST OF FIGURES

Chapter 1

Introduction

1.1 Motivation

Deltas often form at the intersection of fluvial and coastal landscapes, where river channels deliver water and sediments to a basin in a dynamic interplay of hydrologic, sedimentologic, and antecedent factors that ultimately govern the morphology and evolution of the resulting landscape. While research on deltas is longstanding (e.g., Gilbert, 1885; Russell et al., 1936; Fisk, 1944), the rates and patterns of delta evolution are not well-resolved over centennial to millennial timescales. For example, it is unknown if radial bayhead delta progradation observed in decadal-scale systems (e.g., Shaw and Mohrig, 2014) can be sustained for centuries, or if deltas ultimately prograde in a spatially episodic fashion characterized by discrete lobes operating within a larger region (e.g., Frazier, 1967). Distributary channels are the primary pathways of sediment delivery to the coast, and so, quantifying their activity is highly relevant to patterns of delta growth. Some recent studies have claimed that avulsion of distributary channels occurs at a single node related to backwater dynamics (Chatanantavet et al., 2012; Ganti et al., 2016), although this has not been conclusively demonstrated in the Mississippi Delta.

In addition to the growth of new deltaic land, decay processes such as subsidence are an important component of delta evolution (Penland et al., 1988; Roberts, 1997). A growing body of work suggests that subsidence of deltas is driven primarily by

compaction of shallow sediment (Törnqvist et al., 2008; Jankowski et al., 2017) or human activities such as artificial drainage (Higgins et al., 2013), although faulting (Dokka et al., 2006) and subsurface fluid extraction (Morton et al., 2006) have also been invoked. Previous work has shown that load-induced compaction may result in the loss of about 35% of elevation scaled to the thickness of the overburden (Törnqvist et al., 2008), however this estimate is based on relatively inland data underlain by organic-rich sediment and does not reveal how coastward localities such as shallow bays may respond to loading.

This dissertation aims to build knowledge of fundamental processes of delta evolution including land growth and subsidence, and to develop new approaches to establishing geochronology and inferring sediment transport processes in deltas. These aims are met through a collection of four projects employing stratigraphy, modeling, and luminescence measurements. The work herein is enabled by optically stimulated luminescence (OSL) dating, a technique that was first introduced in the late 20th century and evolved for use on fluvial deposits in the early 21st century. This dissertation presents many novel concepts because the luminescence tools used herein have only become available to the delta-research community within the last two decades.

1.2 Optically stimulated luminescence dating

OSL dating (Fig. 1.1) provides a timing for sediment deposition based on the last exposure to light of quartz or feldspar minerals (Huntley, 1985). The phenomenon of luminescence arises from charges that are stored within the mineral crystal lattice and produce a very small light flux when released. These charges accumulate at a

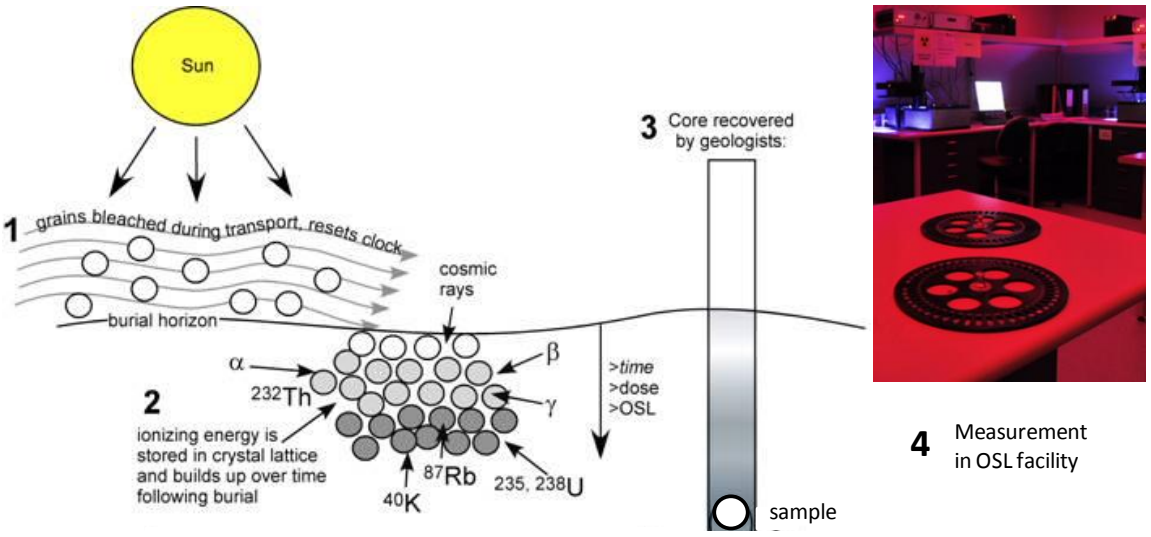

Fig. 1.1. *The luminescence signal of sediment (represented by circles) may be bleached during transit (1), and begins to accumulate upon burial (2). The accumulated dose is indicated by shading: white grains contain little to no dose, and gray grains contain more dose and therefore greater luminescence signals. Buried sediment is recovered (3) and the burial dose is estimated in a luminescence facility (4). Modified from Mallinson (2008).*

measureable rate, referred to as the dose rate, that is driven by the decay of radionuclides in the surrounding sediment matrix, cosmogenic dosing, and internal dosing through the decay of U, Th, and K inclusions within the mineral crystal lattice (e.g., Durcan et al., 2015). The trapped charges are released upon exposure to light or heat and produce a signal that is proportional to the dose received during burial. In the laboratory, this natural signal is related to an equivalent dose (D_e), thought to represent the total dose received by the grains of one aliquot during burial. D_e is estimated for a number of aliquots by first measuring the natural signal, then measuring signals for the same grains that arise in response to known doses of radiation given in the laboratory, referred to as regenerative doses. This produces a dose-response curve that allows for estimating D_e (Fig. 1.2). When more than one grain is measured per subsample, this technique is referred to as the single-aliquot regenerative-dose (SAR) protocol (Murray and Wintle,

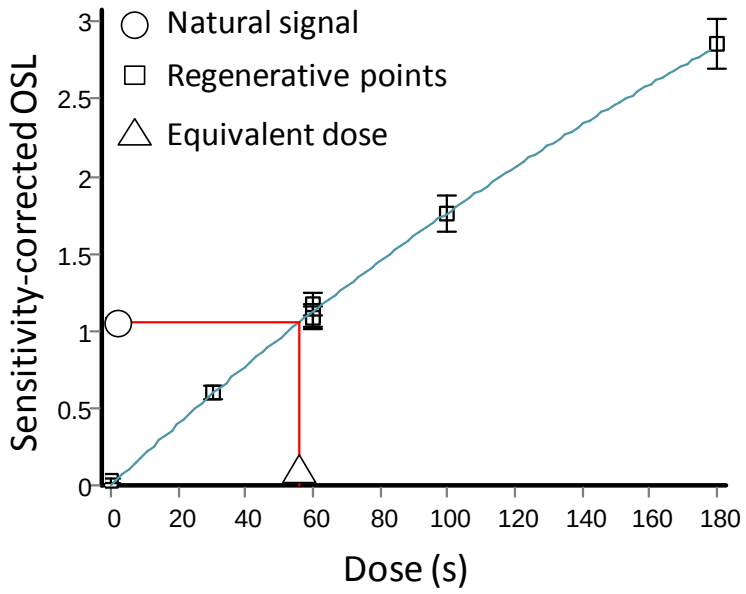

Fig. 1.2. *Example of a dose-response curve used to estimate the equivalent dose of a sample, through the SAR protocol.*

2000, 2003). Statistics ("age models") are used to select one paleodose, thought to represent the average dose absorbed by the measured grains since burial, from a set of D_es. Age is calculated as the paleodose divided by the natural dose rate.

The development of the SAR protocol for OSL dating has improved the accuracy and environmental range of this chronologic tool, enabling dating of quartz grains with depositional ages ranging from a few years to hundreds of thousands of years. In addition, recent statistical advances (e.g., Galbraith et al., 1999; Cunningham and Wallinga, 2010) have enabled dating of sediments for which only a fraction of grains were completely bleached prior to deposition. These methods have extended OSL dating to fluvial sediments, of which not all grains may be reset prior to deposition. Despite major advances in OSL dating, and subsequent application of the method to broader geographic settings, the degree of bleaching and availability of sensitive quartz are still concerns in applying OSL dating in fluviodeltaic environments. These are discussed in Chapters 4 and 5.

While luminescence measurements have been traditionally used for sediment dating purposes, recent studies have explored the potential of luminescence approaches for inferring geologic processes beyond sedimentary geochronology. For example, Sohbati et al. (2012) used attenuation of the luminescence signal with depth in boulders for surface exposure dating, and Reimann et al. (2015) used differential bleaching of luminescence signals to infer transport of sand grains along the Dutch coast.

This dissertation applies luminescence dating to establish a chronology for deltaic deposits, and also presents new luminescence methods. These novel methods aim to extend luminescence dating to regions in which it has been historically underused, and to infer sediment transport in deltas using differential bleaching of the luminescence signal of polymineral sediments. Drivers of bleaching in a large meandering river and its delta are also explored.

1.3 Scientific contributions of this dissertation

The following portion of this dissertation is equally composed of chapters that describe deltaic evolution (Chapters 2 and 3) quantified through luminescence approaches, and chapters that advance the use of luminescence dating in deltas through methodological advances (Chapters 4 and 5). Through this dissertation and its resulting and pending publications, my coauthors and I make the following contributions to science:

- *Clarifying processes of centennial- to millennial-timescale deltaic land growth.* This is tested in a major relict subdelta of the river-dominated Mississippi Delta. The 6,000-8,000 km^2 bayhead portion of the subdelta is shown to have grown in a

radially symmetric fashion characterized by distributary channel coactivity. Progradation rates (100-150 m/yr) were sustained for almost a millennium before abandonment, providing no evidence for autoretreat within this system. Avulsions, and thus the delivery of sediment to the deltaic plain, are shown to have taken place over a broad zone extending more than 700 linear km inland, well beyond the delta.

- *Quantifying total subsidence and its primary drivers, over centennial- to millennial-timescales.* This is also tested in the Mississippi Delta. Subsidence over long timescales is found to be strongly correlated to loading of new sediment, but unlikely to be linked to total Holocene sediment thickness or faulting. Up to 50% of elevation gained by deposition of fresh sediment is ultimately lost, likely due to the combined effects of compaction of fresh sediments and deformation of underlying strata due to loading.
- *Assessing bleaching of the quartz luminescence signal of river-delta sediment by grain size and transport mode.* This is explored using archival data from the Mississippi Delta geologic record in combination with new samples collected from the modern Mississippi River. The degree of bleaching of sands is shown to be highly time- and space-dependent. By contrast, silt is shown to be generally sufficiently bleached in both the modern Mississippi River and its deposits, regardless of age.
- *Establishing and validating a luminescence dating protocol for use in a deltaic setting where standard geochronology methods are unlikely to work.* This is tested in the Ganges-Brahmaputra-Meghna Delta, a delta fed by up ~ 1 billion

tons of sediment per year mobilized from rapidly uplifting igneous and metamorphic rocks. Silt is found to be sufficiently bleached and suitable for luminescence dating through the SAR protocol. Advances are made toward identifying sediment transport processes through the application of a bleaching index that describes light exposure of sediments.

1.4 Broader impacts

It is no secret that deltas worldwide are among the most at risk, biodiverse, productive, and populated regions on the planet (e.g., Blum and Roberts, 2009; Syvitski et al., 2009; Brammer, 2014; Auerbach et al., 2015b; Allison et al., 2016). In addition to satisfying scientific curiosity, research on deltaic processes is needed to inform science-based management of deltas. Quantifying rates and patterns of deltaic growth through distributary channel activity is important because distributaries are the primary control of the delivery of fresh water and sediment resources to a delta plain. The delivery of new sediment is essential for keeping pace with relative sea level rise (e.g., Paola et al., 2011), maintaining cultivated and inhabited delta land area, and protecting relatively inland population centers from the damaging effects of tropical cyclones and coastal flooding. The delivery of fresh water is important to sustaining livelihoods in deltas, where it is essential for municipal infrastructure and agriculture. Knowing the rates and drivers of subsidence is equally important to managing deltas and predicting which regions may be the most vulnerable to inundation due to sinking land. Validating methods to date sediment deposition in deltas is essential to measuring processes of delta evolution and the patterns and rates over which they operate.

Chapter 2

Anatomy of Mississippi Delta growth and its implications for coastal restoration

Collaborators: Torbjörn Törnqvist, Zhixiong Shen, Barbara Mauz, Jakob Wallinga

Abstract

The decline of several of the world's largest deltas has spurred interest in expensive coastal restoration projects to make these economically and ecologically vital regions more sustainable. The success of such projects depends in part on our understanding of how delta plains evolve over timescales longer than the instrumental record. Building on a new set of optically stimulated luminescence (OSL) ages, we demonstrate that a large portion (~10,000 km^2) of the late Holocene river-dominated Mississippi Delta grew in a radially symmetric fashion for almost a millennium before abandonment. Sediment was dispersed by deltaic distributaries that formed by means of bifurcations at the coeval shoreline and remained active throughout the lifespan of this landform. Progradation rates (100-150 m/yr) were surprisingly constant, producing 6-8 km^2 of new land per year. This shows that robust rates of land building were sustained during pre-industrial conditions despite high rates of relative sea-level rise (on the order of 1 cm/yr). However, these rates are several times lower than rates of land loss over the past century, indicating that only a small portion of the Mississippi Delta may be sustainable in a future world with continued acceleration of sea-level rise.

2.1 Introduction

Many of the world's largest deltas are undergoing rapid transformations due to reductions in sediment supply (Syvitski et al., 2005), accelerating rates of sea-level rise (Ericson et al., 2006), plus some of the world's highest subsidence rates (Milliman and Haq, 1996). The Holocene stratigraphic record contains abundant information on the ability of delta plains to grow within the constraints of these controls. However, this archive has only partially been explored, in part due to a historic lack of geochronological tools that are necessary to quantify rates of change. Previous studies have assessed the timing of delta lobe (subdelta) activity through radiocarbon dating of bounding peat (Maselli and Trincardi, 2013) and shoreline progradation through optically stimulated luminescence (OSL) dating of beach-ridge deposits (Giosan et al., 2006; Tamura et al., 2012). However, delta growth is fundamentally driven by distributary channel activity. Currently available records of delta growth rely largely on instrumental data obtained over recent decades. For example, the mean land growth rate of the Wax Lake Delta, a recent bayhead delta within the Mississippi Delta, USA (Fig. 2.1a,b), is about 0.8 km^2/yr (Shields et al., 2017). However, the assessment of delta growth over small temporal and spatial scales may reveal little about how river-dominated deltas operate over longer timescales.

Understanding the rates and patterns of delta growth through distributary channel activity is essential for predicting future deltaic land change (Blum and Roberts, 2009), managing sediment resources (Paola et al., 2011), and understanding the effects of human perturbations on deltas (Maselli and Trincardi, 2013). This information will be of paramount importance in the 21st century as major population and economic centers in

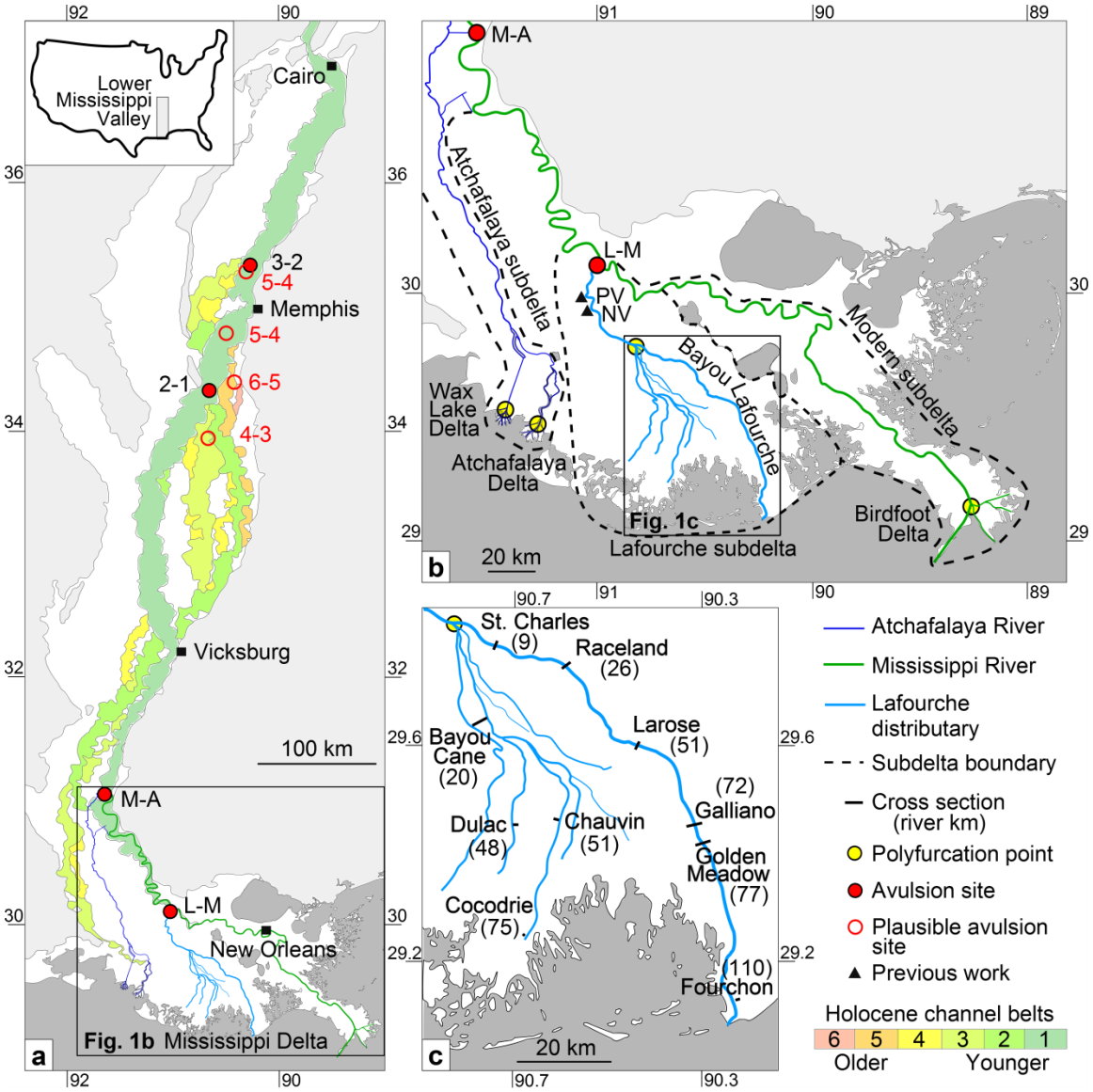

Fig. 2.1. *Major past and present paths of the Mississippi River. a, Channel belts and avulsion sites in the Lower Mississippi Valley and Mississippi Delta (for location see inset), after Saucier (1994). b, Mississippi Delta, including the Lafourche subdelta, the Modern (Balize) subdelta with the Birdfoot Delta, and the Atchafalaya subdelta with the Wax Lake and Atchafalaya deltas. Trunk channels that feed these subdeltas branch into multiple distributaries at polyfurcation points which define the landward limit of bayhead deltas. The two most recent deltaic avulsion sites are the Lafourche-Modern (L-M) and Modern-Atchafalaya (M-A) avulsions. Previous work was conducted at Paincourtville (PV) and Napoleonville (NV). c, Location of cross sections, with distance in river kilometers from the Lafourche subdelta polyfurcation point shown in parentheses.*

large deltas struggle with rapid environmental change. These issues are exemplified well by the Mississippi Delta, where the deposition of clastic sediment by the trunk channel of the Mississippi River (the primary population and infrastructure corridor) is severely hampered due to flood-protection levees. Despite the growth of new land in the Wax Lake and Atchafalaya deltas (Fig. 2.1b), net land loss rates for the delta plain are about 45 km^2/yr, averaged over the past century (Couvillion et al., 2017).

Land loss in deltas can be offset by the controlled delivery of new sediment to the delta plain (Paola et al., 2011; Auerbach et al., 2015a; CPRA, 2017). For example, a $50 billion management plan for coastal Louisiana includes proposals to create new land by the year 2065 through engineered river diversions (CPRA, 2017) that would reintroduce clastic deposition by means of sediment-laden river water. Developing realistic expectations for the efficacy of these strategies requires an understanding of the natural deltaic processes (e.g., distributary channel growth rates, drivers of avulsion) that govern land growth over timescales well beyond decadal-scale instrumental records and the slightly longer historical records (~165 years, Ellet, 1853). In addition to information on fluvial sediment loads (Allison et al., 2012) and deltaic sediment retention efficiency (Esposito et al., 2017), centennial- to millennial-scale records of rates of land growth in the Mississippi Delta are needed to evaluate whether it is possible to significantly offset the high rates of present-day land loss by means of river diversions. There is currently a lack of field data to answer these questions.

Here, we use OSL dating of mouth-bar deposits from the Lafourche subdelta (Fig. 2.1b) to determine the rates and patterns of growth of the Mississippi Delta. Luminescence techniques enable the direct dating of fluviodeltaic deposits (Wallinga,

2002a) and have proven successful for dating the deposition of Mississippi River sediment (Rittenour et al., 2007; Shen et al., 2015). Mouth bars form as distributaries deliver their sediment load to a receiving basin and reflect deposition of the coarsest sediment fractions as flow decelerates when it meets a standing water body. This results in a sand-dominated deposit that progrades and aggrades to fill the basin (Edmonds et al., 2009). By OSL dating mouth-bar sands, we directly capture the time of emergence of new land, and thus, the progradation of the shoreline.

2.2 Geologic setting

The Mississippi Delta is comprised of a series of subdeltas that formed when quasi-periodic avulsions of major distributaries relocated the depocenter (Fisk, 1944). The 10,000 km^2 Lafourche subdelta was active from about 1.6-0.6 ka (Törnqvist et al., 1996; Shen et al., 2015) under conditions of fairly constant relative sea-level rise, and was the primary depocenter during the time period of interest. Water and sediment discharge was shared with the Modern (Balize) subdelta after 1.4 – 1.0 ka (Hijma et al., 2017). The abandonment of the Lafourche subdelta likely preceded the initiation of the Atchafalaya subdelta (Fisk, 1952; Hijma et al., 2017) so river discharge was never shared between these two subdeltas.

We selected the Lafourche subdelta for this study because it is the most recently abandoned subdelta in the Mississippi Delta. The Lafourche subdelta has experienced a complete delta cycle (Roberts, 1997) and therefore provides an archive for river-dominated delta growth from initiation to termination, yet it has experienced limited reworking compared with older subdeltas. In addition, this system has a well-constrained

sea-level history (González and Törnqvist, 2009). In the uppermost reach (about 55 river km long), the Lafourche system essentially features one trunk distributary channel that fed sediment to the surrounding delta plain through episodic overbank deposition, including abundant crevassing on top of a widespread wood peat bed (Shen et al., 2015). This demonstrates that the region between the avulsion site (L-M) and the polyfurcation point (Fig. 2.1b) was subaerial prior to the initiation of the Lafourche subdelta (Törnqvist et al., 1996). Here, we focus on the lower reach of the subdelta (downstream from the polyfurcation point) based on ten cross sections roughly perpendicular to both the main distributary (Bayou Lafourche) and the lesser distributaries (Fig. 2.1c). Ages are presented in ka relative to 2010.

2.3 Methods

2.3.1 Stratigraphy and OSL sample collection

Boreholes were drilled with an Edelman hand auger and gouge. Cores were discretized to 10 cm intervals and described in the field with attention to grain size following the US Department of Agriculture texture classification scheme, sedimentary structures, and fossil content, which informed the interpretation of lithogenetic units (Appendix A, Table A.A.1). The surface elevation at borehole sites was obtained from publicly available LiDAR data. OSL samples were captured with a stainless steel Eijkelkamp sampler that prevents light exposure.

2.3.2 OSL sample preparation and measurement

OSL samples were prepared under amber light at Tulane University following standard procedures (Mauz et al., 2002; Mauz and Lang, 2004). Luminescence measurements were performed at the University of Liverpool using 1-2 mm aliquots of 75-125 µm (~110 grains) or 125-180 µm (~50 grains) purified quartz sand, adhered to 10 mm stainless steel disks. The coarsest grain-size fraction for which sufficient sediment was available was used. Descriptions of measurement facilities are given in previously published work (Shen and Mauz, 2012). A standard single-aliquot regenerative-dose (SAR) protocol (Murray and Wintle, 2000, 2003) with a 200 or 220 °C preheat, 180 °C cut heat, 3-4 regenerative points, one recuperation point, and recycling checks including infrared (IR) depletion of the OSL signal (Duller, 2003) (Appendix A, Table A.A.4) was used to extract the equivalent dose (D_e). Note that D_e herein refers solely to the absorbed radiation dose estimated from luminescence measurement for a single aliquot. Luminescence measurements were made for 40 s over 250 channels. The OSL signal was integrated over the first 0.48 s and an early background interval, integrated over 0.48 – 1.76 s, was subtracted (Cunningham and Wallinga, 2010). Aliquot acceptance criteria included recycling and OSL IR depletion ratios of 10% (Duller, 2003), a maximum test dose error of 20%, and recuperation of 5% relative to the natural signal.

2.3.3 OSL age calculation

D_e datasets were cleaned to remove potential outliers prior to age modelling (see Appendix A) and then treated with a bootstrap minimum age model (bootMAM) (Galbraith et al., 1999; Cunningham and Wallinga, 2012) to obtain the paleodose for each

sample. The paleodose is defined as the best estimate of the true burial dose (the average dose absorbed by the dated quartz sand grains within the sample since burial). The bootstrap approach provides the benefit of incorporating uncertainty on the width of the D_e distribution (sigma_b) expected for well-bleached sands in this setting (Cunningham and Wallinga, 2012). To define the sigma_b input to bootMAM, this study employed a new method for quantifying overdispersion based on the assumption that at least some samples contain only well-bleached quartz grains. This assumption was supported by initial tests which showed that some samples (n=5) had overdispersion values equal to or less than those considered characteristic of well-bleached Mississippi Delta sands by previous studies (Shen and Mauz, 2012; Shen et al., 2015). First, each D_e dataset (n=23, see Appendix A) was analyzed with a central age model (CAM) (Galbraith et al., 1999) which gives a central value and overdispersion of the D_e distribution of the sample (Appendix A, Table A.A.5). The values for overdispersion obtained through the CAM were grouped by grain size (75-125 μm or 125-180 μm) and input with their uncertainties into bootMAM (Cunningham and Wallinga, 2012) with sigma_b = [0,0]. The output revealed the overdispersion that is characteristic of the best-bleached samples within a given grain-size fraction. Overdispersion quantified with this approach was 11 ± 3% for 75-125 μm sand and 11 ± 4% for 125-180 μm sand. The exclusion and addition of samples to the overdispersion analysis are discussed in Appendix A.

The natural radiation of bulk sediment was determined using activity concentrations of ^{40}K and several radionuclides from the uranium and thorium series, measured with a gamma spectrometer at Tulane University (Appendix A, Table A.A.6). The dose rate was calculated using standard dose rate conversion (Guérin et al., 2011)

and cosmogenic contribution (Prescott and Hutton, 1994) factors (Appendix A, Table A.A.6). No external alpha contribution was included because the outer layer of the quartz grains was removed by etching. Beta dose attenuation was corrected for grain size (Mejdahl, 1979) and attenuation due to pore water was calculated (Aitken, 1985). Water content was measured by drying bulk sediment for each sample in a low-temperature oven, with 5% uncertainty added.

OSL ages were calculated by dividing the paleodose obtained from the bootMAM by the dose rate presented in Appendix A (Table A.A.6). Two samples were dated per cross section and paired ages that agreed within 2σ unshared uncertainty were accepted. One age (St. Charles I-2) was rejected; this is discussed further in Appendix A. Paired ages and their unshared uncertainties were treated with a weighted mean following the separation of shared (i.e., instrument source calibration, dose rate conversion factors, gamma spectrometer calibration) and unshared (i.e., the spread of the D_e distribution assigned by the age models, dose rate measurement error due to counting statistics, and water content) errors (Rhodes et al., 2003) to obtain a single age for land emergence at each cross section. Shared errors were returned in quadrature to the uncertainty of the weighted mean ages after application of the weighted mean.

2.3.4 Progradation and land change rates

The range of the Lafourche bayhead delta progradation rates was obtained by dividing the distance between the most landward (St. Charles) and most seaward (Fourchon) cross sections by the minimum and maximum time span between emergence at these localities. The land area produced by the Lafourche bayhead delta was obtained

by estimating different shoreline positions at the time of Lafourche subdelta abandonment; other boundaries are better constrained. The minimum area was calculated using the current position of the transgressive barrier island chain. The maximum area was estimated by projecting the Lafourche subdelta beyond the most seaward cross section, assuming constant progradation rate was sustained by all distributaries for the remainder of subdelta activity. The contemporary rate of land loss for the deltaic plain was calculated as the sum of areas lost from the Atchafalaya Delta, Barataria, Breton Sound, Mississippi River Delta, Pontchartrain, Teche-Vermillion, and Terrebonne basins over the time period of 1932-2016 (Couvillion et al., 2017).

2.3.4 Avulsion lengths

Avulsion lengths in the Mississippi Delta are presented in river kilometers, obtained along the center of river channels using Google Earth. The avulsion length range associated with the establishment of the present-day Mississippi River in the Mississippi Delta was obtained from the distance between the L-M avulsion site and the most seaward and landward positions possible for the Lafourche paleo-shoreline at the time of the avulsion (1.4 to 1.0 ka, Hijma et al., 2017) and by placing the timing of Lafourche subdelta initiation at 1.6 ka. The most landward position was determined by multiplying the minimum time the Lafourche subdelta had been active when the L-M avulsion occurred by the minimum rate of progradation. Multiplying the maximum time by maximum rate of progradation projected the most seaward position of the paleo-shoreline beyond the realistic region constrained by the OSL ages, and so we established this boundary by using the 1 ka isochron (see Results and discussion).

Holocene channel belts and their relative chronology have been mapped by Saucier (1994). Avulsion sites associated with the creation of new channel belts were identified based on the following criteria: 1) likely redirection of all flow to form a new channel belt, rather than partial redirection of flow via bifurcation, and 2) the most inland departure between two sequential channel belts, rather than a point where channel belts may crosscut downstream. Distinction was made between avulsion sites that unequivocally met these criteria versus those that were classified as plausible avulsion sites (Fig. 2.1a). Other avulsions within this region have been suggested by previous work (Aslan et al., 2005). However, those "avulsions" cannot be ruled out as instances of crosscutting, given the lack of chronologic data. Avulsion lengths of Holocene channel belts were estimated relative to the modern shoreline using Google Earth and rounded to the nearest 50 km. They are presented in linear kilometers due to the unknown sinuosity of relict alluvial channels.

2.4 Results and discussion

2.4.1 Stratigraphy

The Lafourche trunk channel splits into multiple smaller distributaries at 55 river km downstream of its divergence from the modern Mississippi River. This polyfurcation marks the pre-Lafourche shoreline and produced a distributary network that geomorphologically resembles a bayhead delta. Similar polyfurcations mark the antecedent shorelines of modern bayhead deltas such as the Wax Lake and Atchafalaya deltas and give rise to the birdfoot shape of the Modern (Balize) subdelta (Fig. 2.1b). Downstream of the Lafourche polyfurcation point, the Lafourche distributary system

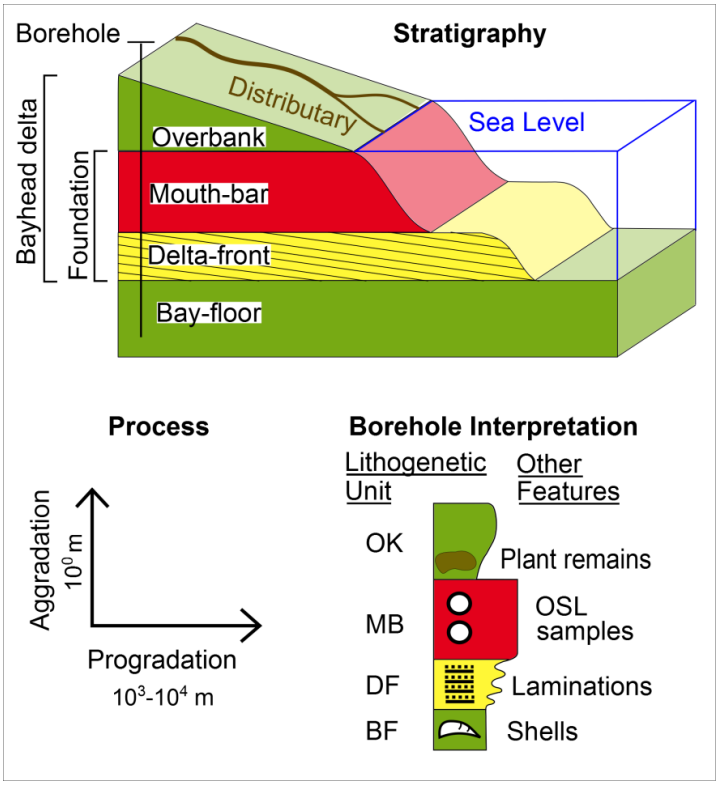

Fig. 2.2. *Schematic illustration of the stratigraphy associated with bayhead delta progradation and aggradation. Red = sand, yellow = silt, green = clay, OK = overbank deposits, MB = mouth-bar deposits, DF = delta-front deposits, BF = bay-floor deposits.*

built new land by prograding into a shallow bay (Fig. 2.2). We refer to the area of new land created during Lafourche activity as the "bayhead delta" (~6,000-8,000 km^2), and the broader area in which Lafourche sedimentation occurred as the "subdelta" (~10,000 km^2). The bayhead delta exhibits a common succession of shell-rich bay-floor muds overlain by 1.3 ± 0.5 m thick laminated delta-front silts, then 2.1 ± 0.8 m thick mouth-bar sands, capped by overbank sediments of varying textures that thin both seaward and away from the channel (Figs. 2.3 and 2.4; Appendix A, Fig. A.A.1). Overbank deposits are relatively fine-grained and somewhat organic near the base. In the more mature regions of the subdelta, the overbank unit grades vertically into a patchwork of relatively coarse deposits that pinch out coastward and away from the channel (Fig. 2.4). This shows that initial, channel-proximal elevation gain in the newly formed bayhead delta was dominated by the deposition of clays, likely through annual flooding. Later, elevation

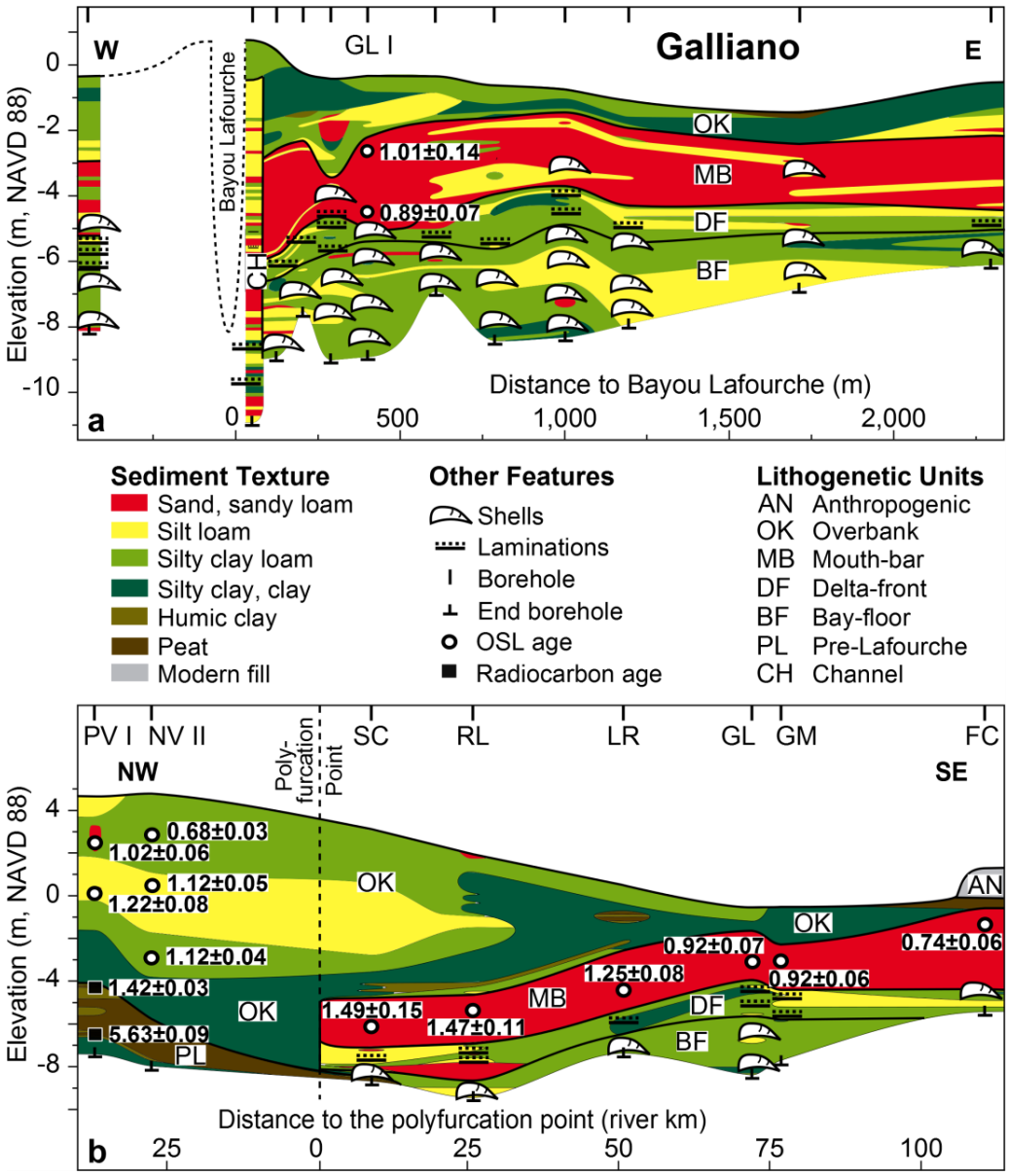

Fig. 2.3. *Cross sections illustrating the stratigraphy adjacent to Bayou Lafourche. a, Example of a cross section perpendicular to the main distributary at Galliano; additional cross sections are presented in Appendix A (Fig. A.A.1). Location and orientation of cross sections are shown in Figs. 2.1b and 2.1c. b, Cross section parallel to the main distributary of the Lafourche subdelta. Deposits underlying the Lafourche bayhead delta that formed in a subaerial setting are referred to as "Pre-Lafourche". In b, weighted mean OSL ages and average sample depths are shown for locations seaward of the polyfurcation point, and the chronology for the PV I and NV II boreholes is from previous studies. Note that the uppermost portion of the overbank unit is highly generalized; for details see Shen et al (2015). All ages are presented in ka relative to 2010.*

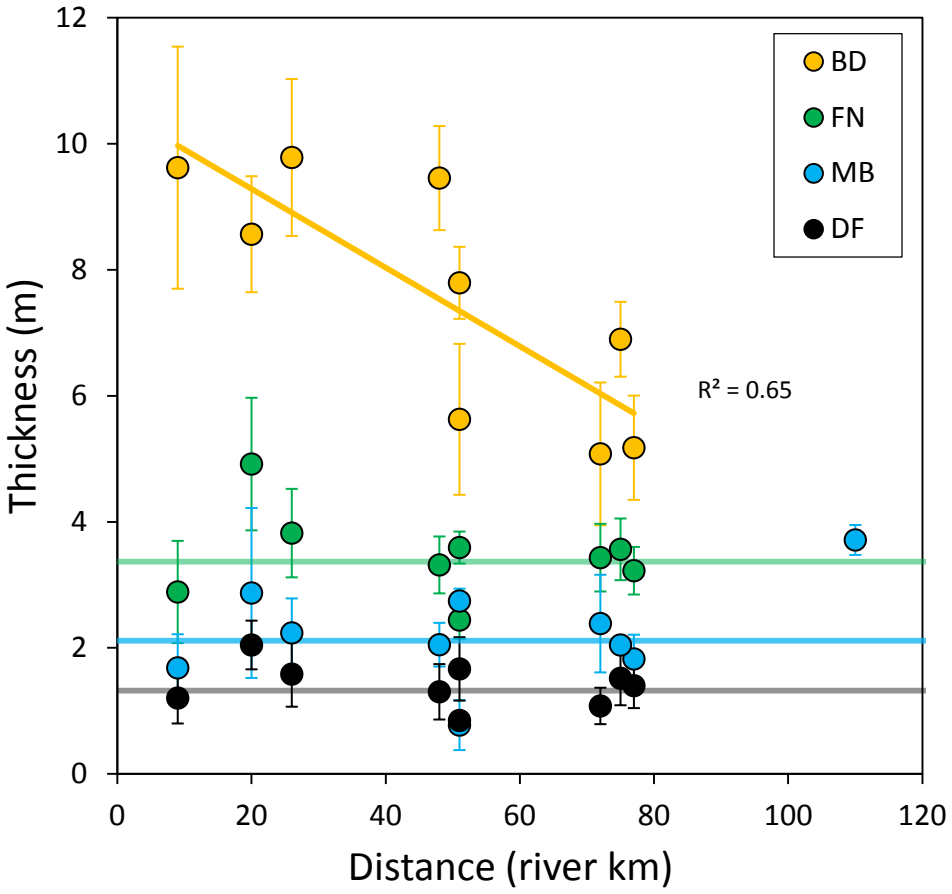

Fig. 2.4. *Downstream trend in the thickness of lithogenetic units. The average thickness of the mouth-bar (MB) and delta-front (DF) deposits for each transect are plotted against distance with reference to the Lafourche polyfurcation point (Fig. 1c). The thickness of the bayhead-delta (BD) and foundation (FN) strata is also shown. The colored horizontal lines show the average thickness of the MB, DF, and FN deposits and the orange line indicates the trend in thickness of the BD deposits. See Appendix A (Fig. A.A.2 and Table A.A.3) for uncertainties on the average thickness.*

gain was characterised by deposition of dominantly silts associated with crevasse channels.

The thickness of bayhead-delta strata is similar between the main and lesser distributaries (Appendix A, Fig. A.A.2). The combined thickness of mouth-bar and delta-front deposits (referred to as "foundation deposits") that aggraded to sea level and

subsequently supported the growth of the subaerial delta through overbank deposition, is consistent throughout the bayhead delta (Fig. 2.4). This indicates that the pre-Lafourche bay-floor depth was fairly uniform (3.4 ± 0.8 m) and remarkably similar to basin water depths of modern incipient bayhead deltas of the Atchafalaya subdelta (Neill and Allison, 2005). The Lafourche subdelta is therefore a good analogue for present-day processes of bayhead delta growth, such as the proposed river diversions that are planned to convert open water into land.

2.4.2 Growth patterns

Modern bayhead deltas have been shown to prograde in a radially symmetric pattern at their onset (Shaw and Mohrig, 2014). This is consistent with observational and modelling studies demonstrating that the most seaward portion of a delta is characterized by bifurcations that produce coeval distributaries (Edmonds and Slingerland, 2007; Jerolmack and Swenson, 2007). Yet, other studies suggest that radial growth of deltas may be restricted to these early stages, while more mature systems may prograde in succession by means of repeated avulsions within the subdelta distributary network. Such a mechanism has found support from a widely used Holocene Mississippi Delta radiocarbon chronology (Frazier, 1967), as well as historical records of the human-modified Po (Nelson, 1970) and Huanghe (Shu and Finlayson, 1993) deltas that feature distributary avulsions within 20 and 100 km of the present-day shoreline, respectively.

Our results show that distributary mouth bars of the Lafourche subdelta at similar distances from the polyfurcation point have matching OSL ages, indicating that growth was characterized by coeval distributary channels throughout of its period of activity (Fig. 2.5). Contrary to what has been proposed by previous work (Frazier, 1967), there is

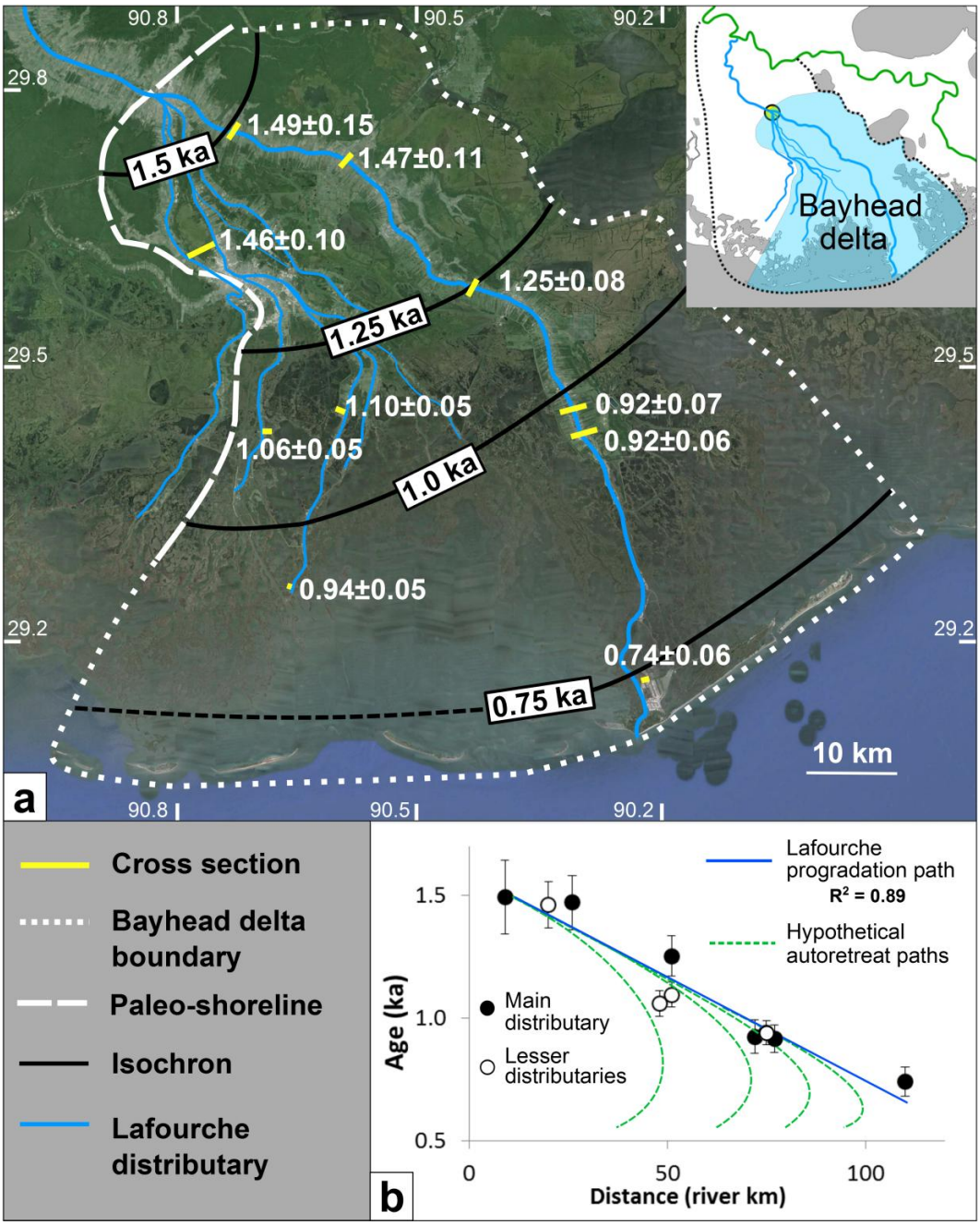

Fig. 2.5. *Growth history of the Lafourche bayhead delta. a, Weighted mean OSL ages determine the timing of new land creation through progradation of the bayhead delta of the Lafourche subdelta (inset). The bayhead delta is bounded to the north and west by the paleo-shoreline, to the south by transgressive Lafourche barrier islands, and to the east by open water (interdistributary lakes). b, The progradational history of mouth-bar deposits associated with the main channel (filled symbols) and lesser distributaries (open symbols) compared to the hypothetical paths that could be expected due to autoretreat (green dashed lines).*

no evidence for avulsions within the distributary network of the Lafourche bayhead delta. We therefore conclude that the Lafourche distributaries formed by means of bifurcation. This demonstrates that radial growth through distributary channel progradation can persist in river-dominated deltas for nearly a millennium. These data also underscore a principle of distributary evolution evident in both modern and past landscapes of the Mississippi Delta: river-dominated delta systems branch at coastal polyfurcation points (Fig. 2.1b). This observation provides a framework by which the antecedent shoreline and stratigraphy of other river-dominated deltas may be inferred. Based on this, we hypothesize that the paleo-shoreline of the Modern (Balize) subdelta was positioned near the polyfurcation point of the Birdfoot Delta (Fig. 2.1b) at the time of Modern subdelta initiation.

2.4.3 Growth rates

It has been previously hypothesized that progradation slows and reverses with delta maturity as the area of the delta plain becomes too large to be supported by a constant sediment supply under conditions of constant accommodation creation (Muto and Steel, 1992). This process of "autoretreat" has been replicated in laboratory (Muto, 2001) and model (Parker et al., 2008) experiments, and has been offered as a possible explanation for transgressive successions found in the ancient stratigraphic record (Hampson, 2010). Progradation rates of deltas during the late Holocene have been assessed elsewhere (Saito et al., 2000; Hori et al., 2004; Maselli and Trincardi, 2013), however, the autoretreat concept has never been tested in a real-world setting with a well constrained sea-level history and geochronology.

The Lafourche bayhead delta grew at an average rate of 6-8 km^2/yr, associated with distributary mouth-bar progradation at a relatively constant rate of 100-150 m/yr (see Methods) throughout the majority of Lafourche activity (Fig. 2.5). This is a surprising result, considering that discharge was shared between the Lafourche distributaries and the modern Mississippi River after 1.4 to 1.0 ka (Hijma et al., 2017). Furthermore, at least one major crevasse splay in the upstream reach of the Lafourche subdelta extracted a considerable amount of sediment from 0.8-0.6 ka (Shen et al., 2015). Thus, we find no evidence for autoretreat in this system and we tentatively propose that deltas situated on relatively open coasts and unconstrained by topography may avulse before they enter a state of autogenic decline.

2.4.4 Avulsions

Avulsions are the principal mechanism that shift the depocenter within deltas, thereby driving delta evolution over centennial to millennial timescales. Our new results show that avulsions did not occur within the Lafourche subdelta, suggesting that subdeltas function fundamentally differently and should not be seen as miniature versions of the broader delta. Here we zoom out to the entire Mississippi Delta to identify avulsion sites and to test the hypothesis that avulsions are preferentially located near a single node (Parker et al., 1998; Ganti et al., 2014) corresponding to the backwater transition where channel-bed deposition is relatively rapid (Chatanantavet et al., 2012; Ganti et al., 2016).

The two most recent avulsion sites within the Mississippi Delta include the partial shift of the modern Mississippi River to the Atchafalaya River (M-A avulsion), and the shift of Bayou Lafourche to the modern river (L-M avulsion) (Fig. 2.1a,b). The M-A

avulsion initiated at 0.5-0.3 ka (Hijma et al., 2017) and is 490 river km inland (see Methods), comparable to the backwater length of the modern Mississippi River (Chatanantavet et al., 2012). There is no information to suggest that the modern river mouth has prograded significantly since the M-A avulsion occurred (Fisk et al., 1954). The L-M avulsion occurred between 1.4 and 1.0 ka (Hijma et al., 2017). At this time, the Lafourche bayhead delta had prograded between 20 and 70 km beyond the polyfurcation point, yielding an avulsion length (that is, the channel length between the avulsion site and the shoreline at the time of the avulsion) of 75-125 km (see Methods), significantly shorter than the M-A avulsion length and most likely well within the backwater length of the Lafourche system.

Evidence of other Holocene Mississippi River avulsions, in the form of relict channel belts, can be found more than 700 linear km inland, within the uppermost reaches of the Lower Mississippi Valley (Fig. 2.1a) (Saucier, 1994). This region has seen considerable (10 m or more, Saucier, 1994) Holocene aggradation, making avulsions almost inevitable. The locations of the two most recent avulsion sites in this region are relatively well-defined, yet, three or more older avulsions likely occurred within a ~250 km linear zone centered around Memphis, Tennessee (see Methods).

From this evidence we conclude that avulsions of the Mississippi River are at least partially dictated by fluvial processes that occur far landward of the delta and extend well beyond the backwater transition. This is consistent with observations of avulsion nodes occurring over an ~80 km linear distance and extending beyond the backwater transition in the Rhine-Meuse Delta (Fernandes et al., 2016), The Netherlands, an area with significantly more data to address this problem (Stouthamer and Berendsen, 2000).

Within the Mississippi Delta as well as in other muddy, river-dominated deltas, avulsions may be partly steered by factors such as sediment cohesion (Ganti et al., 2016) which may drive the river to reoccupy easily erodible (sandy) channel belts (Aslan et al., 2005) rather than forging new tracks through cohesive, muddy overbank strata.

2.5 Implications for coastal management

Avulsions of the Mississippi River are shown to most likely occur over a broad spatial zone that is only partly mediated by backwater dynamics, with a considerable density of avulsion sites 450-700 linear km inland. In contrast, since no evidence was found for avulsions in prograding distributary channels, it seems unlikely that new bayhead deltas associated with river diversions will exhibit avulsions. Rather, they can be expected to grow radially by means of bifurcation.

We document high progradation rates of 100-150 m/yr and land-area creation rates of 6-8 km^2/yr within the Lafourche subdelta, sustained for nearly a millennium, i.e., rates that are an order of magnitude higher than present-day growth rates in the Wax Lake Delta (Shields et al., 2017). These rates are especially noteworthy considering that the sediment input was shared between the Lafourche subdelta and the Modern (Balize) subdelta (at least during part of its existence) and the region experienced rates of relative sea-level rise on the order of 1 cm/yr (Jankowski et al., 2017), given that the high subsidence rates observed today likely prevailed over the past few millennia. This finding is relevant to coastal planning because it shows that channels with diminished sediment flux, including proposed river-sediment diversions that siphon only a fraction of modern Mississippi River discharge during relatively short time periods, can be very effective in

building new land. However, the average prehistoric rates of land growth are several times (by a factor of about 5-7) lower than recent rates of Mississippi Delta land loss (Couvillion et al., 2017). While areas beyond the Lafourche subdelta such as the Modern (Balize) subdelta may have also experienced growth during the time period of concern, there was undoubtedly significant decline in other portions of the Mississippi Delta (i.e., pre-Lafourche subdeltas) and so it is unlikely that net growth of the delta plain exceeded 6-8 km^2/yr. Considering recent land-loss rates (~45 km^2/yr, Couvillion et al., 2017) in combination with the global sea-level rise acceleration (Church et al., 2013), net land loss in the modern delta will likely continue regardless of coastal restoration strategies, ultimately producing a deltaic landscape that will be very different from the present one.

2.6 Acknowledgements

We thank Jon Bridgeman, Chris Esposito, and Jayur Mehta for field assistance and acknowledge all land owners for allowing us to work on their property. Susan Packman and Mhairi Birchall of the University of Liverpool assisted with OSL measurements. Tony Reimann of the Netherlands Centre for Luminescence Dating shared insights about the OSL data analysis. Mead Allison and Steven Goodbred, Jr. provided comments on an earlier version of this manuscript. We acknowledge funding from the National Science Foundation (EAR-1148005 and EAR-1349311), the Gulf Coast Association of Geological Societies student grant program, and the Coastal Protection and Restoration Authority of Louisiana Applied Research Program (CPRA-2013-T11-SBO2-DR).

Chapter 3

The inconvenient truth of fresh sediment: Insights from a new method for quantifying subsidence in the Mississippi Delta

Collaborators: Zhixiong Shen, Torbjörn Törnqvist

Abstract

Subsidence is a complex process driven by many potential factors, with rates dependent on the timescale and depth interval over which they are measured. There is growing consensus that relatively shallow processes such as compaction and artificial drainage are dominant drivers of subsidence in deltas, although other processes such as faulting have not been entirely discounted. Here we use a new method to quantify subsidence in the Mississippi Delta over centennial to millennial timescales using the depth of the mouth-bar-to-overbank stratigraphic boundary formed near sea-level, in combination with OSL chronology. The contributions of isostatic processes are removed by subtracting a relative sea-level rise term previously obtained from basal peat. We find that displacement rates, averaged over 750 to 1500 years, are on the order of a few mm/yr. Subsidence appears unrelated to the thickness of underlying Holocene strata and the occurrence of previously mapped faults. There is a strong correlation between overburden thickness and cumulative displacement, suggesting that roughly 50-57% of elevation added through overbank deposition is ultimately lost to subsidence associated with the combined effects of compaction of fresh sediments and deformation of underlying strata due to loading. Load-induced subsidence is greater at locations

underlain by mouth-bar sand and bay-floor deposits than at locations underlain by peat and relict subdelta deposits. These findings have major relevance to coastal restoration in the Mississippi Delta through engineered river diversions, which will inevitably accelerate compaction at diversion sites, especially those building into open-water settings.

3.1 Introduction

Subsidence has been widely recognized as a major driver of deltaic land loss that endangers the future sustainability of these economically and culturally significant regions (e.g., Mazzotti et al., 2009; Syvitski et al., 2009; Marriner et al., 2012; Higgins et al., 2013). In the Mississippi Delta, USA, subsidence has been attributed to human activities such as fluid extraction (Morton et al., 2006; Kolker et al., 2011), deep natural processes such as faulting (Dokka et al., 2006), and compaction of Holocene sediments (Törnqvist et al., 2008) occurring primarily in the upper 5-10 m of deltaic deposits (Jankowski et al., 2017). However, these measurements are highly sensitive to the timescales and technologies used for measurement (Meckel, 2008; Blum and Roberts, 2012). For example, GPS (Karegar et al., 2015) and tide gauge records (Kolker et al., 2011) are anchored to monuments often at undocumented depths below the land surface and therefore exclude processes happening in the shallowest subsurface. Rod surface-elevation table-marker horizon measurements (Webb et al., 2013) mostly capture these shallowest processes, and can be very effective in measuring present-day subsidence when combined with deep measurement approaches such as GPS monitoring stations (Jankowski et al., 2017). Yet, these instrumental records reveal little about how

subsidence has operated over geologic timescales in the delta, and therefore do not yield information about rates of subsidence associated with natural processes that occurred prior to human modification of the delta.

Developing this information in critical to predicting the land-building capacity of river diversions, a significant component of the $50 billion coastal management strategy outlined in the Louisiana Coastal Master Plan (CPRA, 2017). River diversions aim to counteract land loss in the Mississippi Delta by reconnecting the Mississippi River with its floodplain, thereby resuming the natural processes of land-building though sedimentation. This restoration strategy has the best likelihood for success if diversions are positioned into basins that are least likely to experience high rates of subsidence. Geologic-timescale rates of subsidence have been previously addressed through the depth occurrence of basal peats at a relatively inland locality in the Mississippi Delta (Törnqvist et al., 2008). More work is needed to assess rates of subsidence across a larger area including coastward localities, which are those most directly vulnerable to inundation.

Here, we present an innovative and largely unused approach to measure subsidence in the Mississippi Delta. Values of subsidence are extracted from the depth occurrence and timing of formation of the mouth-bar-to-overbank (M-O) transition, a common stratigraphic boundary in many coastward localities of the delta (see Chapter 2). Subsidence rates and cumulative displacement over geologic timescales are assessed at strategically-selected coastward localities in the Lafourche subdelta (Fig. 3.1). This region of the Mississippi Delta includes overburden deposits of variable thickness that are part of a thicker Holocene sediment package, subsurface fluid extraction hotspots, and is crosscut by multiple roughly coast-parallel faults. These features enable an exploration of

the primary drivers of subsidence, which can be used to predict regions of the delta that will be most likely to experience high subsidence rates in the future.

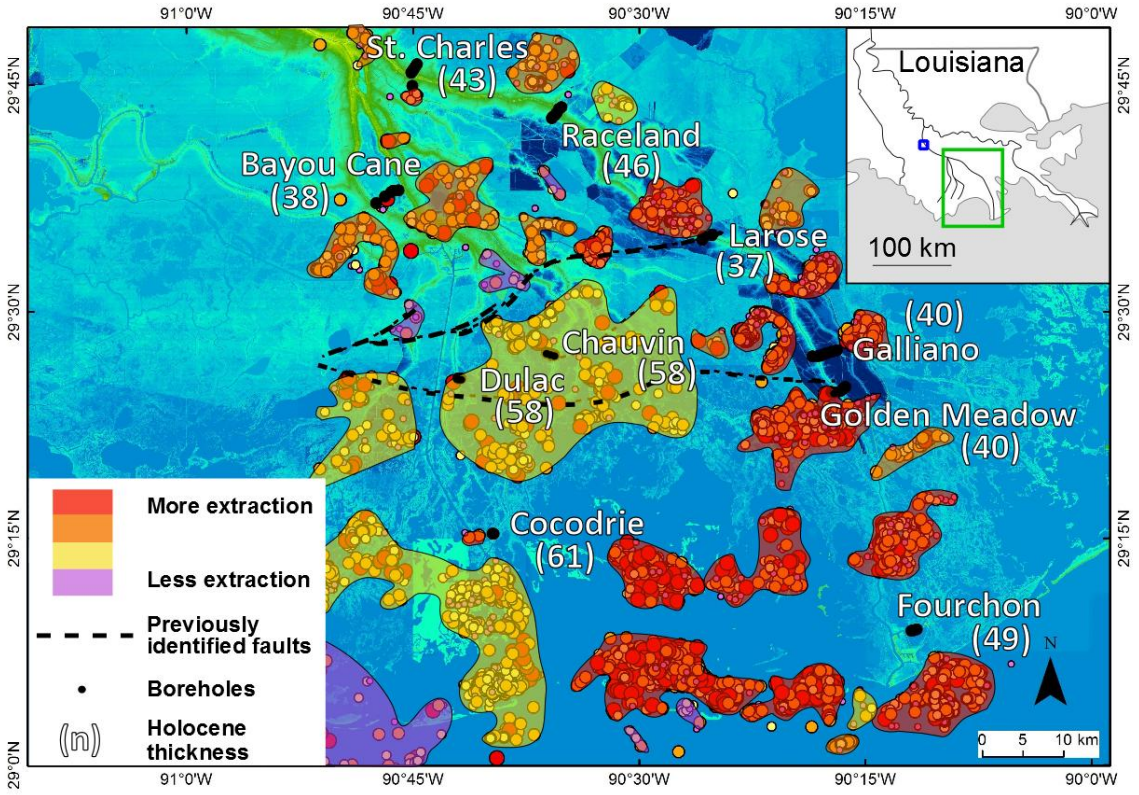

Fig. 3.1. *The location of cross sections relative to Holocene sediment thickness (Heinrich et al., 2015), oil- and gas-extraction hotspots, and previously mapped faults (Kuecher et al., 2001). The inset shows the location of the study area (green box) as well as the study area of Törnqvist et al. (2008) (blue box). Oil and gas extraction values are given in Appendix B, Figs. A.B. 1 and A.B.2.*

3.2 Geologic setting

Subsidence was assessed at 10 locations in the Lafourche subdelta (Fig. 3.1), a ~10,000 km^2 portion of the Mississippi Delta that was formed 1.6-0.6 ka (Törnqvist et al., 1996; Shen et al., 2015) and created 6,000-8,000 km^2 of land through progradation into a shallow (3.4 ± 0.8 m) bay environment similar to Atchafalaya Bay (see Chapter 2).

Therefore, the Lafourche subdelta provides a reasonable analogue for inferring natural processes such as subsidence due to loading within present-day bayhead deltas such as the Wax Lake Delta and proposed river diversions discharging into open water. The emergence of new bayhead delta land in the Lafourche subdelta was recorded as a ubiquitous succession of shell-rich bay-floor, laminated delta-front, sandy mouth-bar, and overbank lithogenetic units (see Chapter 2) (Fig. 3.2). The timing of land formation in the Lafourche bayhead delta was previously determined through optically stimulated luminescence (OSL) dating of mouth-bar deposits (see Chapter 2) .

This study considers the influence of overburden thickness, faults, and total Holocene sediment thickness on subsidence in the Lafourche subdelta (Fig. 3.1). Overbank sediment thickness was calculated between the land surface and the top of the mouth bar (see Chapter 2). The overbank unit thins coastward (Fig. 3.3a) with sedimentation time, that is, the time between the emergence of the mouth bar and the abandonment of the Lafourche subdelta at 0.6 ka (see Chapter 2). Overbank deposits accumulated at an average rate of 0.71 mm/yr over the lifespan of the subdelta (Fig. 3.3b) and range in thickness from about 1-8 m at the sites studied herein. Because the mouth-bar and delta-front deposits are fairly uniform, the thickness-trend of the overbank deposits yields a wedge-shaped bayhead delta deposit that thins coastward (see Chapter 2, Fig. 2.4). The surface expression of fault traces in the lower Lafourche subdelta (Kuecher et al., 2001) and total Holocene sediment thickness (Heinrich et al., 2015) were compiled from previous studies. Oil and gas production data were compiled using the SONRIS database (Appendix B, Figs. A.B.1 & A.B.2). Study sites are located away from

oil- and gas-extraction hotspots (Fig. 3.1), thereby minimizing the contribution of extraction to subsidence and allowing this study to focus on other factors.

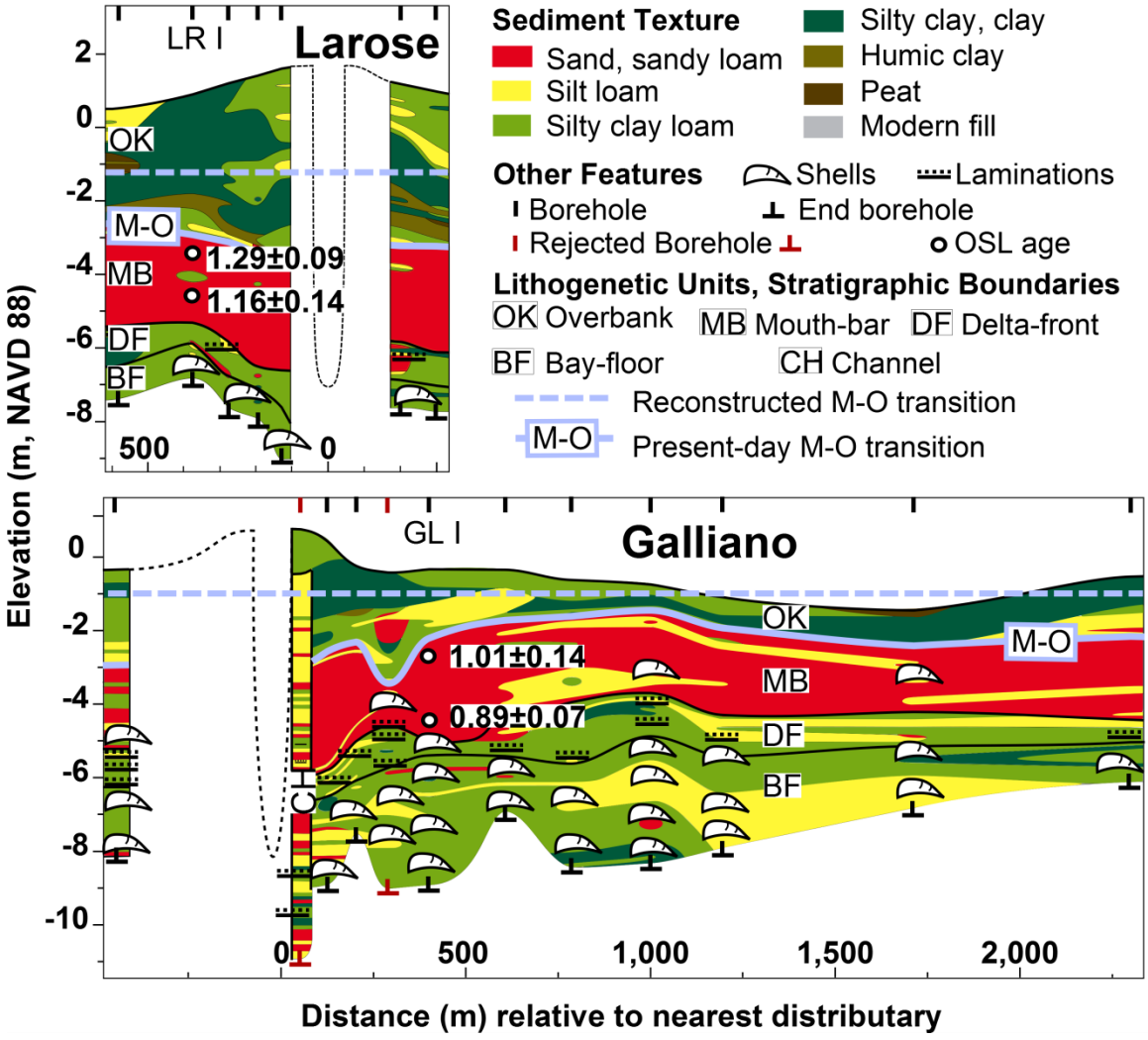

Fig. 3.2. *Two examples Lafourche subdelta stratigraphy in the bayhead delta. Larose is a relatively landward locality with thicker overbank deposits, and Galliano is a relatively seaward locality with thinner overbank deposits. The reconstructed position of the M-O transition at the time of its formation and preset day position are indicated. All cross sections are presented in the Chapter 2 appendix. See Fig. 2.2 for a schematic illustration of the stratigraphy associated with bayhead delta progradation and aggradation.*

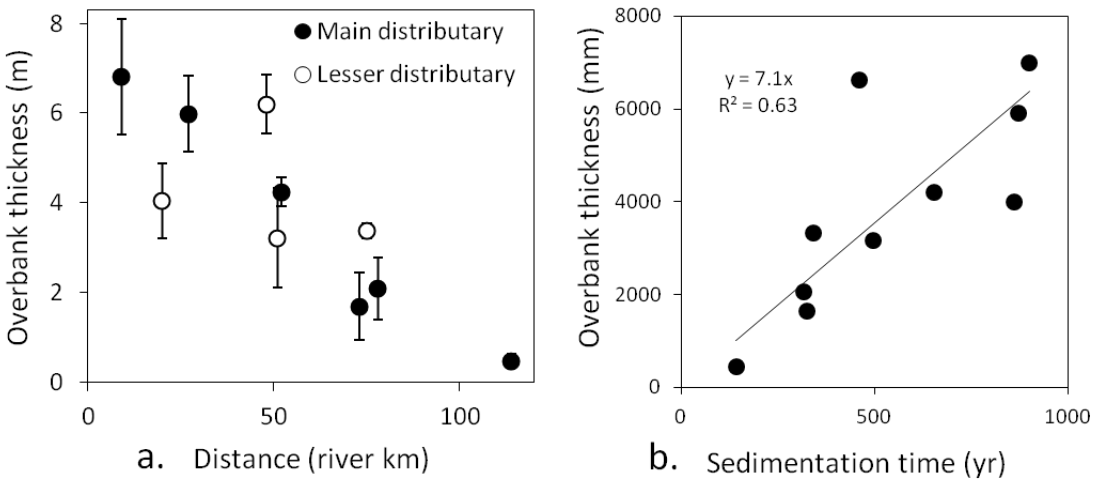

Fig 3.3. *Thickness of overbank deposits with distance below the polyfurcation point (a), and the centennial-timescale average overbank aggradation rate (b).*

3.3 A new approach to calculating subsidence

Mouth bars form through clastic deposition by distributary channels at the marine-terrestrial interface and reflect the coarsest sediment delivered by the distributary (e.g., Fisk et al., 1954). In systems with sufficient coarse sediment such as the Mississippi Delta, this results in a sand-dominated deposit that fills the accommodation space (e.g., Wright, 1977; Edmonds et al., 2009). As the top of the mouth bar approaches sea level, vegetation colonizes the deposit and enhances trapping of fine-grained sediments. This produces an abrupt lithologic transition from sand to mud referred to herein as the M-O transition. This boundary has been shown to correspond to sea level in the Mississippi Delta (Fisk et al., 1954; Roberts et al., 1997; Shen and Mauz, 2012), and forms specifically at low mean tide in the Wax Lake Delta (Wellner et al., 2005). Low mean tide in the Mississippi Delta occurs at -0.2 ± 0.1 m NAVD 88 and is relatively constant across the delta (González and Törnqvist, 2009). It is likely that the tidal range has not changed significantly over the late Holocene (Hill et al., 2011).

Because the M-O transition corresponds to sea level and is a common stratigraphic boundary in bayhead regions of the Mississippi Delta and likely other systems as well, its depth occurrence in the geologic record is a valuable and largely unexplored relative sea-level indicator. A similar innovation was presented by Fisk et al. (1954), based on the observation that both total thickness of "bar" sands adjacent to distributary channels in the Birdfoot Delta of the Modern (Balize) subdelta (see Chapter 2, Fig. 2.1) and the depth of the base of overlying natural levee deposits are a record of total subsidence. However, Fisk et al. (1954) lacked the chronologic and relative sea level data needed to apply their insight to calculate subsidence rates. Here, we use stratigraphic data in combination with OSL ages of mouth-bar deposits, which capture the timing of formation of the M-O transition, and a previously established record for compaction-free relative sea-level rise in the Mississippi Delta (González and Törnqvist, 2009). This allows for the calculation of subsidence rates (S) using the formula:

$$S = \frac{(E_2 - E_1) - (R_2 - R_1)}{(T_2 - T_1)}, \quad (3.1)$$

where (E_1) is the elevation of the M-O transition relative to sea level at the time of formation (-0.2 ± 0.1 m), (E_2) is the elevation of the M-O transition at the time of coring, relative to NAVD 88, (T_1) is the mouth-bar sand OSL age relative to present-day (T_2), and (R_2) is modern sea level and (R_1) is the paleo-sea level for the Mississippi Delta at T_1 (González and Törnqvist, 2009) (Fig. 3.4). Deep subsidence, including the effects of glacial isostatic adjustment (GIA) and sedimentary isostatic adjustment (SIA), were removed through the subtraction of this relative sea-level rise term, which is based on the

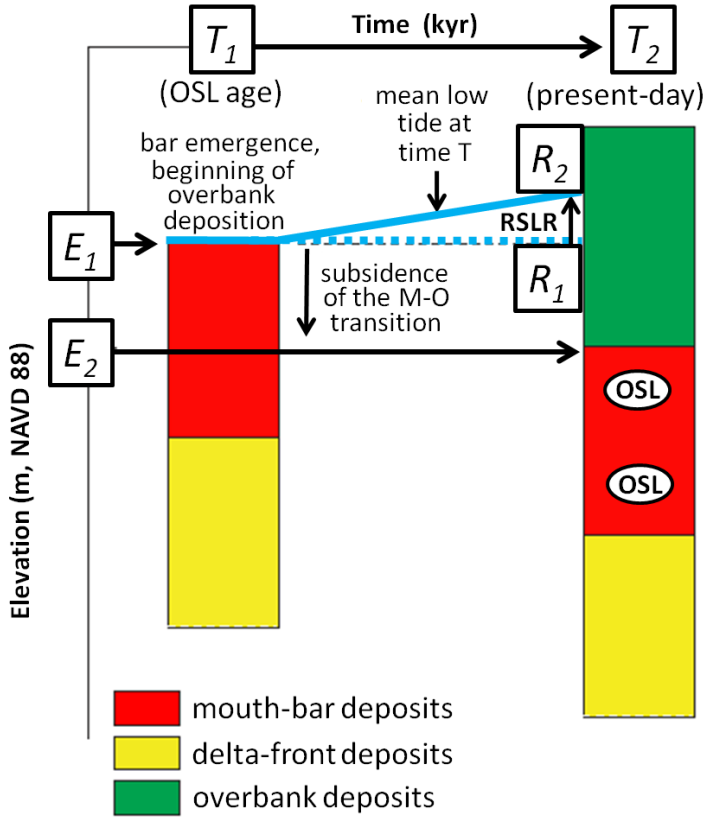

Fig. 3.4. *Schematic illustration of how subsidence is calculated based on the depth of the mouth bar (red) to overbank (green) (M-O) transition, time since formation of the M-O stratigraphic boundary obtained from OSL ages of mouth-bar deposits, and corrected for relative sea-level rise (RSLR). E, T, and R are explained further in the text.*

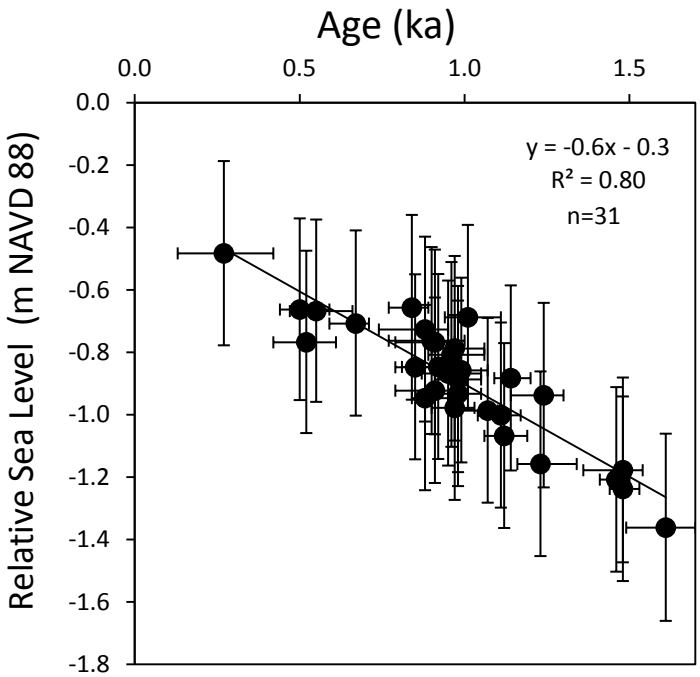

Fig. 3.5. *Rate of relative sea-level rise obtained from radiocarbon dating of peats formed directly above the compaction-free Pleistocene surface in the Mississippi Delta (after González and Törnqvist, 2009).*

depth occurrence of basal peat that formed in the Mississippi Delta during Lafourche activity (Fig. 3.5).

3.4 Values and drivers of subsidence in the Lafourche subdelta

Rates of subsidence measured with this new method ranged from 0-4 mm/yr (Appendix B, Fig. A.B.3), consistent with previously modeled rates of Holocene Mississippi Delta sediment compaction (Meckel et al., 2006). Cumulative subsidence was found to correlate to overburden thickness and therefore also downstream distance, yet showed no clear relationship to total thickness of the Holocene package (Fig. 3.6).

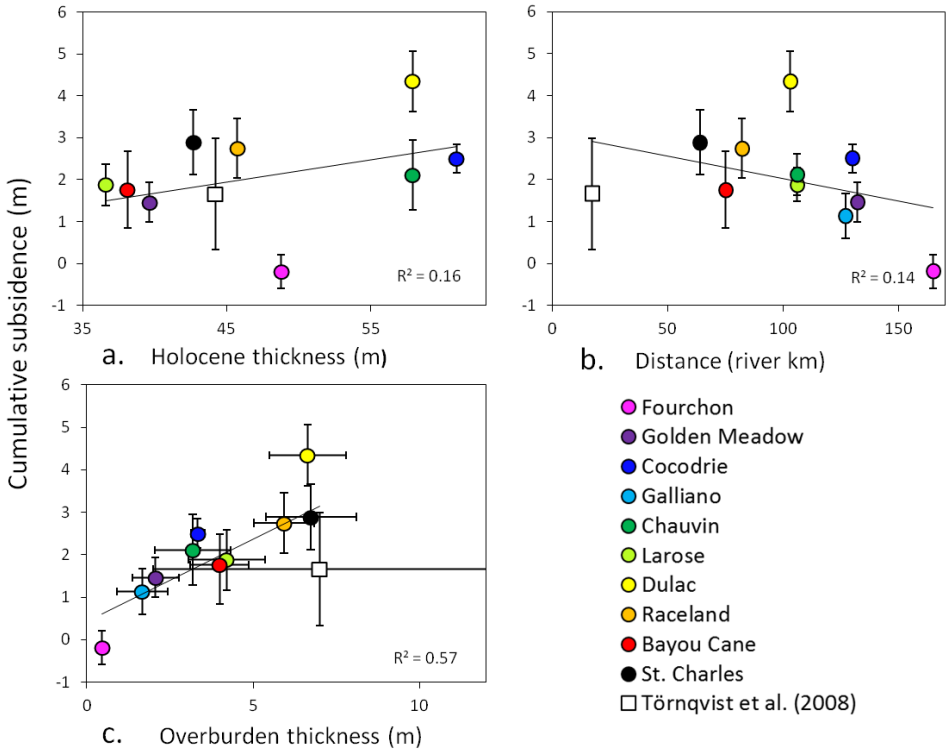

Fig. 3.6. *Values obtained at each cross section for total subsidence and their relationship to (a) thickness of Holocene deposits, (b) distance along Bayou Lafourche, and (c) overburden thickness.*

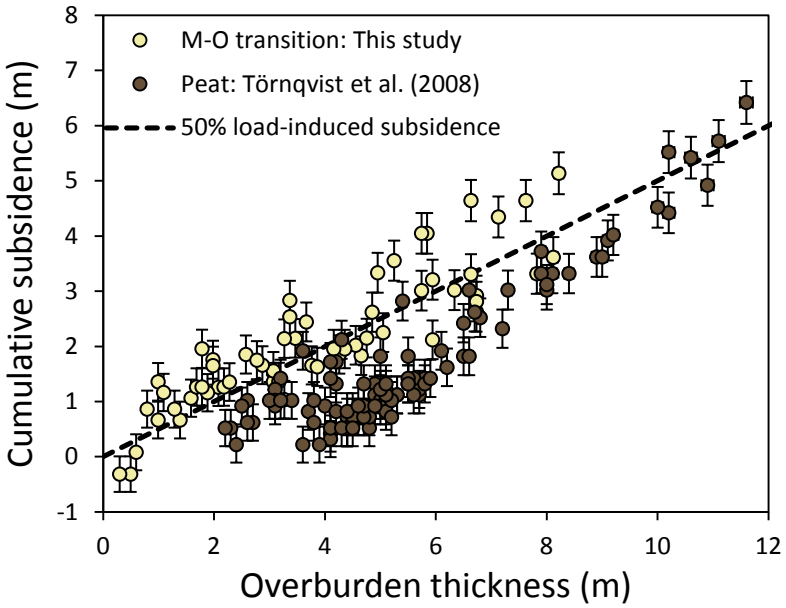

Fig. 3.7. *The relationship of overburden thickness to cumulative subsidence assessed with the depth occurrence of two stratigraphic surfaces, the M-O transition (this study) and peats (Törnqvist et al., 2008). The dashed line indicates subsidence scaled to 50% of the overburden thickness.*

By reconstructing the original position of the M-O transition at the time of its formation (Fig. 3.2), and calculating the fraction of the overlying deposit occurring below this boundary at present day, we estimate that 50-57% of elevation gained through overbank deposition is ultimately lost to subsidence of the bayhead delta (Fig. 3.7). Our values are significantly higher than the 35% value for load-induced subsidence presented by Törnqvist et al. (2008), obtained through a similar method using the same assumptions with regard to tidal range and uncertainties. However, it is important to recognize that load-induced subsidence at our study localities is not sourced solely to the overbank deposit; the weight of the mouth-bar and delta-front deposits that directly underlie the M-O transition likely also drive subsidence of the deeper bay floor deposits, perhaps through the displacement of mud lumps or similar phenomena. Further, mouth-bar and delta-front deposits represent relatively young strata and highly unconsolidated strata, that likely experienced primary compaction (Terzaghi and Peck, 1967) concurrent with

Lafourche overbank deposition. In other words, the subsidence measured herein probably represents the combined effects of compaction of fresh sediment within the Lafourche subdelta deposits and deformation of underlying strata due to loading by the Lafourche subdelta deposits. It is also possible that the alternating layers of sand and clay typical of bayhead delta stratigraphy may yield optimal conditions for compaction because the high permeability of sand allows water to exit the strata, thereby lowering the pore pressure and driving compaction (Meckel et al., 2006). By contrast, peats confined by clays may be more likely to retain water and therefore less likely to compact. Regardless of the driving mechanism(s), our findings suggest that that bayhead delta deposits are more prone to subsidence than deposits at relatively inland localities underlain by older subdelta strata, even when the inland localities are rich in organics. This is a surprising result, considering that the prevalence of subsurface peat has been previously linked to exceptionally high rates of subsidence (Hooijer et al., 2012).

Subsidence in the Lafourche subdelta does not appear to correspond to previously mapped faults (Fig. 3.1). For example, the rate of subsidence of the Golden Meadow transect (1.59 ± 0.52 mm/yr) located coastward of a previously mapped fault (Kuecher et al., 2001), is not significantly different from the rate of subsidence at the Galliano transect (1.22 ± 0.59 mm/yr) located landward of this fault. It is unclear whether this is due to fault inactivity or inaccurate mapping of the fault. There is ongoing work by others to compile a "fault atlas" for south Louisiana, informed by high resolution 3D seismic data, however this work is not complete nor peer-reviewed at present. Despite uncertainty in the exact surface expression of faults in our study area, we know that the study area is generally crosscut by multiple faults (Gagliano, 1999). Previous studies have claimed that

fault movement over recent millennia in the Mississippi Delta has driven a general trend of increasing subsidence coastward, associated with the submergence of large blocks of coastal land (Gagliano et al., 2003; Dokka et al., 2006). This trend is not present in our data, suggesting that faulting is at most a minor source of Mississippi Delta subsidence producing only very regional effects, and is not driving broad-scale subsidence in this part of the delta.

The load-driven compaction component of subsidence has been previously shown to be greatest at the onset of loading and to decrease exponentially with time (e.g., Holtz and Kovacs, 1981), with the majority of compaction occurring within the first ~20 years (Mazzotti et al., 2009). To further investigate the time-depended nature of the subsidence rates calculated here, we normalized rates by overburden thickness, producing rates of subsidence (mm/yr) per meter of overbank sediment. These rates, averaged over 750-1500 years, were found to be higher at younger locations and lower at older locations (Fig. 3.8). This indicates that load-induced subsidence is ongoing in the Lafourche subdelta, despite the passage of hundreds to more than 1000 years since loading began and about 600 years since loading ceased. Still, the present-day contributions of load-induce subsidence are likely only a minor component of the millennial to centennial average produced by our method.

3.5 Conclusions

This and other recent studies suggest that subsidence is largely sourced to processes acting within shallow Holocene strata (e.g., Jankowski et al., 2017), while subsidence produced by deep processes is a relatively minor component (Wolstencroft et al., 2014) of the present-day rates of land surface subsidence in the Mississippi Delta

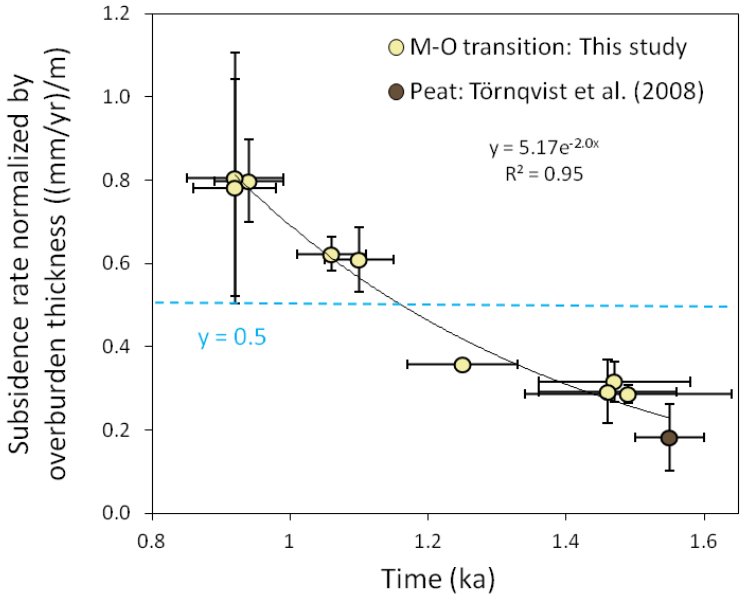

Fig. 3.8. *Subsidence rates normalized by overburden thickness are shown to decrease exponentially with time since formation of the M-O boundary. The blue dashed line indicates the average normalized subsidence rate. Subsidence rates at the Fourchon locality were excluded from this analysis.*

(on the order of 9 mm/yr, Nienhuis et al., 2017). Centennial- to millennial-timescale average rates of subsidence of the M-O boundary are shown to be fairly low (only a few millimeters per year). Total subsidence decreases coastward, coincident with thinning of the bayhead delta package. This supports previous findings that sediment loading is a primary driver of subsidence in the Mississippi Delta (Törnqvist et al., 2008), while deeper processes such as faulting and compaction of the entire Holocene sediment package appear to have little if any broad-scale effect. Additional subsidence may occur within the upper 1-8 m of overbank sediments, not captured by our method.

Our findings imply that inactive regions of the delta can be fairly stable if they are not loaded or otherwise perturbed by human activities. However, loading of the deltaic plain with fresh sediment will inevitably accelerate shallow subsidence, potentially reducing elevation gain by more than 50% at coastward sites where new land is built into open-water basins. In addition to heightened rates of load-driven subsidence, coastward and exposed localities have been shown to experience lower sediment retention relative

to inland and sheltered localities (Esposito et al., 2017). This means that diversions discharging into open water will require significantly more sediment input to produce the same area of land as inland diversions, and are therefore less efficient and effective strategies for mitigating Mississippi Delta land loss. Our findings support the notion that relatively inland diversions underlain by relatively old and previously compacted strata will have the greatest likelihood for success. These findings will be applied in the future to a delta growth model (Kim et al., 2009) adapted to predict the land-building potential of river diversions under realistic scenarios of load-induced subsidence scaled to bayhead delta thickness.

3.6 Acknowledgements

This work was supported by grants from the Coastal Protection and Restoration Authority of Louisiana Applied Research Program (CPRA-2013-T11-SBO2-DR) and the Gulf Coast Association of Geological Societies student grant program. We thank Jon Bridgeman, Christopher Esposito, and Jayur Mehta for field assistance, Samantha McKinley and Sage Anderson for performing fluid extraction analyses. This manuscript was improved by comments made on an earlier draft by Mead Allison, Steven Goodbred, and Jakob Wallinga.

Chapter 4

OSL bleaching of sediments in a major meandering river and its delta: The Mississippi system, USA

Collaborators: Zhixiong Shen, Barbara Mauz, Jakob Wallinga

Abstract

Understanding the degree of bleaching as a function of grain size, transport history, and depositional environment is needed for designing effective sampling strategies and producing accurate luminescence ages. Here, we explore bleaching of the luminescence signal of modern and late Holocene quartz sediment in the Mississippi River and Delta, USA. We compare measured residual doses of sand and silt sampled from within the modern Mississippi River channel with estimated residual doses of sand isolated from Mississippi Delta mouth-bar and overbank deposits formed about 1600 to 600 years ago. Further insight in bleaching is obtained from a comparison of burial ages of paired quartz sand and silt of Mississippi Delta overbank deposits. Contrary to previous studies of smaller and/or braided river systems, we find that coarser sand of the meandering Mississippi River and its delta is less likely on average to be completely bleached than finer sand. However, there is significant variability in the degree of bleaching of sand within grain size fractions, which corresponds to the timing of subdelta-switching and is potentially caused by changes in channel-belt pathways within the alluvial valley or distributary channel dynamics within the delta. This demonstrates that the degree of bleaching of sands in a large delta is highly time- and space-dependent.

Silt is shown to be generally sufficiently bleached in both the modern Mississippi River and associated deposits regardless of age. Therefore, fines should be further tested as a viable option rather than avoided for obtaining luminescence chronologies in megadeltas.

4.1 Introduction

A fundamental requirement of luminescence dating is complete bleaching (zeroing) of the optically stimulated luminescence (OSL) signal prior to burial, for at least a population of grains. Sediment that does not receive sufficient light exposure prior to burial retains a residual dose acquired during previous episodes of burial, which may lead to overestimation of the timing of the most recent burial event. Populations of sediment grains (e.g., sediment samples) may be well/completely-bleached and contain only zeroed grains, or may be incompletely-bleached and contain at least some grains with residual doses. Incompletely-bleached sediment populations may be classified as heterogeneously- (containing both zeroed grains and grains with residual doses), or poor-bleached (containing few to no zeroed grains).

The degree of bleaching is a major consideration in dating of fluvial deposits (e.g.,Wallinga, 2002a), which are less likely to be completely-bleached than aeolian sediments. Assessing bleaching is especially important for dating of fluvial sediments deposited within the most recent millennium, because relatively small residual doses can produce inaccurate ages due to relatively low uncertainties compared with multi-millennial aged deposits (Jain et al., 2004). Yet, if identified, heterogeneous bleaching of sand can be accommodated through the use of appropriate measurement approaches (e.g., measuring small-diameter aliquots or even single grains, Duller, 2008) in combination

with statistical procedures (e.g., application of a minimum age model to isolate the best-bleached grains, Galbraith et al., 1999; subtraction of an early background interval to isolate the most light-sensitive signal, Cunningham and Wallinga, 2010).

Bleaching of quartz sand has been shown to increase with transport distance in some rivers, associated with exposure to daylight during temporary storage on bar surfaces (Stokes et al., 2001). Bleaching of sediments sampled from rivers may also decrease downstream due to the addition of poorly-bleached grains by tributaries or local bank erosion (McGuire and Rhodes, 2015). Fluvial sediments are considered less likely to be completely-bleached if they are contained within channelized flow and do not experience temporary storage, because turbid water greatly reduces the intensity of light exposure and restricts the light spectrum (Berger et al., 1990). Nevertheless, river sediments have complex and numerous potential pathways prior to deposition which may afford various opportunities for bleaching which may differ greatly by river system. The mode of transport is known to vary with grain size (e.g., Gilbert and Murphy, 1914; Hjulstrom, 1935) and is therefore likely to have variable effects on OSL bleaching of sediments of different calibers. It has been previously suggested that finer sediment may be better bleached than coarser sediment because fines are more evenly distributed throughout the water column and therefore more likely than sands to experience transport near the water surface for at least a portion of their travel time (Fuller et al., 1998). However, measurements of some fluvial sediments have found that coarser sand grains possess lower residual doses than finer sand grains (Olley et al., 1998, Murrumbidgee River, Australia; Truelsen and Wallinga, 2003, Rhine Meuse Delta, The Netherlands).

Modern sediments in-transit may experience different bleaching than those preserved in the stratigraphic record (Jain et al., 2004).

Here, we explore bleaching of modern and late Holocene quartz sediment of various transport modes, grain sizes, and depositional environments, in the Mississippi Delta, USA (Fig. 4.1). This is approached through comparing measured residual doses of sands and silts sampled from within the modern Mississippi River channel with estimated residual doses of sands isolated from Mississippi Delta mouth-bar and overbank deposits formed about 1,600 to 600 years ago (Shen et al., 2015). Further insight into bleaching is obtained from a comparison of the burial ages of paired quartz sand and silt of Mississippi Delta overbank deposits (Shen et al., 2015; Chapter 2), reanalyzed here with early background subtraction (Cunningham and Wallinga, 2010). A description of all samples investigated for this study is provided in the Supplementary File (Appendix C, Table A.C.1).

4.1.1 Mississippi River hydrology

The Mississippi River is among the largest rivers in the world in terms of catchment size, sediment, and water discharge. Its catchment includes about 3.3×10^6 km^2 (Milliman and Syvitski, 1992) and drains about 41% of the continental United States (Fig. 4.1) (Milliman and Meade, 1983). Therefore, sediment grains arriving in the Mississippi Delta may originate as far as 2,400 linear kilometers upstream and have experienced lengthy and convoluted transport, or as near as a few meters or less from nearby river cutbanks and have experienced minimal transport since their last major storage event.

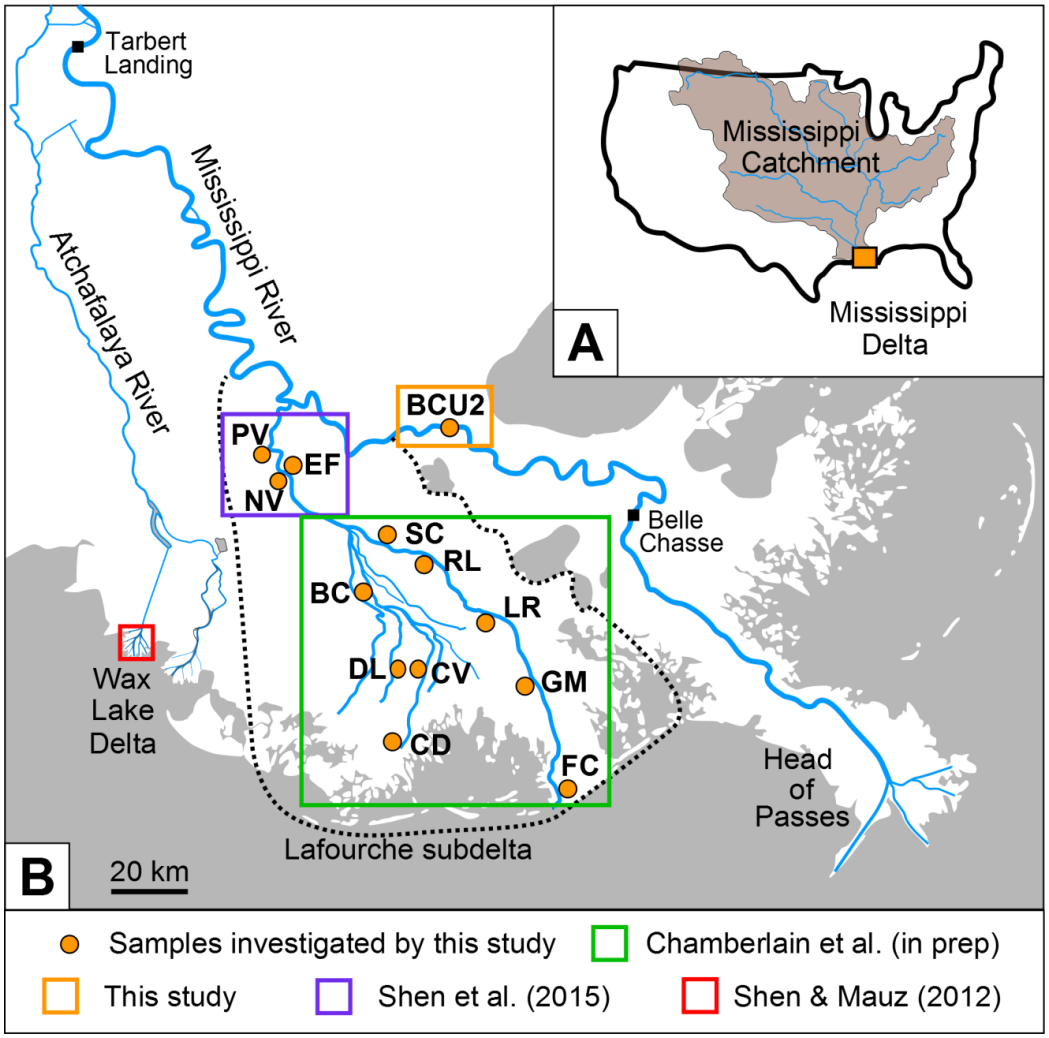

Figure 4.1. *The Mississippi Delta and catchment (A), and locations of modern Mississippi River and Lafourche subdelta samples used for this study and their primary references, plus the locations of previous research in the Wax Lake Delta and of river gauge stations (B).*

The hydrograph of the Mississippi River is generally highest in the spring due to snowmelt and increased precipitation in the catchment, and has multiple spring peaks with an average discharge of 25,000 m^3/s or more (Appendix C, Fig. A.C.1) (Galler and Allison, 2008). The first springtime "freshet" serves to mobilize and flush sediment from

the lower reaches of the Mississippi River channel that has accumulated during preceding autumn-time low flow (less than 8500 m^3/s) conditions (Galler and Allison, 2008). Historical discharge records (1964-2012) for the US Army Corps of Engineers gauge at Tarbert Landing (river km 492 above the polyfurcation of the modern river at Head of Passes) (Fig. 4.1) show that cumulative annual discharge is highly variable between years, and can range from around 3×10^{11} m^3/yr to greater than 6×10^{11} m^3/yr (Allison et al., 2014). Mud is the primary material transported in suspension during low flow conditions in the lower reach of the river, and is generally evenly distributed throughout the water column at all discharges (Ramirez and Allison, 2013). The mass of suspended sand in the lower reach, thought to be mobilized from lateral bars on the river bed, is minimal during low flow events and becomes similar to that of fines during the highest flow events (Allison et al., 2014). This indicates that there is a seasonal opportunity for light exposure of sands, and a year-round opportunity for light exposure of silts entrained within the river channel.

In addition to being a major river with significant variance driven by natural sources, the Mississippi is one of the most highly engineered river systems in the world (Kesel, 2003; Allison et al., 2012). Flow within the Lower Mississippi River is generally contained due to human-made levees, which limit the degree of interaction of the modern channel with its floodplain by containing annual floodwaters within the engineered floodplain, and decrease the cannibalization of banks by restricting river migration (Kesel, 2003). The construction of dams and flood and navigation control structures in the catchment has reduced the suspended sediment load reaching the delta by reported values of 50-70 %, although the effects of these structures on sand transport to and within

the deltaic reach has been debated (Blum and Roberts, 2014; Nittrouer and Viparelli, 2014). Similar changes in hydrology and sediment transport due to engineering have been documented in other river-delta systems (e.g., Erkens, 2009; Hobo, 2015). The hydrology and related luminescence bleaching opportunities of grains in the Mississippi River and other major channels worldwide may have been quite different prior to human modification of rivers.

4.1.2 Mississippi Delta sedimentology and luminescence characteristics

The Holocene Mississippi Delta first emerged around 7 ka, as sediment delivery to the basin outpaced regional sea-level rise (Törnqvist et al., 2004), and is comprised of a series of stacked sediment lobes (subdeltas) fed by discrete distributary networks (Fisk, 1944). This study investigates deposits of the Lafourche subdelta (Fig. 4.1) that was active from 1.6 to 0.6 ka (Törnqvist et al., 1996; Shen et al., 2015). The Lafourche subdelta was co-active with the Modern (Balize) subdelta for the latter portion of Lafourche activity. Modern (Balize) subdelta initiation has been constrained to 1.4-1.0 ka (Hijma et al., 2017), although the exact timing and nature of the discharge split is not well-known.

Previous research has shown that Mississippi River and Delta deposits contain suitable quartz for luminescence dating (Rittenour et al., 2005; Shen and Mauz, 2012). The Lafourche subdelta in particular has been extensively luminescence dated for geologic research (Shen et al., 2015; Chapter 2). These studies mainly relied on the measurement of small-diameter aliquots of quartz sand in combination with the application of minimum age models (Galbraith et al., 1999; Cunningham and Wallinga,

2012) to extract paleodoses, because equivalent dose (D_e) distributions indicated that at least some of the fluvial deposits in this setting were not completely bleached. Incomplete bleaching of Mississippi Delta grains was also suggested by Shen and Mauz (2012). They found that the subtraction of an early background interval (Cunningham and Wallinga, 2010) produced more accurate and younger luminescence ages for contemporary deposits associated with the nascent Wax Lake Delta of the Mississippi Delta. Results were validated by an independent chronology from historical records.

With regard to the Lafourche subdelta, Shen et al. (2015) employed late background subtraction for dating overbank sands and silts. They showed that late-background-subtracted luminescence ages for paired silt and sand fractions extracted from the same overbank samples agreed within 2σ, indicating that silt was sufficiently reset in this depositional environment for accurate dating of these centennial- to millennial-aged deposits.

So far, the bleaching of the luminescence signals of sediments within the modern river channel has not been investigated, and a comprehensive assessment of the degree of bleaching of the luminescence signal of Mississippi Delta deposits by depositional environments, grain size, and transport mode has not yet been conducted. The present study aims to begin filling this niche, thereby guiding luminescence sample selection and measurement approaches in the Mississippi Delta and potentially other megadeltas.

4.2 Methods

4.2.1 Sample selection

Modern Mississippi River bedload and suspended load sediments were sampled at Bonnet Carre Upstream 2 (BCU2), a site 221 river kilometers above the Mississippi

River mouth at Head of Passes (Fig. 4.1). This site corresponds to the AboveBC2 site in Allison et al. (2013). Sampling took place in the Mississippi River channel center during high-flow conditions of 18,320 m^3/s on May 5th, 2014, when the channel depth at BCU2 was 21.9 m. A 5 L Niskin bottle was used to capture suspended sediment samples (n=5) at 0% (0 m), 25% (5.5 m), 50% (11.0 m), 75% (16.4 m), and 90% (19.7 m) water depths and a grab sampler was used to obtain bedload sediment (n=1). Care was taken not to expose the samples to light.

To investigate bleaching of older sediments, we revisited samples of late Holocene Mississippi Delta deposits previously collected and measured for geological research. These Lafourche subdelta channel-proximal mouth-bar (n=17, BC, CD, CV, DL, FC, GM, LR, RL, and SC localities, see Chapter 2) and overbank (n=23, EF, NV, and PV localities, Shen et al., 2015) (Fig. 4.1) deposits were captured with a Van der Horst sampler, which extracted 30 cm-long by 5 cm-diameter cores in a rigid plastic liner within a light-proof stainless steel cylinder.

4.2.2 Sample preparation and measurement

Samples were prepared under amber light conditions at Tulane University, USA, to isolate quartz sand and silt fractions of known grain sizes. Preparation followed standard procedures described in Mauz et al. (2002). These included wet sieving of sand and settling-velocity separation of silt, chemical treatment with 30% H_2O_2 and 10% HCl, and density separation of minerals at 2.62 and 2.73 g/cm^3. The grain size used for dating purposes was guided by the available sediments, using the coarsest grains possible. Mouth-bar deposits were typically coarser and so these were most often dated using 125-

180 μm sands, although 75-125 μm grains were also used at some localities (see Chapter 2). Overbank deposits were typically dated using finer sand fractions that included grains less than 125 μm (Shen et al., 2015). Etching of all sand and of the silt isolated from overbank deposits was performed at the University of Liverpool, UK, using hydrofluoric acid as described by Mauz and Lang (2004). The modern river silt was etched with 20% hydrofluoric acid for only 10 minutes, shorter than the standard etching time, because sediment was scarce.

Luminescence measurements of all samples were performed at the University of Liverpool on a Risø TL/OSL DA- 15 B/C reader (Bøtter-Jensen et al., 2003). Luminescence signals were detected through a 7.5 mm Hoya U340 filter. Sand aliquots were prepared on stainless steel disks, with hand-painted 1-2 mm sized aliquots. These were estimated to have an average diameter of 1.2 mm because the target diameter was 1 mm, but this was difficult to achieve given the painting tools. Silt was suspended in acetone and pipetted onto aluminum disks to produce 10 mm diameter aliquots containing 1-2 mg of sediment per aliquot.

4.2.3 Equivalent dose estimation

Equivalent doses (D_es) of aliquots were extracted through the single-aliquot regenerative-dose (SAR) protocol (Murray and Wintle, 2000, 2003) with recuperation and recycling checks including infrared (IR) depletion of the OSL signal (Duller, 2003) (Table 4.1). All sand and late Holocene silt were measured with 3-4 regenerative points, while modern river silt was measured with a simplified SAR protocol using one regenerative point (Ballarini et al., 2007). Luminescence measurements were made at 125

°C for 40 s over 250 channels. Luminescence signals were integrated over the first 0.48 s and an early background interval, integrated over 0.48-1.76 s, was subtracted (Cunningham and Wallinga, 2010). Acceptance thresholds for aliquots were recycling and OSL IR depletion ratios with 10% unity (Duller, 2003), a maximum test dose error of 20%, and recuperation of <5% relative to the highest regenerative signal. Age model inputs and usage are described below (see below, "Calculating overdispersion of Mississippi Delta sand", and "Calculating residual doses").

We had to reconcile differences in luminescence approaches across samples because this project utilized archival data (Appendix C, Table A.C.2). To avoid systematic biases associated with the application of different methods to different sets of samples, we reanalyzed all archival data repurposed from Shen et al. (2015) and from Chapter 2 using the methods described above. As such, D_es presented in this study differ somewhat from those presented in the original sources.

4.2.4 Overdispersion of Mississippi Delta sand

Following the extraction of D_es from aliquots, age modeling is often applied to a D_e dataset to extract a "paleodose", the best estimate of the average radiation dose received by quartz sand grains within the sample since burial. Accurate paleodose estimation of heterogeneously-bleached sand requires knowledge of the degree of scatter of D_es (overdispersion) arising from non-bleaching sources such as beta dose heterogeneity (e.g., Mayya et al., 2006) and measurement reproducibility (Thomsen et al., 2005). An estimate of the overdispersion of well-bleached material is needed for input to the sigma_b parameter (assumed overdispersion) of minimum age models. In addition to machine reproducibility and environmental factors such as dosing, overdispersion is

Table 4.1. *SAR protocol.*

Step	1	2	3	4	5	6
Treatment	Dose	Pre-heat	OSL	Test dose	Cutheat	OSL
Lafourche mouth-bar sand	Natural, 3-4 regenerative doses (2.5 to 15 Gy)*, recuperation (0 Gy), recycling (2.5 to 5 Gy)*, recycling (2.5 to 5 Gy)*	200 or 220 °C for 10 s*	125 °C for 40 s	4 to 5 Gy^	180 °C for 0 s	125 °C for 40 s
Lafourche overbank silt	Natural, 3-4 regenerative doses (1.5 to 7 Gy)*, recuperation (l0 Gy), recycling (lowest regeneration dose Gy)*, recycling (lowest regeneration dose Gy)*	200 or 220 °C for 10 s*	125 °C for 40 s	3-5 Gy	180 °C for 0 s	125 °C for 40 s
Lafourche overbank sand	Natural, 3-4 regenerative doses (2-15 Gy)*, recuperation (0 Gy), recycling (lowest regeneration dose, Gy)*, recycling (lowest regeneration dose, Gy)*	200 or 220 °C for 10 s*	125 °C for 40 s	3-5 Gy	180 °C for 0 s	125 °C for 40 s
Mississippi River suspended load fine silt	Natural, 1 regenerative doses (3 Gy), recuperation (0 Gy), recycling (3 Gy), recycling (3 Gy)	180 °C for 10 s	125 °C for 40 s	3 Gy	160 °C for 0 s	125 °C for 40 s
Mississippi River suspended load coarse silt	Natural, 1 regenerative doses (2.4 or 4 Gy)*, recuperation (0 Gy), recycling (4 Gy), recycling (4 Gy)	180 °C for 10 s	125 °C for 40 s	4 Gy	160 °C for 0 s	125 °C for 40 s
Mississippi River bedload sand	Natural, 3-4 regenerative doses (2.4 to 25 Gy)*, recuperation (0 Gy), recycling (4.8 or 6 Gy)^, recycling (4.8 or Gy)^	200 °C for 10 s	125 °C for 40 s	4 or 5 Gy^	180 °C for 0 s	125 °C for 40 s

*parameters were not standardized across samples, and so a range of values are provided

^ measured on two different machines providing different dose rates

sensitive to the number of grains measured per disk and the proportion of grains that produce a signal (Cunningham et al., 2011). The number of grains measured per disk is a function of the grain size and aliquot diameter. The proportion of luminescent grains can vary by setting and has been reported to range from less than 1 to 5% (Duller, 2008; Harrison et al., 2008).

Mississippi Delta sediment is ideal for developing and testing new methods for quantifying overdispersion because quartz is suitable here for luminescence dating and there is a large archive of luminescence ages constrained by radiocarbon and historical chronologies (e.g., Shen and Mauz, 2012; Shen et al., 2015; Chapter 2) that can be used to inform selection of the assumed overdispersion parameter (sigma_b). Shen et al. (2015) used a sigma_b value of 10% for 1-2 mm diameter aliquots of quartz sand of variable grain sizes (48-108 grains per disk) based on the observation that this value was characteristic of the overdispersion of D_es for samples they identified as well-bleached. Chapter 2 of this dissertation presented sigma_b values of 1-2 mm diameter aliquots of 75-125 μm (108 grains, overdispersion = 11 ± 2%) and 125-180 μm (46 grains, overdispersion = 11 ± 4%) aliquots of quartz sand calculated with a new method. These sigma_b values were obtained by first determining the overdispersion of D_es for each sample with the central age model (CAM) (Galbraith et al., 1999). Overdispersion and the uncertainty were then grouped by grain size and input to the bootstrap (Cunningham and Wallinga, 2012) minimum age model (bootMAM) (Galbraith et al., 1999) to select the sigma_b characteristic of the best-bleached sediment within each grain size group.

Our study builds on the sigma_b estimation technique presented used in Chapter 2. Sand samples were grouped by grain size range (75-125, 75-180, 90-180, 100-200, 125-180, or 180-250 μm). Values for overdispersion, quantified with CAM following a 4 standard deviation cleaning of the aliquots to remove the most anomalous outliers, were input to bootMAM to estimate sigma_b for each grain size range (Appendix C, Table A.C.3). We refer to these values as "calculated sigma_b".

For this approach to be effective, each group must contain a sufficient number of samples that are completely bleached (that is, they only contain well-bleached grains) for reliable statistics as well as enough samples to run bootMAM. The 90-180 μm (n=4) and 100-200 μm (n=2) groups did not have enough samples for bootMAM to run, and so we do not present calculated sigma_b values for these two groups. If effective, a trend of increasing calculated sigma_b with grain size would be expected because 1) coarser sediment is more likely than finer sediment of the same potassium content to have radiation "hotspots" separated by distances exceeding the travel range of ^{40}K beta particles (e.g., Mayya et al., 2006) due to the larger grain size and therefore higher matrix heterogeneity over a given distance, and 2) there is less averaging of signals during luminescence measurements of coarser sediment because there are fewer grains per constant-diameter aliquot (Duller, 2008). While most calculated sigma_b values met the expected range (~10-11%) within their uncertainties, we did not see the anticipated trend in calculated sigma_b with grain size (Table 4.2). Rather, calculated sigma_b appeared directly tied to the number of samples per grain size group (Appendix C, Fig. A.C.2), indicating that there were not a sufficient number of completely-bleached samples for at least some groups.

To overcome this challenge, we selected a single calculated sigma_b for one grain size group and modeled sigma_b values of the other grain size groups from this benchmark by applying procedures outlined in Cunningham et al. (2011). We refer to these modeled values as "adapted sigma_b". This approach assumed that the overdispersion of well-bleached sand measured as single grains is 20% (Duller, 2008; Arnold and Roberts, 2009) and decreases in a predictable fashion with increasing numbers of grains per aliquot (Cunningham et al., 2011). The 125-180 μm group (calculated sigma_b = 10.6 ± 3.4%) was selected as the benchmark because this collection had the greatest number of samples and was therefore most likely to have captured the overdispersion of well-bleached samples. The adapted sigma_b values (Fig. 4.2, Table 4.2) were input to bootMAM for residual dose estimation.

4.2.5 Calculating residual doses

Modern sediments that are sufficiently reset in transit should yield zero D_es, and so, any residual dose on these sediments can be easily identified as positive D_es (e.g., Murray et al., 1995; Stokes et al., 2001). As such, residual doses of the modern river bedload and suspended load samples (BCU2 I-1, I-2, I-3, I-4, I-5, and I-6) were defined as the weighted mean values of D_es obtained using the unlogged central age model (CAMul) (Arnold et al., 2009) for sands and a mean and standard error for silts. Doses of sand samples were also calculated using the bootstrap unlogged minimum age model (bootMAMul), to test how well an accurate paleodose may be isolated from these grains. The unlogged versions of the age models (Arnold et al., 2009) were necessarily for these modern samples because some aliquots produced near-zero or negative D_es.

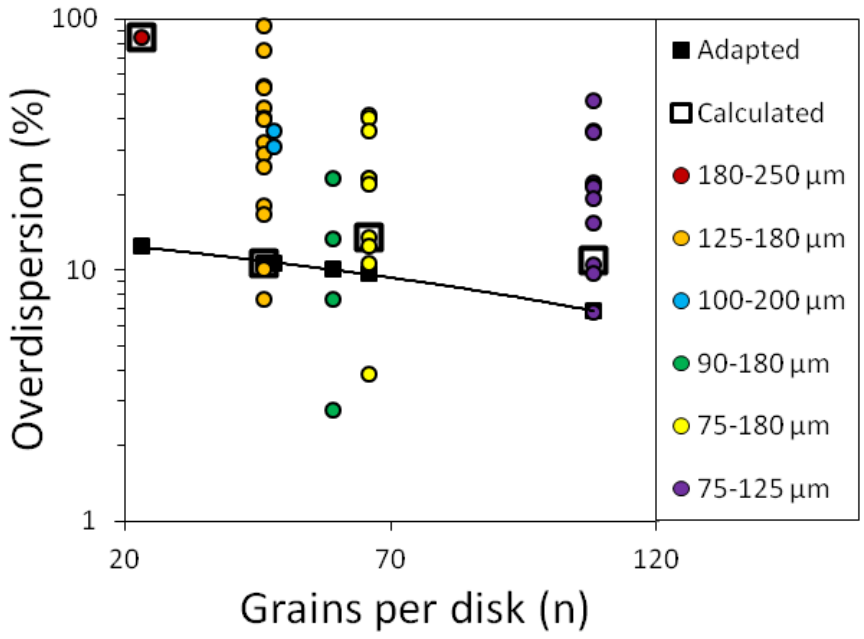

Fig. 4.2. *Values for overdispersion of each sample obtained with CAM (filled circles), and values for calculated sigma_b (open squares), and adapted sigma_b (filled squares) of each grain size group.*

Table 4.2. *Selection of sigma_b values for overdispersion. Bold values were ultimately used for input to the bootstrap minimum age model for residual dose estimation.*

Grain size grouping (µm)	**samples (n)**	**Calculated average grains per disk (n)**	**Calculated sigma_b (%)**	**Adapted sigma_b (%)**
125-180	14	46	10.6 ± 3.4	**10.6 ± 3.4**
75-125	11	108	11.0 ± 2.3	**6.9 ± 2.2**
75-180	10	66	13.5 ± 3.2	**9.7 ± 3.1**
90-180	4	59	n/a	**10.1 ± 3.2**
100-200	2	48	n/a	**10.6 ± 3.4**
180-250	1	23	84.9 ± 11.6	**12.5 ± 4.0**

Estimating residual doses of sedimentary deposits without independent chronology is less straightforward. Such assessments have often relied on dose

distributions obtained from measurements of small-diameter aliquots (e.g., Olley et al., 1998). However, those can be highly influenced by grain size (i.e., the number of grains per aliquot) and require knowledge of the overdispersion arising from non-bleaching sources (Mayya et al., 2006) that is not well-developed in many localities. Additionally, D_e distributions act as a sort of pass/fail test for bleaching; high scatter can indicate bleaching heterogeneity but does not quantify exactly how this heterogeneity may affect the OSL age estimate of the sample. Other approaches to checking bleaching include analyzing the form of the optical decay curve (e.g., Singhvi and Lang, 1998; Bailey, 2000; Shen and Lang, 2016), comparing different luminescence signals measured for the same sample (e.g., Roberts et al., 1994) and, more recently, multiple-signal comparisons of polymineral sediment (Reimann et al., 2015; Chapter 5). For this project, residual doses of quartz sand isolated from Lafourche overbank (EF, NV, and PV samples) and mouth-bar deposits (BC, CD, CV, DL, FC, GM, LR, RL, and SC samples) were estimated as the differences between a central D_e value determined by the central age model ($D_{e,CAM}$) and paleodose estimate obtained from the bootstrap minimum age model ($D_{e,bootMAM}$) following a 3 standard deviation cleaning of D_e datasets (see Chapter 2), so that:

$$4.1.\ \text{Residual dose} = D_{e,CAM} - D_{e,bootMAM}$$

This approach to quantify residual dose assumes that the minimum age model has successfully estimated the burial dose (by isolating the D_es of the well-bleached grains within the sample), an assumption that is supported by the stratigraphic correctness of sand ages for these samples demonstrated by Shen et al. (2015) and in Chapter 2, and by prior radiocarbon dating of underlying peat that provide an upper age limit of 1.6 ka for

Lafourche deposits (Törnqvist et al., 1996). Sand was classified as well-bleached if the residual dose minus uncertainty was equal to or less than zero. This means that some samples considered to be well-bleached may have possessed small residual doses.

Checking for residual doses retained by silt in the absence of independent age control is also not straightforward, because the high degree of averaging of luminescence signals produced by the measurement of up to 1 million grains per aliquot (Duller, 2008) renders dose distributions and statistical approaches largely ineffective in most settings (Wallinga, 2002a). For this study, bleaching of late Holocene silt was checked by comparing silt burial ages estimated with CAM to sand burial ages estimated with bootMAM, for paired sand-silt fractions extracted from the same samples (PV I-4, PV I-5, NV II-3, NV VIII-1, NV X-1, EF II-2, EF II-3, Shen et al., 2015), using the D_es obtained for this study with early background subtraction.

4.2.6 Dose rate and residual age estimation

Remnant doses preserved in grains upon burial have little direct relationship with the dose rate of the matrix from which the grains are ultimately isolated for luminescence dating, although the dose rate of this matrix is used to determine residual age. The bulk sediment characteristics and geological context (e.g., cosmogenic exposure, water content, radionuclide activities) under which the residual doses were acquired are generally unknown. For this reason, we primarily used residual dose rather than residual age to describe the bleaching of sediments. Approximations of residual age are also discussed. These were informed by average dose rates of 2.43 ± 0.06 Gy/ka calculated from 40 reported dose rates of sands and 2.96 ± 0.05 Gy/ka calculated from 22 reported

dose rates of silt sampled within the Lafourche subdelta (Shen et al., 2015; Chapter 2) and an average of 2.06 ± 0.05 Gy/ka for Lower Mississippi River Valley sand calculated from 69 reported dose rates of Pleistocene-aged fluvial deposits (Rittenour et al., 2005). Details of these dose rates are given in the original publications. Here, we assumed that sand experienced dosing prior to deposition at a rate of 2.25 ± 0.52 Gy/ka, calculated as the average ± 2 standard deviations of rates reported for Lafourche subdelta and Lower Mississippi River Valley deposits. We assumed a dose rate of 2.96 ± 0.70 Gy/ka for silt, using the average rate reported for Lafourche subdelta silts and applying 24% relative uncertainty, matching the relative uncertainty assigned to modern sand dose rates for this study. Ages calculated for the comparison of sand and silt fractions isolated from the same sample used dose rates particular to those samples, presented in Shen et al. (2015) and updated here to use the radionuclide conversion factors of Guérin et al. (2011).

4.3 Results and interpretation

4.3.1 Residual doses of modern river sediments

Residual doses of all samples are provided in Table 4.3. Modern river sediments show a trend of increasing residual dose with both grain size and channel depth (Fig. 4.3). We found that residual doses of modern river silt, moving in suspension within the channel, are very low regardless of water depth. These ranged from 0.027 to 0.135 Gy for the 4-20 μm grains, with a mean value of 0.078 ± 0.044 Gy. This corresponds to an estimated residual age of 10-42 years.

Table 4.3. *Minimum doses ($D_{e,bootMAM}$), central doses ($De,_{CAM}$), and residual doses for modern river sediments and sands isolated from sedimentary deposits, with (n) accepted aliquots ("al."), calculated following a 3 standard deviation cleaning.*

Sample name	Grain size (µm)	Al. (n)	$D_{e,bootMAM}$ (Gy)	$D_{e,CAM}$ (Gy)	Residual dose (Gy)	Minimum residual dose (Gy)
Modern river suspended load						
BCU2 I-1	4-20	4	----------	0.027 ± 0.001[a]	0.027 ± 0.001	0.026
BCU2 I-2	4-20	2	----------	0.088 ± 0.031[a]	0.088 ± 0.031	0.057
BCU2 I-3	4-20	3	----------	0.040 ± 0.014[a]	0.040 ± 0.014	0.026
BCU2 I-4	4-20	2	----------	0.100 ± 0.022[a]	0.100 ± 0.022	0.078
BCU2 I-5	4-20	2	----------	0.135 ± 0.013[a]	0.135 ± 0.013	0.122
BCU2 I-3	45-75	---	----------	did not produce a measurable signal		
BCU2 I-5	45-75	4	----------	0.227 ± 0.149[a]	0.227 ± 0.149	0.078
Modern river bedload						
BCU2 I-6	125-180	36	0.027 ± 0.051[b]	1.617 ± 0.288[b]	1.617 ± 0.288	1.329
BCU2 I-6	180-250	30	0.791 ± 0.534[b]	10.507 ± 1.673[b]	10.507 ± 1.673	8.834
Lafourche mouth-bar deposits						
GM I-2	75-125	64	1.992 ± 0.082	2.119 ± 0.060	0.127 ± 0.104	0.023
BC I-1	75-125	68	2.936 ± 0.291	3.866 ± 0.158	0.930 ± 0.338	0.592
CV I-1	75-125	84	2.686 ± 0.124	2.810 ± 0.036	0.124 ± 0.132	-0.008
CV II-1	75-125	82	2.525 ± 0.096	2.663 ± 0.034	0.138 ± 0.104	0.034
RL I-1	125-180	54	2.794 ± 0.225	4.357 ± 0.245	1.563 ± 0.339	1.224
RL I-2	125-180	58	2.897 ± 0.246	4.029 ± 0.212	1.132 ± 0.331	0.801
FC I-2	125-180	29	1.386 ± 0.101	1.466 ± 0.053	0.080 ± 0.116	-0.036
FC I-1	125-180	48	1.084 ± 0.214	1.415 ± 0.078	0.331 ± 0.232	0.099
GM I-1	125-180	40	2.000 ± 0.092	2.242 ± 0.104	0.242 ± 0.142	0.100
LR I-1	125-180	54	2.548 ± 0.121	3.534 ± 0.185	0.986 ± 0.225	0.761
LR I-2	125-180	47	2.697 ± 0.290	5.879 ± 0.555	3.182 ± 0.639	2.543
SC I-1	125-180	30	3.408 ± 0.241	5.142 ± 0.441	1.734 ± 0.513	1.221
BC I-2	125-180	53	3.320 ± 0.164	4.067 ± 0.137	0.747 ± 0.218	0.529
CD I-2	125-180	59	2.044 ± 0.066	2.091 ± 0.042	0.047 ± 0.080	-0.033
CD I-1	125-180	71	1.808 ± 0.126	2.018 ± 0.043	0.210 ± 0.135	0.075
DL I-2	125-180	69	2.337 ± 0.064	2.355 ± 0.032	0.019 ± 0.073	-0.054
DL I-1	125-180	72	2.371 ± 0.093	2.420 ± 0.034	0.049 ± 0.101	-0.052

Table 4.3.*Continued.*

Lafourche overbank deposits						
EF II-2	75-125	11	2.759 ± 0.140	2.729 ± 0.213	-0.030 ± 0.260	-0.290
EF II-3	75-125	25	3.222 ± 0.115	3.279 ± 0.082	0.057 ± 0.144	-0.087
NV II-4a	75-125	37	2.545 ± 0.155	2.821 ± 0.129	0.276 ± 0.205	0.071
NV X-3	75-125	27	3.640 ± 0.146	4.800 ± 0.338	1.160 ± 0.376	0.784
EF II-1	75-125	13	1.913 ± 0.227	1.979 ± 0.118	0.065 ± 0.261	-0.196
EF II-6	75-125	34	2.807 ± 0.077	2.815 ± 0.067	0.009 ± 0.104	-0.095
EF III-1a	75-125	51	2.579 ± 0.234	3.656 ± 0.158	1.076 ± 0.288	0.788
NV II-2	90-180	51	2.746 ± 0.109	2.794 ± 0.071	0.048 ± 0.133	-0.085
NV II-3	90-180	50	2.626 ± 0.079	2.642 ± 0.067	0.016 ± 0.105	-0.089
PV I-7	90-180	34	2.310 ± 0.048	2.321 ± 0.049	0.011 ± 0.070	-0.059
PV I-8	90-180	31	3.406 ± 0.197	5.020 ± 0.356	1.614 ± 0.415	1.199
NV VIII-1	75-180	51	1.897 ± 0.068	1.967 ± 0.054	0.070 ± 0.089	-0.019
NV X-1	75-180	53	3.821 ± 0.185	4.230 ± 0.140	0.478 ± 0.237	0.241
NV III-1	75-180	47	1.689 ± 0.127	1.912 ± 0.066	0.223 ± 0.145	0.078
NV III-3	75-180	56	2.678 ± 0.057	2.684 ± 0.047	0.006 ± 0.075	-0.069
NV IV-1	75-180	31	1.780 ± 0.214	2.110 ± 0.101	0.330 ± 0.241	0.089
NV-IV-2	75-180	61	2.044 ± 0.112	2.126 ± 0.044	0.082 ± 0.123	-0.041
NV V-1	75-180	44	2.392 ± 0.152	3.063 ± 0.141	0.671 ± 0.212	0.459
NV V-2	75-180	42	2.389 ± 0.090	2.893 ± 0.112	0.504 ± 0.146	0.358
NV VII-1	75-180	49	2.230 ± 0.082	2.282 ± 0.065	0.053 ± 0.107	-0.054
NV IX-1	75-180	68	2.381 ± 0.113	2.543 ± 0.065	0.161 ± 0.133	0.028
PV I-4	100-200	31	2.470 ± 0.249	3.145 ± 0.146	0.675 ± 0.294	0.381
PV I-5	100-200	45	2.947 ± 0.245	3.517 ± 0.120	0.570 ± 0.278	0.292

[a]Central age calculated using a mean and standard error
[b]unlogged versions of the age models were used

Only the deeper (19.7 m) sample (BCU2 I-5) of the 45-75 µm suspended silt produced a measurable quartz luminescence signal, while the shallower fraction of this sample (BCU2 I-3) was not sufficiently luminescent and will not be discussed further. The residual dose of BCU2 I-5 was 0.227 ± 0.149 Gy, suggesting that bleaching of coarser silt transported deeper in the water column may be less complete than bleaching of finer silt moving in more shallow suspension (Fig. 4.3).

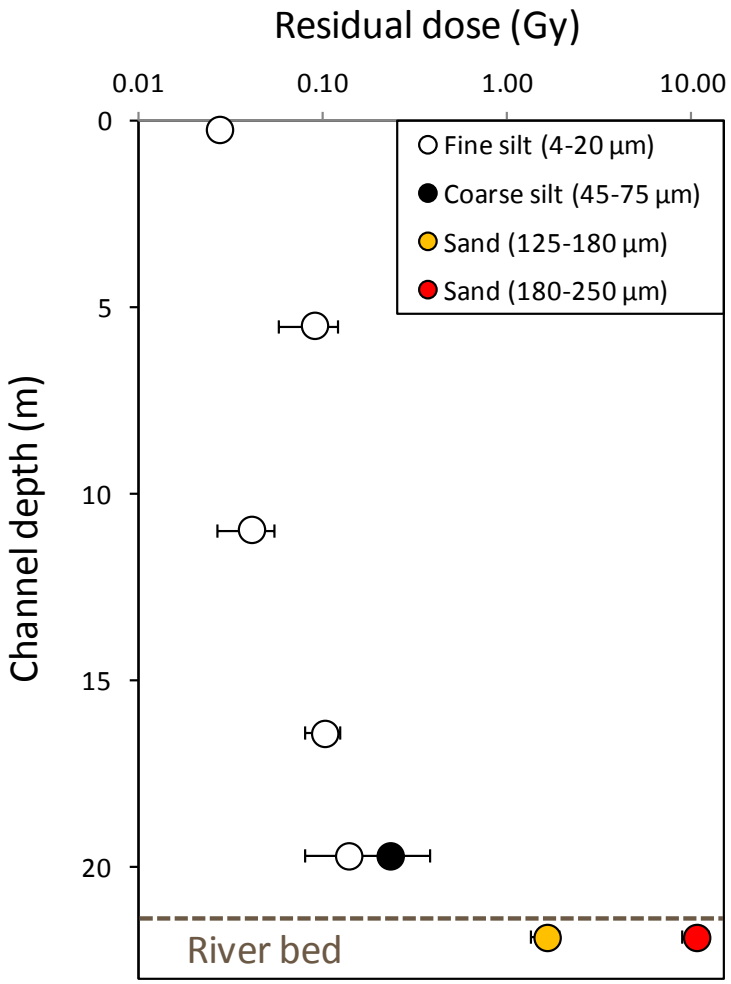

Fig. 4.3. *Residual doses of quartz sediments in transit in the modern Mississippi River sediments, with depth in the river channel*

By contrast, both grain size fractions of modern river bedload sand (BCU2 I-6) appeared to be heterogeneously- to poorly-bleached. The residual dose of the 125-180 μm fraction of BCU2 I-6 was 1.617 ± 0.288 Gy. This corresponds to a 0.51-0.93 ka estimated residual age. A bootMAMul D_e of 0.027 ± 0.051 Gy indicated that this grain size fraction contained some well-bleached quartz grains capable of producing an accurate luminescence age. The residual dose of the 180-250 μm fraction of BCU2 I-6 was 10.507 ± 1.673 Gy, corresponding to a 3.36-5.98 ka estimated residual age. A bootMAMul D_e of 0.791 ± 0.534 Gy indicated that this grain size fraction contained very few, if any, well-bleached quartz grains. We note that some aliquots provided D_e*s* of more than 20 Gy, indicating that some coarser sand grains transported by the modern Mississippi River have not been exposed to light for about 10,000 years.

4.3.2 Residual doses of late Holocene deposits

Sand isolated from mouth-bar and overbank deposits ranged from well- to heterogeneously-bleached for both depositional environments (Fig. 4.4). This was indicated by residual doses, calculated as $D_{e,CAM}$ - $D_{e,bootMAM}$, ranging from zero to greater than 3 Gy. These values correspond to residual ages estimated to be in the range of 0 - 1.5 ka. Mouth-bar deposits had a smaller proportion of well-bleached sand samples (29%), while overbank deposits contained a greater proportion of well-bleached sand samples (48%). Bleaching was more complete for samples with D_e*s* less than about 2.3 Gy. Above 2.7 Gy, mouth-bar sand was found to be heterogeneously-bleached with considerable (>0.5 Gy) residual doses, while overbank sand of similar D_es ranged from well- to heterogeneously bleached (Fig. 4.4).

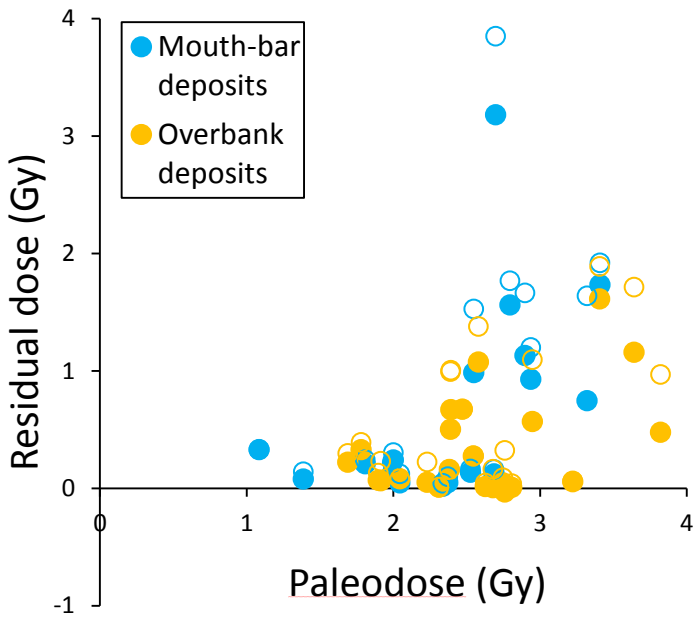

Fig.4.4. Residual doses calculated as $D_{e,CAM} - D_{e,bootMAM}$ versus the paleodose estimated as $D_{e,bootMAM}$ for mouth bar and overbank deposits of the Lafourche subdelta. Filled circles indicate doses calculated following a 3 standard deviation cleaning, while open circles indicate central doses that were not cleaned. Uncertainties, not shown here due to the high density of data points, are given in Table 4.3.

4.3.4 Bleaching by grain size

Among all samples, we observed a trend of increasing residual dose with increasing median grain size (Fig. 4.5), suggesting that coarser sand is the least likely grain size to be completely bleached. Still, each sand grain size fractionalso contains some well-bleached samples, indicating that sand grains of all sizes had the potential for bleaching prior to preservation in mouth-bar and overbank deposits. The 180-250 μm fraction of the river bedload sample (BCU2 I-6) yielded an exceptionally high residual dose of more than 10 Gy. While results for this grain size fraction fit the observed trend of bleaching degree with grain size, they are informed by only one sample of sediment that was still in-transit in the river channel when captured and may not be representative of bleaching of these coarser grains, both moving in the channel and preserved in the stratigraphic record. For example, BCU2 I-6 180-250 μm grains may have originated

very close to the sample site (e.g., through erosion of a nearby bank or channel scour) and not have had sufficient opportunity for bleaching during fluvial transport. It is also possible that 180-250 µm sands receive additional bleaching prior to deposition and sequestration in the stratigraphic record (Jain et al., 2004). For these reasons, we caution against over-interpreting the results of BCU2 I-6, and the coarser fraction of this sample is omitted from Figure 4.5.

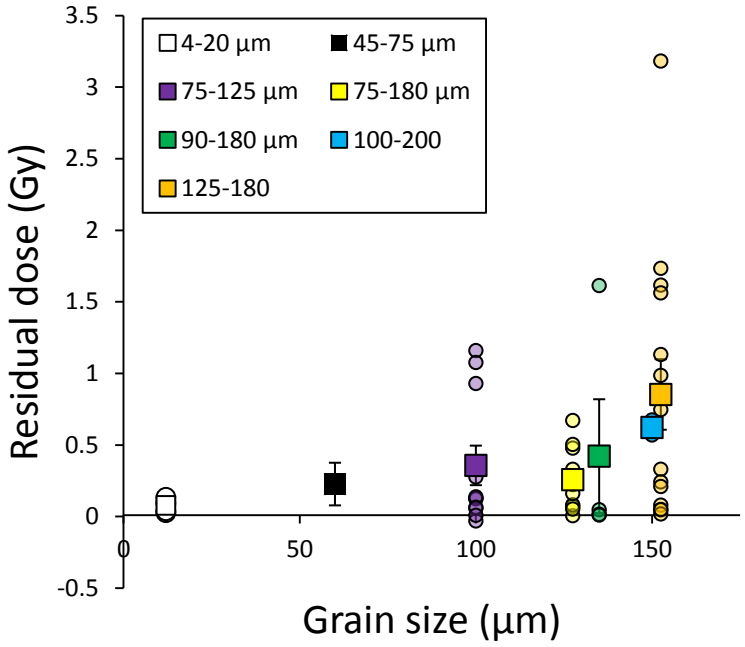

Fig. 4.5. *Mean (boxes) and individual (circles) residual doses by grain size for silt and sand samples. Data are not shown for the 180-250 µm fraction, which consisted of only one sample and would plot outside the graph.*

4.3.5 Bleaching of sand with time

Bleaching of mouth bar sand was highly time-dependent (Fig. 4.6). Prior to 1.1 ka, all mouth bar sand samples (n=7) had very high residual doses, ranging from about 1 to more than 3 Gy. Bleaching of sand isolated from mouth-bar deposits younger than 1.1 ka (n =10) was much improved, with all samples yielding residual doses less than 0.1 Gy within uncertainty. Bleaching of overbank sand showed a trend of improvement with

time, although there was significant variability of the degree of bleaching, with both well- and heterogeneously-bleached sands of all ages (Fig 4.6).

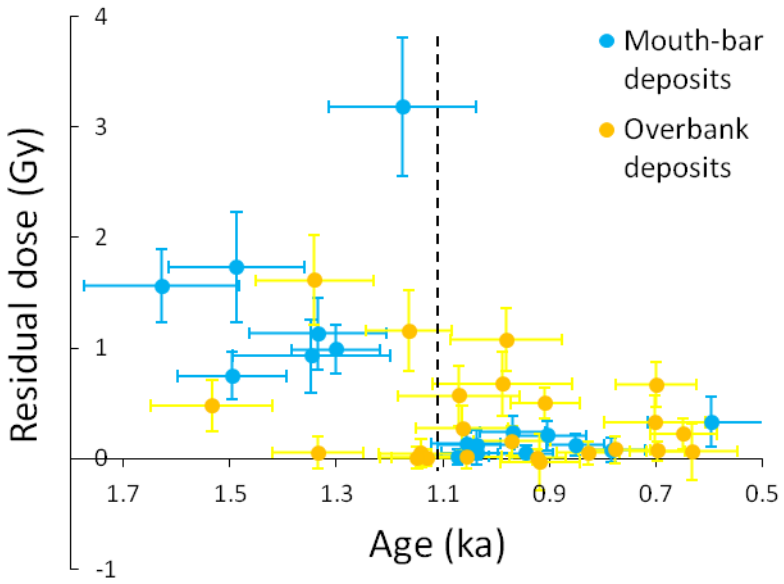

Fig. 4.6. *Bleaching with time obtained from OSL ages of sand isolated from mouth-bar and overbank deposits.*

4.3.6 Bleaching of late Holocene silt inferred from dating of sand/silt pairs

Good agreement was found between the majority (n=5) of sand and silt pairs dated from the same overbank samples (n=7) (Fig. 4.7). Silt ages scattered both higher and lower than sand ages, indicating that these silts were generally sufficiently bleached for dating. Two samples, PV I-4 and PV I-5, produced silt ages that exceed sand ages by ~ 450 and 580 years respectively. The age overestimation by silt may be due to poor quartz bleaching (Shen et al., 2012). Alternatively, there is evidence that these two samples were contaminated with feldspar, which is less readily bleached than the fast-component signal of quartz (Godfrey-Smith et al., 1988; Wallinga, 2002a). Despite strong luminescence signals, PV I-4 and PV I-5 had 20% and 17% of aliquots, respectively, rejected for poor reproducibility. One additional aliquot (5%) of PV I-4 and

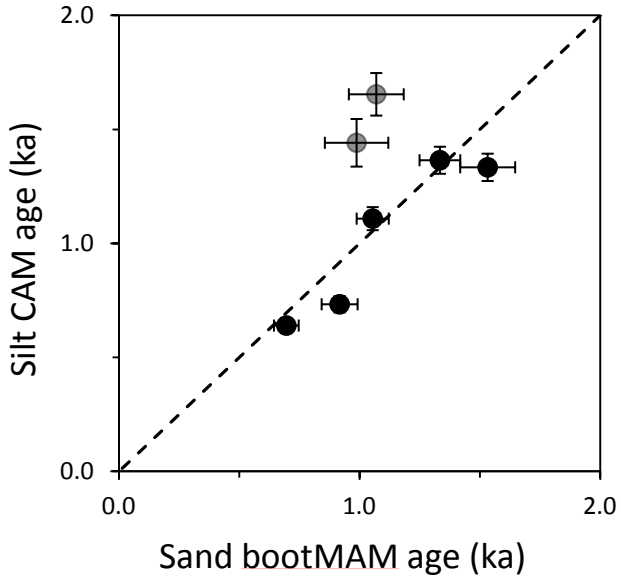

Fig. 4.7. *Comparison of ages of paired sand and silt fractions isolated from the same samples (n=7) of overbank deposits. Gray circles indicate PV I-4 and PV I-5, two samples possibly affected by feldspar contamination or containing poorly bleached silt.*

4 additional aliquots (13%) of PV I-5 were rejected for IR depletion, indicating that etching may not have been entirely effective at removing feldspars for these two samples. No aliquots of the other five samples that produced agreeing sand/silt ages were rejected for IR depletion. PV I-4 did not exhibit a suitable 110 °C TL peak; rather, the TL signal increased from 110 °C onward (Appendix C, Fig. A.C.3).

By coincidence, the samples selected for the paired sand/silt analysis featured mainly well-bleached sand, with little difference between sand ages obtained with CAM and bootMAM (Appendix C, Fig. A.C.4). It is possible that greater differences between bleaching of sand and silt could be identified if this analysis was performed on sediment pairs extracted from deposits with heterogeneously-bleached sand.

4.3.7 Overdispersion and sigma_b of Mississippi River Delta sediments

Adapted sigma_b values were generally lower than the calculated sigma_b values (Table 4.2). The adapted sigma_b values lay within the range of overdispersion

quantified with CAM for individual samples within each grain size group, with the exception of the 180-250 µm group for which there was only one sample (Fig. 4.2). This demonstrated that the adapted sigma_b values were realistically constrained by the field data.

To test whether the use of adapted sigma_b values which varied by grain size group may affect our results, we also calculated $D_{e,bootMAM}$ using a constant sigma_b value of 11 ± 3% for all sands regardless of grain size. This constant value was informed by Chapter 2 analyses. We anticipated that this would cause the greatest offset in the 75-125 µm group, because this group had the greatest difference between the adapted (6.9 ± 2.2%) and constant (11 ± 3%) sigma_b values. Surprisingly, there was little difference between the $D_{ebootMAM}$ values estimated with these two approaches for all grain size fractions (Fig. 4.8).

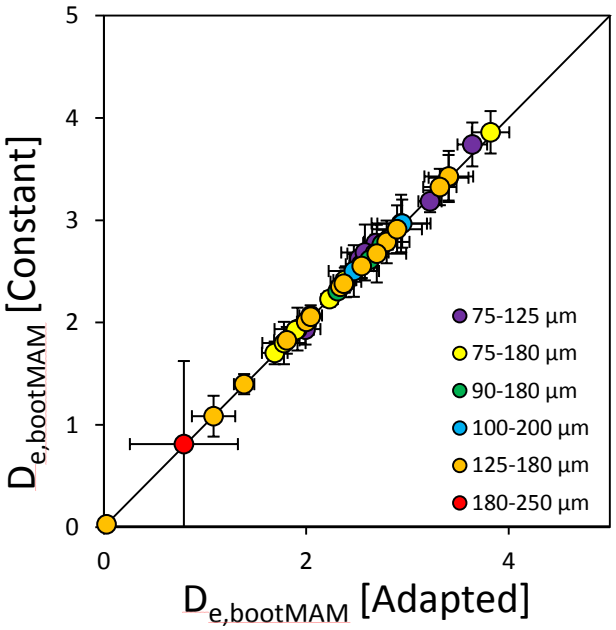

Fig.4.8. *Comparison of D_es obtained with the bootstrap minimum age model using constant sigma_b values of 11 ± 3% for all samples and adapted sigma_b values that varied with the number of grains per aliquot (i.e., grain size of the samples).*

To explore further, the effects of overdispersion on paleodose estimation via bootMAM were tested for 5 samples of 125-180 μm mouth bar sand representing various degrees of bleaching (Fig. 4.9). The tested samples and their residual doses included LR I-2 (3.182 ± 0.639 Gy), RL I-1 (1.563 ± 0.339 Gy), BC I-2 (0.747 ± 0.218 Gy), GM I-1 (0.242 ± 0.142 Gy), and CD I-2 (0.047 ± 0.080 Gy). Sigma_b values ranging from 0 to 100% were input to bootMAM at 5% intervals with a constant uncertainty of 3%. These values are referred to as "experimental sigma_b". The resulting $D_{e,bootMAM}$ values were normalized by the *paleodose* of each sample quantified with bootMAM using the calculated benchmark sigma_b value of 10.6 ± 3.4%. This produced a Dose Overestimation Ratio, defined as:

$$2.\ \text{Dose Overestimation Ratio} = \frac{D_{e,bootMAM}[Experimental]}{D_{e,bootMAM}[Adapted]}$$

This ratio describes how responsive $D_{e,\ bootMAM}$ is to forcing by sigma_b, and allowed for comparison across samples with different burial doses. The Dose Overestimation Ratio was plotted against experimental sigma_b. A high slope indicated that the paleodose could be greatly affected by the selection of the sigma_b value, while a low slope indicated that the paleodose was not very responsive to sigma_b.

We found that the paleodoses of the most heterogenously bleached samples (e.g., LR I-2, RL I-1) showed the greatest response to the sigma_b value input to bootMAM, while the paleodoses of the better bleached samples (e.g., GM I-1, CD I-2) were less affected by varying sigma_b input to bootMAM (Fig. 4.10). $D_{e,bootMAM}$ increased with the experimental sigma_b up to roughly the overdispersion of the sample identified with CAM and then plateaued, demonstrating that paleodose estimations cannot be pushed much beyond the central values constrained by the D_es of the aliquots (Fig. 4.10). The

lack of difference between paleodoses estimated with adapted and constant (11 ± 3%) sigma_b values (Fig. 4.6) is attributed to 1) similar adapted and constant sigma_b values for the coarser, more poorly bleached sands, and 2) better bleaching of the finer fractions and therefore less sensitivity to sigma_b input.

We further tested the relationship of sigma_b to $D_{e,bootMAM}$ for all samples classified as well-bleached (Fig. 4.11; Appendix C, Fig. A.C.5). Results supported that the bootMAM produced D_es similar to those obtained with CAM, regardless of sigma_b input.

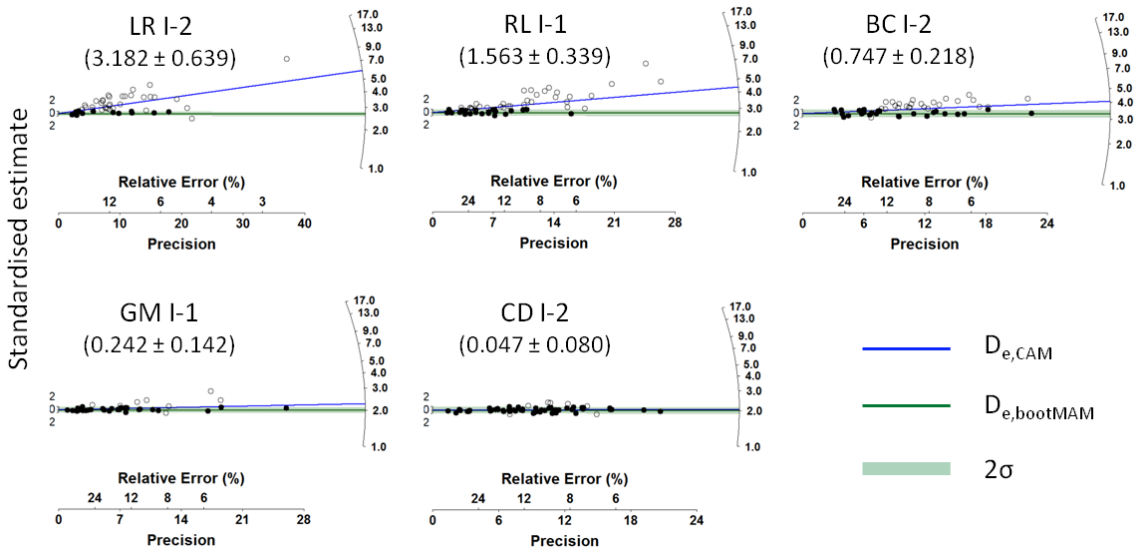

Fig. 4.9. *Radial plots showing D_es quantified with the central age model ($De_{,CAM}$) and bootstrap minimum age model ($De_{,bootMAM}$) for samples with varying degrees of bleaching. Residual doses (Gy) are listed in parentheses.*

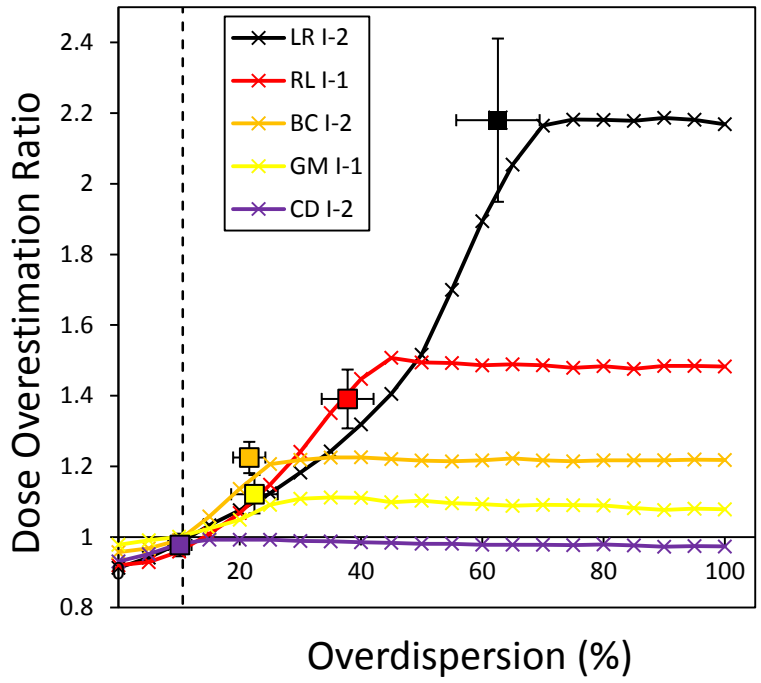

Fig. 4.10. *Dependence of paleodose on sigma_b input to bootMAM, for five samples with varying degrees of bleaching. Values for De,bootMAM obtained with the 10.6 % benchmark input for sigma_b (dashed line) lie at the intersection of the dashed line and y=1. Squares indicate values obtained using the central age model.*

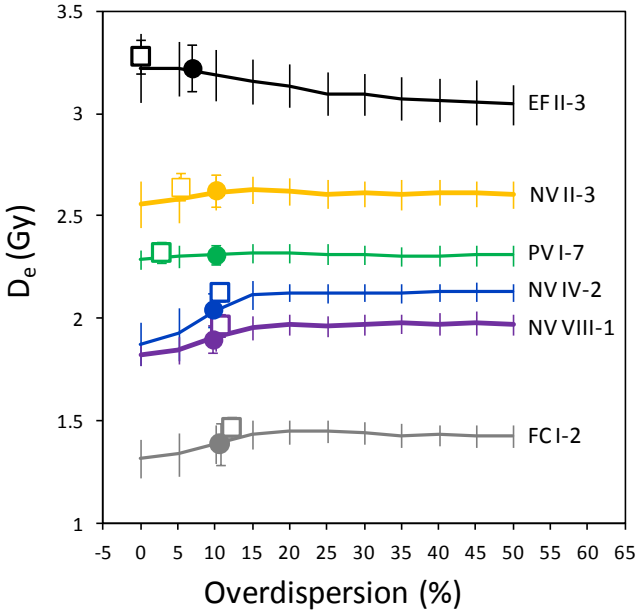

Fig. 4.11. *D_es obtained with the central age model (open boxes) and bootstrap minimum age model with the adapted sigma_b input (filled circles), plotted against D_es obtained from the bootstrap minimum age model with experimental sigma_b input (lines). Results for six examples of sediments classified as well-bleached are shown.*

4.4 Discussion

4.4.1 Controls on bleaching of fluviodeltaic sediment

This study identified lower average residual doses for finer sand grains than for coarser sand grains in transit in the deltaic reach of a large meandering river and preserved in its deltaic deposits (Fig. 4.5). Our findings are different from those of bleaching studies conducted in the Rhine Meuse Delta, The Netherlands, (Truelsen and Wallinga, 2003) and Murrumbigbee River, Australia (Olley et al., 1998), which identified better bleaching of coarser sand grains than of finer sand grains.

Fine silt, moving in suspension within the modern river channel, was found to be more completely bleached than sands moving as bedload (Fig. 4.3). This is consistent with recent studies in the Yangtze (Sugisaki et al., 2015) and Ganges-Brahmaputra (Chapter 5) river deltas, which showed that silt (in suspension, and deposited within recent decades up to a couple centuries, respectively) carried low residual doses and was therefore sufficiently bleached for accurate dating of Holocene deposits.

Bleaching of mouth-bar sand (75-125 and 125-180 μm), generally representing the coarsest material transported by a distributary system (Wright, 1977), increased coastward (Fig. 4.12). This was coincident with the formation of younger land, as the bayhead portion of the Lafourche subdelta prograded into a shallow bay (see Chapter 2). These results show that bleaching of coarse deltaic sand is highly time- and space-dependent; had our study only dated mouth-bar sand of the Lafourche delta younger than 1.1 ka (Fig. 4.6), we may have concluded that coarse grains were the best bleached fraction of sand in the Mississippi Delta.

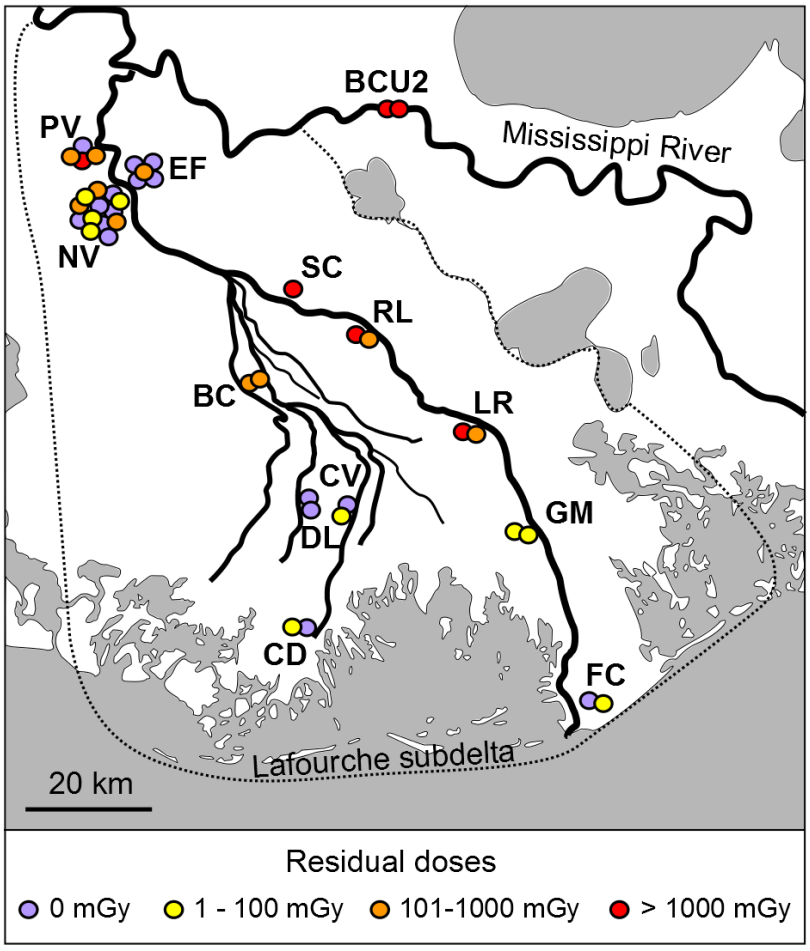

Fig. 4.12. *Geographic distribution of sands and their residual doses.*

We tentatively propose two explanations for the time-dependent bleaching of mouth-bar sand. The primary alluvial channel is known to have avulsed a number of times throughout the late Holocene (Saucier, 1994; Chapter 2), thereby occupying different pathways within the Lower Mississippi Valley, although the timing of these avulsions is not well known. It is plausible that a relatively landward avulsion (450 - 700 linear km inland, see Chapter 2) of the river circa 1.1 ka may have positioned the channel belt in such a way that it mobilized younger deposits, for example by reworking late Holocene channel-belt deposits rather than eroding Pleistocene terrace deposits. Recently-bleached sediments would require less light exposure during transit in the river

system to become well-bleached upon arrival and deposition in the delta. Alternatively, the abrupt change in bleaching of mouth-bar sand may be linked to hydrologic changes within the delta associated with the activation of the Modern (Balize) subdelta circa 1.4 - 1.0 ka (Hijma et al., 2017). For example, after 1.1 ka much of the bedload may have been rerouted toward the Modern (Balize) subdelta, causing suspended-load transport during high-flow events to be the more dominant mode of sand-delivery to the lower reaches of Lafourche. Additionally, decreased discharge in Lafourche distributaries could have allowed marine processes to play a greater role, potentially altering turbulence, turbidity, salinity, and suspension times of sediment at the mouths of Lafourche distributaries. It is also plausible that these two drivers operated in tandem; an avulsion of the alluvial channel may have driven delta-lobe switching circa 1.1 ka. There are not sufficient data at present to test these hypotheses. Bleaching of mouth-bar sand was not found to correlate to depth within the deposit (Fig. 4.13), suggesting that improved bleaching was not related to reworking of mouth bar surfaces or bioturbation, which could be expected to produce greater bleaching for shallower deposits.

Bleaching of overbank deposits was also not found to be improved at shallower depths (Fig. 4.13). Other possible trends in bleaching of overbank sand merit further testing. The degree of bleaching of overbank sand may be linked to proximity to the trunk channel or primary crevasse channels, and opportunities for bleaching during or immediately after deposition (e.g., Cunningham et al., 2011), or even to the time of year (and therefore water velocity and turbulence within the primary channel, e.g., Allison et al., 2014) that deposits formed.

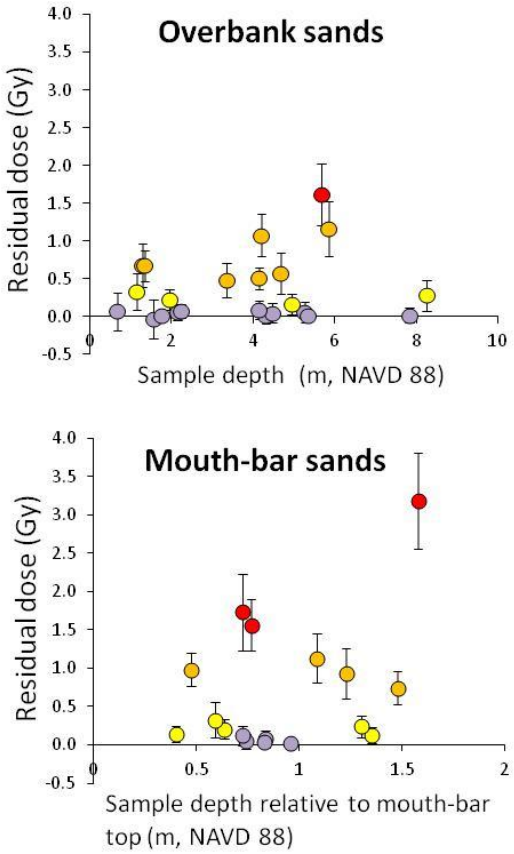

Fig. 4.13. *Bleaching of overbank and mouth-bar sands with depth. Overbank sand depths are relative to mean sea level. Mouth-bar sand depths are relative to the top of the mouth-bar deposit, which formed at roughly sea level.*

4.4.2 Age model selection

Selection of an appropriate age model is regarded as an important component of accurate luminescence dating (e.g., Galbraith et al., 1999; Olley et al., 2004; Arnold and Roberts, 2009). It has been previously suggested that the best-suited age model varies by sample based on such factors as the burial dose and degree of bleaching (Arnold and Roberts, 2009). As such conditions are often unknown, an age model decision process may be applied to guide selection toward the most likely model, however such an approach is self-admittedly "rather convoluted" (Arnold and Roberts, 2009). Generally, the use of a minimum age model has been advocated only for samples in which poor bleaching is suspected based on criteria such as the width or shape of the *De* distribution

(Olley et al., 1999; Olley et al., 2004), while the central age model is suggested for samples that are suspected to be better bleached or where wide D_e distributions may arise from non-bleaching factors such as dose heterogeneity (Galbraith et al., 1999; Olley et al., 2004).

Here, we show that similar paleodoses are obtained through both a minimum and central age model, for well-bleached young fluvial deposits of the Mississippi Delta (Figs. 4.10 & 4.11; Appendix C, Fig. A.C.5). Furthermore, paleodoses of well-bleached sand are generally not responsive to the assumed sigma_b value input to the minimum age model. Because bootMAM is shown to be appropriate for use on both well- and heterogeneously-bleached deposits, and CAM is not appropriate for heterogenously-bleached deposits, we conclude that bootMAM can be applied uniformly to all late-Holocene Mississippi Delta sand deposits. This finding significantly streamlines age model selection for this specific dataset, although we caution that further examination is needed to assess the appropriateness of bootMAM for well-bleached deposits in other settings with different luminescence characteristics, depositional ages, or dosing environments.

4.5 Applications

Modern river silt was shown to carry a residual age of at most a few decades, and silt isolated from late Holocene deposits was determined to be generally well-bleached. This suggests that accurate dating of multi-centennial-aged or older deposits is possible with Mississippi Delta fine silt. Similar conclusions on bleaching of silt have been made for the Ganges-Brahmaputra Delta (Chamberlain et al., 2017), a major delta fed by a

predominately braided-river system. While some sand isolated from of deltaic deposits was well reset, other sand carried high residual ages. This demonstrates that the use of a central age model on poorly bleached deposits may overestimate the depositional age by hundreds of years, or even by millennia. While bootMAM selected younger and likely more accurate paleodoses for heterogeneously-bleached sand, it selected the same *values* as CAM for sand that we judged as well-bleached. Further, paleodoses of well-bleached sand obtained with the bootMAM were found to be not highly affected by the value input for sigma_b. Based on these findings, we conclude that 1) silts should be considered as a viable grain size for luminescence dating in megadeltas, and 2) the bootstrap minimum age model may be used for dating sand in the Mississippi Delta and potentially other settings with similar quartz luminescence characteristics, regardless of the degree of bleaching.

4.6 Acknowledgements

We thank Mead Allison and Michael Ramirez for enabling collection of sediment from the modern Mississippi River. This manuscript was improved by comments on an earlier draft provided by Torbjörn Törnqvist and Mead Allison.

Chapter 5

Luminescence dating of delta sediments: Novel approaches explored in the Ganges-Brahmaputra-Meghna Delta

This chapter is published in *Quaternary Geochronology*.

Chamberlain, E.L., Wallinga, J., Reimann, T., Goodbred, S., Steckler, M., Shen, Z., & Sincavage, R. (2017). Luminescence dating of delta sediments: Novel approaches explored in the Ganges-Brahmaputra-Meghna Delta. *Quaternary Geochronology*, 41: 97-111. doi: 10.1016/j.quageo.2017.06.006

5.1 Abstract

Deltas where luminescence dating is most essential due to organic-poor geologic records are also those where it is often most challenging due to unsuitable luminescence properties of quartz grains, associated with rapid production of young clastic sediment. One example is the Ganges-Brahmaputra-Meghna Delta (GBMD), where Himalaya uplift drives erosion, production, and delivery to the delta plain of poorly sensitized quartz sand. Luminescence dating of fluvial deposits may be further complicated by partial bleaching prior to deposition. Here, we use GBMD quartz and polymineral sediment, including sand and silt fractions, with constrained depositional ages between a few years and a few centuries to test novel approaches to luminescence dating of fluvial deposits in an otherwise challenging setting. This produces the first delta-wide assessment of GBMD sediment luminescence dateability. We use a new multiple-signal SAR (MS-SAR) bleaching index (BI) to explore zeroing of the luminescence signals of sediment prior to

deposition and to quantify the IR, pIRIR, and TL residual doses of GBMD polymineral silt with well-reset BSL signals. This test establishes BI values that can be used to identify sufficient bleaching of Holocene sediment with unknown depositional ages, thereby improving confidence in quartz silt dating. We find that GBMD quartz sand is unsuitable for luminescence dating in most localities. By contrast, GBMD silt is sufficiently bleached and has universally suitable luminescence characteristics, enabling dating of GBMD deposits up to the Last Glacial Maximum. Our findings in the GBMD establish methodology for obtaining and validating luminescence ages for fluvial deposits in challenging settings with unsuitable quartz sand.

5.2 Introduction

The development of luminescence dating has enabled studies of fluvial and deltaic processes not previously possible with radiocarbon and other methods (Wallinga, 2002a; Rittenour, 2008). However, as luminescence dating is more widely adopted, shortcomings in its global applicability have become clear. Establishing comprehensive knowledge of the geographic limitations of luminescence dating based on the availability of suitable quartz (e.g., Preusser et al., 2006; Lukas et al., 2007; Lawson et al., 2012) and likelihood of resetting prior to deposition (Stokes et al., 2001; Olley et al., 2004; Singarayer et al., 2005; Wallinga and Bos, 2010; Shen and Mauz, 2012) is of paramount importance. Developing accurate and robust methods for those regions where coarse-grain quartz optically stimulated luminescence (OSL) dating is not feasible (e.g., Lukas et al., 2007; Madsen et al., 2011; van Gorp et al., 2013) provides a major challenge to the luminescence community.

Here, we explore the utility of luminescence dating for the Ganges-Brahmaputra-Meghna Delta (GBMD), Bangladesh (Fig. 5.1). The GBMD is the second largest and the most populated delta on the planet, with 150 million inhabitants. High population density, increasingly recurrent and severe flooding from multiple sources, and strain on infrastructure and livelihoods (Brammer, 2014) make the GBMD highly susceptible to crises associated with 21st century sea level rise acceleration (Syvitski et al., 2009). Yet,

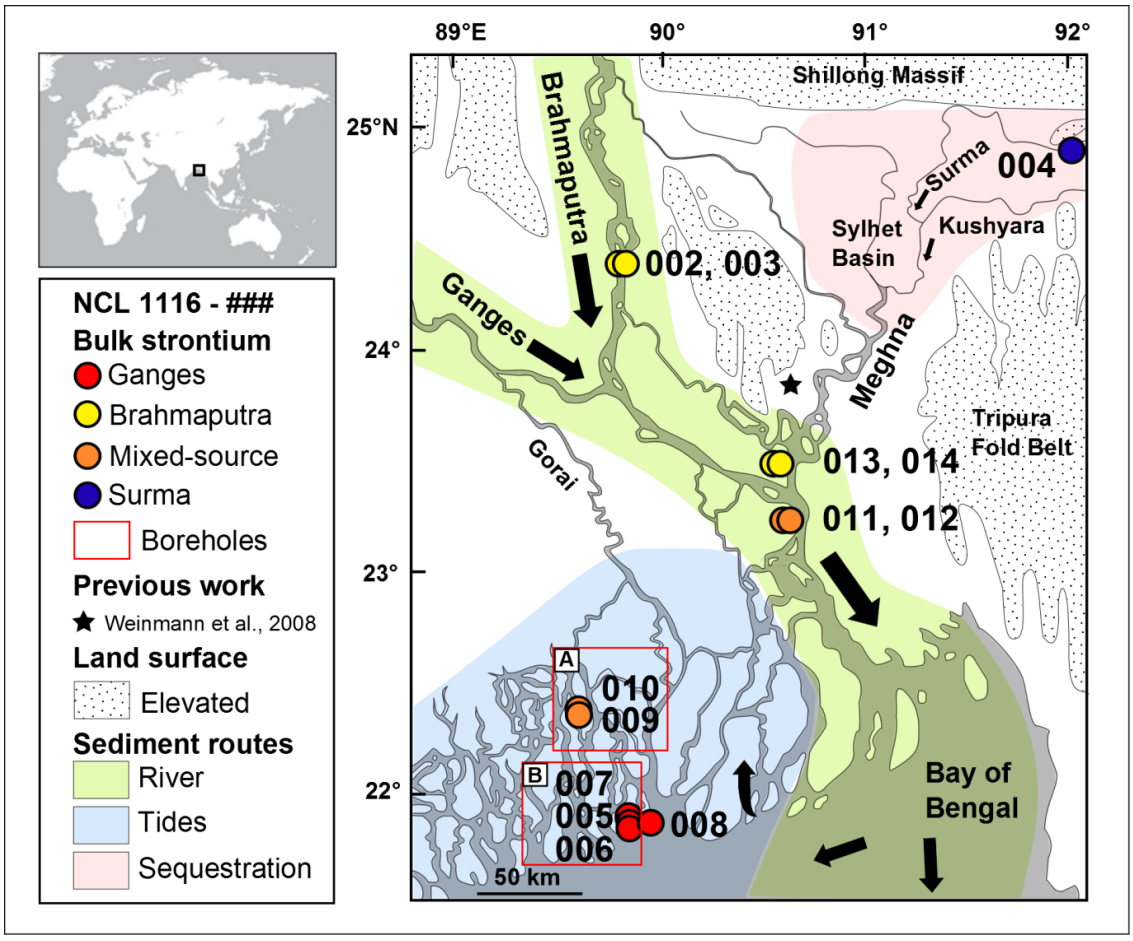

Fig. 5.1. *Sample locations in the GBMD, with relevance to sediment pathways (shaded) and relative sediment flux (black arrows) following Wilson and Goodbred (2015), tectonically or otherwise-elevated features (stippled) following Goodbred and Kuehl (2000), and previous OSL work. Samples are labeled with NCL code and strontium-provenance is indicated by marker color. Red boxes enclose samples obtained from boreholes including KHLC (A) and Katka-A archaeological site (B) borings, while all other samples are from cutbanks.*

due to a wealth of largely Himalaya-derived fluvial sediment (Milliman and Syvitski, 1992; Goodbred and Kuehl, 1999; Sarker et al., 2003) which may serve to offset sea level rise (e.g., Paola et al., 2011) and a relative lack of preexisting hard infrastructure which could otherwise impede nature-based engineering (Jones et al., 2012) the future of the delta may be quite positive if it is managed in a thoughtful way that employs and accommodates natural processes (e.g., Stive et al., 2013).

Establishing reliable geochronological methods for the GBMD is necessary for understanding processes relevant to delta management, such as river avulsion timescales, rates and patterns of sediment deposition and subsidence, frequency of high-magnitude earthquake events, and tropical cyclone recurrence intervals. Further, the GBMD is an excellent example of a system in which establishing new chronologic methods is essential due to complications associated with radiocarbon dating (Suckow et al., 2001). Lessons from this delta can be used to guide dating in other settings.

5.2.1 Dateable deltas

The optimal approach to dating Holocene-aged delta deposits is a function of the composition of the delta's geologic record and the luminescence suitability of its clastic fraction (Fig. 5.2). The necessity for luminescence dating of Holocene deltas may be roughly indicated by sediment yield because this influences the degree of formation and preservation of organic-rich units. Clastics are more efficient than in-situ organics at accreting to fill accommodation space over geologic timescales (Törnqvist et al., 2008; Shen et al., 2015). Therefore, in deltas with high sediment yield, clastics will rapidly fill the available space resulting in organic-poor geologic records. Deltas with low sediment

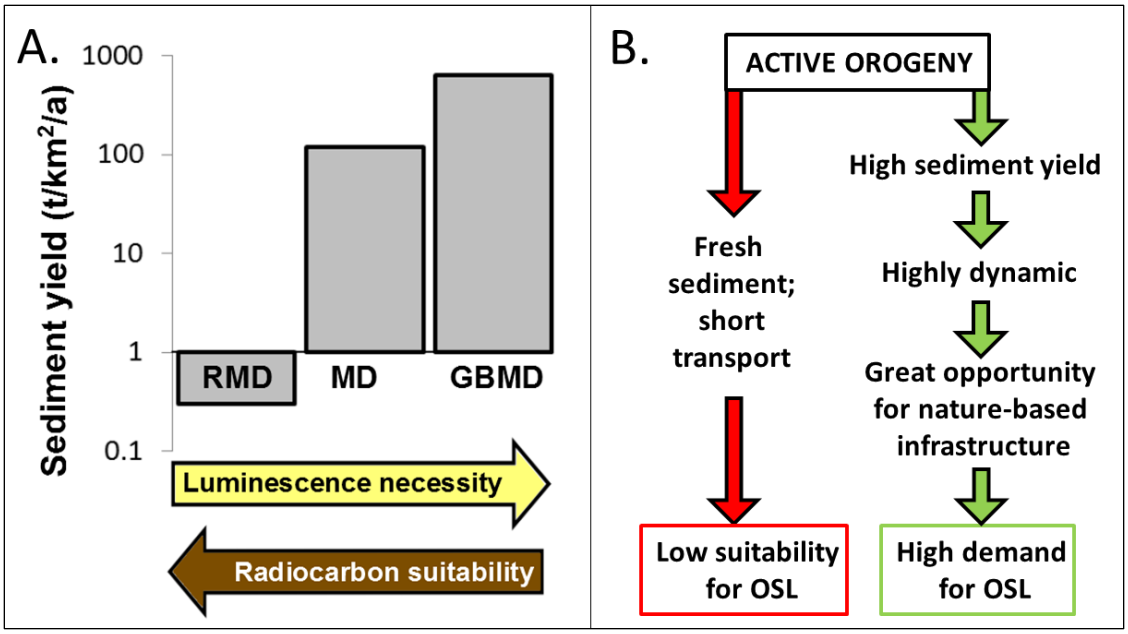

Fig. 5.2. *Necessity (A) and feasibility (B) of OSL in different deltas, with the Rhine Meuse Delta (RMD) and GBMD as end-members and the Mississippi Delta (MD) as an intermediate example. Sediment yield values are from Milliman and Farnsworth (2013); high quantities of fresh sediment are linked to active orogeny because uplift drives erosion and increased sediment production. OSL suitability may be further affected by transport distance.*

yield, on the other hand, provide opportunities for peat formation resulting in more organic-rich geologic records.

Many fundamental questions about delta evolution can be satisfied through well-established radiocarbon dating techniques in organic-rich deltas, such as the Rhine Meuse Delta, Netherlands (e.g., Törnqvist and Van Dijk, 1993; Berendsen and Stouthamer, 2000). By contrast, luminescence dating is essential in organic-poor deltas, such as the GBMD where in situ organics (e.g., peat) are limited within the 50-90 m thick Holocene package (Goodbred and Kuehl, 1999) due to the high lateral mobility of sediment-laden channels that rework the floodplain in the upstream reaches (Wilson and Goodbred, 2015), widespread oxidation of organics during the dry season, and dilution by clastics

and flushing via tidal exchange in the lower reaches (Allison et al., 2003). The Mississippi Delta is an example of a delta that falls in the middle of these extremes; peat is prevalent and clastic subdelta packages are generally bounded by peats (Fisk, 1952; Kosters and Suter, 1993; Törnqvist et al., 1996; Törnqvist et al., 2008), so many broad questions can be answered through radiocarbon dating (e.g., timespan of fluvial system activity, Törnqvist et al., 1996). However, luminescence dating is needed to obtain direct chronologies of clastic deposits related to high energy processes and events (e.g., sedimentation rates and patterns, Shen et al., 2015).

The organic-poor deltas in which luminescence dating is essential are also those in which luminescence dating is often the most difficult (Fig. 5.2). Generally, sediment delivery to deltas is a function of tectonic activity in the hinterland, where uplift drives rapid production and delivery to the delta plain of young material recently eroded from bedrock. Luminescence investigations of bedrock have shown that bedrock quartz OSL sensitivity is minimal (Guralnik et al., 2015) with the exception of sedimentary rocks (Sohbati et al., 2012). Low sensitivity has been documented in sediments associated with active tectonic settings with short transport distances from the orogeny to the basin, including the New Zealand Alps (Preusser et al., 2006) and northwest Himalayas (Jaiswal et al., 2008). Hence, we expect low quartz OSL sensitivity for sediments in organic-poor deltas in general, and GBMD sediments in particular.

5.2.2 Local luminescence

Previous studies have shown that low luminescence sensitivity is common for fluvial Himalaya quartz sand in hinterland localities including Assam, northeast

Himalaya (Thomas et al., 2007), Darjeeling, NE Himalaya (Mukul et al., 2007), and Devprayang, northwest Himalaya (Jaiswal et al., 2008; Ray and Srivastava, 2010). Luminescence dating studies of Himalaya-derived sediment within the Bengal Basin are scarce. Weinman et al. (2008) published four quartz sand OSL ages for the deposition of aquifer sands, Araihazar, Bangladesh (Fig. 5.1), but did not describe the luminescence properties of the quartz sand at this location. Reported ages were between 1 ka and 0.4 ka, with large relative errors between 12.5% and 20%. McArthur et al. (2008) presented quartz OSL ages of western Bengal Basin sediments, also without details of luminescence properties. Other quartz OSL applications in the GBMD employed heated archaeological artefacts (Hanebuth et al., 2013). These are less relevant to sediment dating as heating of quartz increases its luminescence sensitivity (e.g., Poolton et al., 2000). Given the scarcity of information on luminescence properties in the GBMD, there is a need for luminescence investigations of sediments with known depositional ages to validate luminescence dating for Himalaya-sourced sediment in the delta.

5.2.3 Study objectives

Here, we aim to find the best way to luminescence date sediments from an organic-poor delta at the base of an active tectonic margin through a detailed investigation of GBMD fluvial deposits. Sediments with depositional ages constrained within the last few hundred years are used to test the hypotheses that: 1) quartz luminescence of GBMD sediments is poorly sensitized, irrespective of grain size, 2) quartz OSL sensitivity increases with sediment maturity, or source to sink transport times, 3) quartz OSL suitability is in part a function of sediment provenance and

therefore varies among distributaries in the GBMD, and 4) quartz OSL signals in large-river delta sediment are well bleached. This information is used to make recommendations about how to approach luminescence dating of sediment in settings where commonly used dating methods are not applicable.

5.3 Technical approach

We use a multi-pronged approach (Table 5.1) to test the hypotheses of our study, which includes measurement of different mineral and grain size fractions (Appendix D, Fig. A.D.1). We begin with well-established techniques to test the grain-size fractions commonly preferred for luminescence dating, then progress to more experimental measurements of less commonly used fractions. We also test resetting of the luminescence signal upon burial and preservation, using a bleaching index based on differential resetting of multiple luminescence signals within a polymineral sample (Reimann et al., 2015).

Coarse sand is generally selected over finer material in fluvial settings because coarser grains are thought to better bleached than finer grains (Olley et al., 1998), and fewer coarse grains can be measured per disk which makes it possible to check for poor bleaching (e.g., Wallinga, 2002b). In some cases, even single grains of quartz are used to construct equivalent dose distributions in the highest possible resolution, but in many cases poor luminescence sensitivity of quartz grains makes this approach unfeasible (Duller, 2008). In many settings, small-diameter aliquots of quartz sand can be used in combination with statistical analysis (Galbraith et al., 1999; Cunningham and Wallinga, 2012) to obtain accurate ages for heterogeneously bleached quartz because only a small

Table 5.1. *Sequence of measurements used in this study. Abbreviations are used for the following terms: quartz (QTZ), polymineral (PM), single-aliquot regenerative-dose (SAR), thermal transfer (TT), dose recovery (DR) dose response curve (DRC).*

Step	**Mineral**	**Texture**	**Aliquot size**	**Sequence**	**Purpose**
1	QTZ	Sand	3 mm	SAR	check luminescence sensitivity and suitability
2	QTZ	Sand	8 mm	TT-test	find optimal preheat temperature for quartz sand samples that were deemed suitable in Step 1
3	QTZ	Sand	8 mm	DR	verify dose recovery for samples measured in Step 2
4	QTZ	Sand	8 mm	DRC	find age range of samples measured in Step 2
5	QTZ	Sand	3 mm	SAR	determine the depositional age of samples measured in Step 2
6	PM	Silt	2 mg, 10 mm	MS-SAR	quantify pre-depositional bleaching and screen quartz sensitivity
7	QTZ	Silt	2 mg, 10 mm	TT-test	find optimal preheat temperature for quartz silt
8	QTZ	Silt	2 mg, 10 mm	DR	verify dose recovery for quartz silt
9	QTZ	Silt	2 mg, 10 mm	DRC	find age range of quartz silt
10	QTZ	Silt	2 mg, 10 mm	SAR	determine the depositional ages of silt samples

proportion of quartz grains for a sample may luminesce (reported at < 1 % to 5%, e.g., Duller, 2008; Harrison et al., 2008). Fine-grained fluvial sediment has been commonly regarded as undesirable because the small grain-size may yield up to 1 million grains per silt aliquot (Duller, 2008), so the equivalent dose of each aliquot represents an average of the contributions of many grains that may have varied bleaching histories. As a consequence, dose distributions yield no information that allows identifying incomplete bleaching of silts (Olley et al., 1999; Wallinga, 2002b). Single-grain dating is not feasible

for the silt fraction either, due to practical issues with preparing single grains of silt for measurement.

Quartz is the preferred mineral for luminescence dating of Holocene fluvial deposits because it often provides a stable, easily bleached fast component OSL signal (Wallinga, 2002a). However, when quartz luminescence properties are unsuitable, alternative approaches are needed. While quartz OSL sensitivity is highly provenance and site specific, feldspar infrared stimulated luminescence (IRSL) sensitivity is often greater and thus feldspar IRSL may be used in lieu of suitable quartz luminescence properties (e.g., Reimann et al., 2012). However, feldspar IRSL signals are more difficult to bleach than the fast component quartz OSL signal (Godfrey-Smith et al., 1988; Wallinga, 2002a) and, when measured at room temperature (IR-25), are prone to anomalous fading (Spooner, 1994), that is, loss of charge with time from thermally stable traps. Recent research has shown that IRSL measurements of feldspar at elevated temperature following room temperature IRSL measurement, or post-IRIR measurement (e.g., pIRIR-225) target more stable recombination pathways and provide signals that are less affected by anomalous fading (Thomsen et al., 2008; Reimann et al., 2011). These pIRIR measurements avoid proximal trap-recombination center transitions; the greater measurement temperatures correspond to more stable, but also more difficult to bleach signals (Poolton et al., 2002; Jain and Ankjærgaard, 2011; Kars et al., 2014). Therefore, comparisons of multiple IRSL and pIRIR signals for a given sample provide insights into bleaching history of feldspar sands (Murray et al., 2012; Kars et al., 2014). Recently, Reimann et al. (2015) proposed methods to reconstruct bleaching histories from blue stimulated luminescence (BSL), IRSL, pIRIR and thermoluminescence (TL) signals

measured on polymineral samples. The observation that these signals bleach at different rates forms the basis of the bleaching index employed in this study.

5.4 Geology and sample selection

The Ganges, Brahmaputra (Jamuna), and Meghna rivers converge to form the GBMD in the Bengal Basin, Bangladesh (Fig. 5.1), at the intersection of the Indian, Asian, and Burman tectonic plates (Steckler et al., 2008). The actively deforming delta basin is bounded to the north by the Shillong Massif, which overthrusts it, and to the east by the growing IndoBurma Fold Belt which exposes Paleogene-to-Holocene aged sedimentary rocks (Fig. 5.1) (Steckler et al., 2008). The delta is exceptionally dynamic. Rapid uplift in the catchment drives erosion and produces a steep gradient system (5-7 cm/km for main channels in the delta plain, Sarker et al., 2003; 3-10 m/km in the hinterland, Ray and Srivastava, 2010). This system delivers about 1 billion tons/year of sediment to the delta plain and front (Goodbred and Kuehl, 1999) with a relatively short millennial-scale transport time from source-to-sink (Goodbred, 2003). Water and sediment discharge is highly seasonal due to monsoon activity (Islam et al., 1999; Best et al., 2007)

Together the Ganges and Brahmaputra drain an area of 1.72 million km^2, including about 2/3 of the Himalaya orogen (Goodbred et al., 2014). Each river system mobilizes source rocks that are geochemically distinct. The Ganges carries 90 ± 5% Himalaya sediment that is dominantly High Himalayan Crystalline at its entry point to the Bengal basin, plus a minor contribution from the Indian craton (Wasson, 2003; Goodbred et al., 2014). The Brahmaputra erodes mafic batholiths along the suture zone in

Tibet and young Himalayan rocks around the syntaxis, with a smaller component of Lesser Himalaya and Siwalik sources similar to the Ganges load as it passes through the Himalayan foreland in Assam (Singh and France-Lanord, 2002; Goodbred et al., 2014). The Meghna carries locally sourced sediment of principally recycled Tertiary-age Brahmaputra sedimentary rock (Goodbred et al., 2014) introduced by the Surma and Kushyara (Kushiara) tributaries (Fig. 5.1). Strontium content of bulk sediment indicates provenance; Brahmaputra sediment has relatively high strontium content (>140 ppm). Ganges and Surma/Meghna catchment sediment both have low strontium content (<110 ppm), but can be differentiated because they are geographically separate (Goodbred et al., 2014).

The Ganges and Brahmaputra are the main modern sediment conduits to the delta plain and subaqueous delta front, while fluvial sediment in the Meghna is largely sequestered in the subsiding northeast Sylhet basin. Therefore the Meghna contribution to the Holocene sediment package outside the Meghna valley is minimal (Goodbred et al., 2014; Wilson and Goodbred, 2015) (Fig. 5.1). Tides and currents transport sediment from the river mouth to the western coast (Rogers et al., 2013; Wilson and Goodbred, 2015), a fluvially inactive region of the delta that was built and occupied by older Ganges distributaries (e.g., the Gorai, Fig. 5.1) prior to the late-Holocene connection of the Ganges with the Brahmaputra (Allison et al., 2003). In their upstream and middle reaches, the Ganges and Brahmaputra are the archetype of braided rivers with braidbelts averaging 8 ± 4 and 10 ± 4 km wide, respectively. Rapid channel bed aggradation drives high lateral migration and intense reworking of the upper sediments of the delta plain (Wilson and Goodbred, 2015).

Our study employed a sampling strategy to target samples of different grain-size, sites proximal and distal to the coast, sediments of different provenance, and sediments with constrained depositional ages (Table 5.2). Five samples with decade- to century-scale expected ages were obtained by augering and capture with a lined stainless steel Van der Horst sediment sampler. These samples include: 1) coastal tidal flat silty deposits from 0.26, 2.48, and 4.18 m depth (NCL-1116007, 005, 006, respectively) at the Katka-A archaeological site, with the uppermost deposits aged about 250 - 350 a based on luminescence measurements of fired pottery (1640-1750 A.D.) and calibrated radiocarbon dates (1640-1790 A.D.) for mangrove roots embedded in the top meter of sediments (Hanebuth et al., 2013), and 2) tidal channel fill deposited within the last ~20-30 a (NCL-1116010) based on Landsat imagery that captures rapid channel narrowing following human modifications of the system (Wilson et al., in review), and underlying coarser tidal channel sediments likely deposited within the past 30-40 a (NCL-1116009). Tidal channel deposits were sampled at the site of an optical fiber strain meter in Bhanderkote, Khulna District, referred to as KHLC (DeWolf et al., 2013). Eight modern samples were obtained by hammering lined light-proof PVC pipes into cleaned riverbank and river island (char) cutbanks (NCL-1116002, 003, 004, 008, 011, 012, 013, 014), that were presumed to have been deposited within the last 20 years due to the high lateral mobility of these rivers. Where possible, satellite records from Google Earth which generally extend back to the early- to mid-2000's were used to verify and refine the expected depositional ages of these young samples. Our collection includes Ganges silts and sands (NCL-1116005, 006, 007, 008), Brahmaputra silts and sands (NCL-1116002,

003), Upper Meghna catchment sand (NCL-1116004), and mixed-source silts and sands (NCL-1116009, 010, 011, 012, 013, 014) (Fig. 5.1). See Table 5.2 for sample details.

5.5 Sample preparation and bulk sediment analyses

5.5.1 Sand fraction preparation

Sample preparation was performed under amber light conditions at Tulane University, USA, and at the Netherlands Centre for Luminescence dating. Sands were wet-sieved, then chemically processed with 30% H_2O_2 and 10% HCl to remove organics and carbonates, respectively. The washwater was collected during the sieving process because it contained fine silts. Density separation of the sand fraction was performed at 2.72, 2.62, and 2.58 g/cm^3 to isolate a quartz fraction (2.62-2.72 g/cm^3) and a K-feldspar fraction (<2.58 g/cm^3). Quartz sands were washed three times in a sodium pyrophosphate ($Na_4P_2O_7$) detergent solution to remove mica (mainly muscovite) (Kortekaas and Murray, 2005) which was abundant due to the mineralogical immaturity of GBMD sediment. Quartz sands were etched in 40% hydrofluoric acid (HF) for 40 minutes, rinsed with deionized water, treated with 10% HCl for 40 minutes to remove fluorides, and rinsed again with deionized water. Quartz grains were adhered to stainless steel disks using silicon spray and mask sizes that varied with the measurement.

5.5.2 Silt fraction preparation

Silts were isolated from washwater collected during sieving, using settling velocities calculated with Stokes Law to obtain the 4-11 μm fraction and, when additional material was needed, the 11-20 μm fraction. These were treated with 30%

Table 5.2. *Sample details, including the sources of expected ages. The term "river-mouth" is abbreviated as "r-m".*

NCL sample code	Latitude	Longitude	Depth (m)	Sampling mode	Depositional environment	Strontium (ppm)	LOI (%)	D50 (µm)	Expected age (a)
NCL-1116002	24° 24' 03.12"	89° 46' 35.10"	1.25	cutbank	river char	148 ± 4	1	69	10 ± 10[a]
NCL-1116003	24° 23' 13.44"	89° 47' 00.90"	0.35	cutbank	river char	155 ± 4	1	191	10 ± 10[a]
NCL-1116004	25° 06' 32.88"	92° 10' 37.44"	0.35	cutbank	river bank	44 ± 2	1	268	10 ± 10[a]
NCL-1116005	21° 51' 12.84"	89° 46' 04.26"	2.48	borehole	r-m tidal estuary	95 ± 3	5	15	> 300[a,b]
NCL-1116006	21° 51' 12.84"	89° 46' 04.26"	4.18	borehole	r-m tidal estuary	102 ± 3	5	19	> 350[a,b]
NCL-1116007	21° 51' 12.84"	89° 46' 04.26"	0.26	borehole	r-m tidal estuary	96 ± 3	4	17	275 ± 25[b]
NCL-1116008	21° 50' 35.10"	89° 51' 00.96"	0.23	cutbank	coastal sand bar	94 ± 3	1	147	5 ± 5[c]
NCL-1116009	22° 40' 15.60"	89° 34' 11.28"	4.99	borehole	tidal channel	109 ± 3	3	34	35 ± 5[d]
NCL-1116010	22° 40' 15.60"	89° 34' 11.28"	4.44	borehole	tidal channel	107 ± 3	3	42	25 ± 5[d]
NCL-1116011	23° 09' 27.00"	90° 36' 30.42"	0.73	cutbank	river bank	127 ± 4	3	57	5 ± 5[c]
NCL-1116012	23° 09' 27.00"	90° 36' 30.42"	1.48	cutbank	river bank	132 ± 4	1	111	5 ± 5[c]
NCL-1116013	23° 35' 16.32"	90° 34' 38.64"	0.13	cutbank	river bank	162 ± 4	2	93	10 ± 10[a]
NCL-1116014	23° 35' 16.32"	90° 34' 38.64"	1.13	cutbank	river bank	141 ± 4	1*	n/a	10 ± 10[a]

[a]assumed ages based on known lateral mobility of the channels and the stratigraphic principle of superposition. [b]previously published radiocarbon and thermally reset OSL ages (Hanebuth et al., 2013). [c]Google Earth imagery showing landform development with time. [d]Landsat data showing channel infilling with time.

H_2O_2 to remove organics and 10% HCl to remove carbonates to obtain polymineral silt. Note that polymineral silt was not etched in hydrofluoric nor fluorosilicic acid, so these samples are expected to contain quartz, feldspar, and heavy mineral grains (Appendix D, Fig. A.D.1).

To obtain pure quartz silt, up to 1 g sediment per sample was etched in 40 ml 31% fluorosilicic acid (H_2FSi_6) for 80-90 hrs, stirring twice daily roughly following Wang et al. (2006). No efforts were taken to silica-saturate the acid prior to etching. Fluorosilicic acid was decanted and samples were rinsed three times with deionized water, then cleaned with 10% HCl for 1 hr and rinsed four times with deionized water employing settling velocity to isolate the desired quartz grains from the decant. The efficacy of both sand and silt etches was verified with IR depletion measurements (see 'Luminescence experiments and results').

Polymineral and quartz silts were suspended in acetone at a concentration of ~20 mg/ml; 0.1 ml solution was pipetted directly onto 10 mm stainless steel disk. The solution dispersed across the disk to form ~10 mm aliquots each containing ~2 mg sediment (roughly 10^6 grains) that thinned toward the disk edges due to settling patterns.

5.5.3 Dose rate estimation

The natural radiation of the sediment matrixes was assessed from activity concentrations of ^{40}K and several radionuclides from the thorium and uranium series, measured on a gamma spectrometer at Tulane University (Appendix D, Table A.D.1). Dose rate conversion factors were applied following Guérin et al. (2011). The cosmogenic contributions to dose were calculated following Prescott and Hutton (1994)

(Appendix D, Table A.D.1). An alpha efficiency value of 0.025 ± 0.001 was applied to the silt samples (Mauz et al., 2006). Etching of the sand fraction removed the alpha exposed outer layer of the sand grains, therefore no external alpha contribution was included for those samples. Beta dose attenuation was corrected for grain size following Mejdahl (1979). Dose rate attenuation due to water was taken into account following Aitken (1985), based on water contents measured by drying bulk sediment for each sample in a low temperature oven; 5% uncertainty was added to accommodate disturbances due to sampling and/or variations in water content during burial (Appendix D, Table A.D.1).

5.5.4 Strontium provenance, organic content, and grain size measurements

Bulk sediment was sourced to the Ganges, Brahmaputra, and Meghna catchments using strontium content as described by Goodbred et al. (2014) (Fig. 5.1; Table 5.2). For this, bulk major and trace element concentrations were measured with a portable ThermoScientific Niton XL3 Analyzer using 50 g of dried and powdered sediment per sample. Samples were burned in an oven for 48 hours at 600°C at Vanderbilt University to measure loss-on-ignition (LOI) as a proxy for organic content. Following LOI burning, a slurry of sediment was mixed with deionized water and used to measure grain size (Table 5.2) by laser diffraction with a Malvern Mastersizer 2000E particle-size analyzer.

5.6 Luminescence experiments and results

Luminescence measurements were made on an automated Risø D15 TL/OSL reader at the Netherlands Centre for Luminescence dating, Wageningen University. Blue

(~470 nm) and infrared (~875 nm) light emitting diodes (LEDs) were used for optical stimulation and the heating element in the Risø reader was used for heating and TL measurements. The luminescence signals of all polymineral and quartz fractions were detected through a 7.5 mm Hoya U-340 (U-340) filter with a UV detection window. The samples were irradiated with a $^{90}Sr/^{90}Y$ beta-source providing a dose rate of 0.118 ± 0.020 Gy/s to the sands and 0.103 ± 0.02 Gy/s to the fine silts.

IRSL measurements were made for 100 s over 250 channels; the signal was integrated over the first 2 s of the shine down curve and the subtracted background was integrated over the last 20 s (Reimann et al., 2015). BSL measurements were made for 20 s over 1000 channels; the signal was integrated over the first 0.5 s and the subtracted early background was integrated over 0.5-1.8 s to minimize the contribution of medium and slow components (Cunningham and Wallinga, 2010). The TL signal was measured between 250 - 300 °C; subtracted background was measured between 0 - 50 °C (Rink, 2003). Aliquot acceptance criteria included a recycling ratio of 0.9-1.1, recuperation (relative to the largest regenerative dose) of less than 5%, an IR depletion ratio of less than 10% (Duller, 2003), and test dose error less than 20%, including uncertainties. All ages are reported in years (a) relative to 2015, the year of collection for the majority of samples.

5.6.1 Dating the sand fraction: testing quartz BSL

We began with a quick screening of etched quartz sand for all samples to determine luminescence suitability. This assessment employed a standard single-aliquot regenerative-dose (SAR) protocol (Murray and Wintle, 2000, 2003) of 3 mm aliquots,

with a 200 °C preheat, OSL measurement at 125 °C, one 5.90 Gy regeneration point, a recuperation point, and recycling checks including IR depletion of the OSL signal (Duller, 2016). Signals were normalized with a 2.95 Gy test dose. For each sample the coarsest available sand fraction was measured; in addition a finer sand fraction was measured when available (see Table 5.3 for grain size details).

The SAR quartz sand measurements showed that quartz is generally dim across the middle and lower delta plain for our samples including Ganges, Brahmaputra, and the majority of mixed river localities, and exhibited low sensitivity consistent with previous studies (Fig. 5.3) (e.g., Jaiswal et al., 2008) indicated by the low number of accepted aliquots (Appendix D, Table A.D.2). Many of the accepted quartz sand aliquots were not ideal for dating; they had weak luminescence signals and fell within the acceptance range

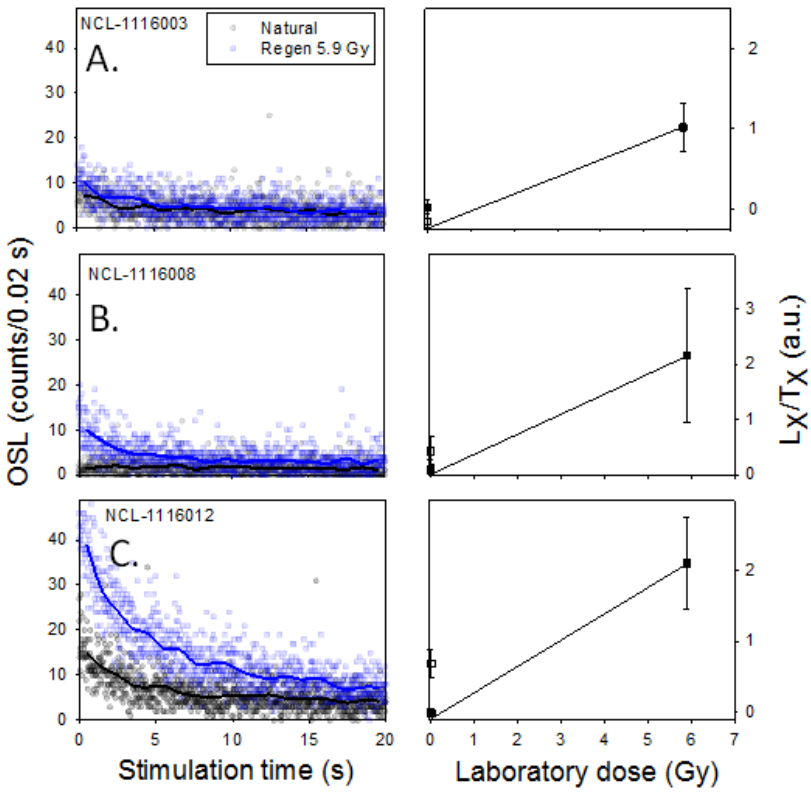

Fig. 5.3. *Examples of typical dose response and decay curves demonstrating poor sensitivity for 3 mm aliquots of (A) Ganges 125-180 µm quartz (B) Brahmaputra 180-250 µm quartz, and (C) mixed-source 125-180 µm quartz sampled below the Padma-Meghna confluence. Aliquots shown in examples A and B were rejected because error on the test dose was greater than 20%. The aliquot shown in example C was accepted.*

due to large uncertainties on the recycling and recuperation values. These low-sensitivity, high-uncertainty aliquots would contribute little to an equivalent dose estimated with weighted statistics.

Notable exceptions to the dim quartz are found in NCL-1116004, upper Meghna catchment sediment, which exhibited suitable characteristics and sensitivity for OSL dating (Fig. 5.4) and NCL-1116012, mixed-source sediment just below the Meghna-Padma confluence, which contained a smaller population of suitable quartz sand grains based on the initial quartz sand screening. Thermal transfer (Truelsen and Wallinga, 2003) and dose recovery to inform equivalent dose measurement, and dose response

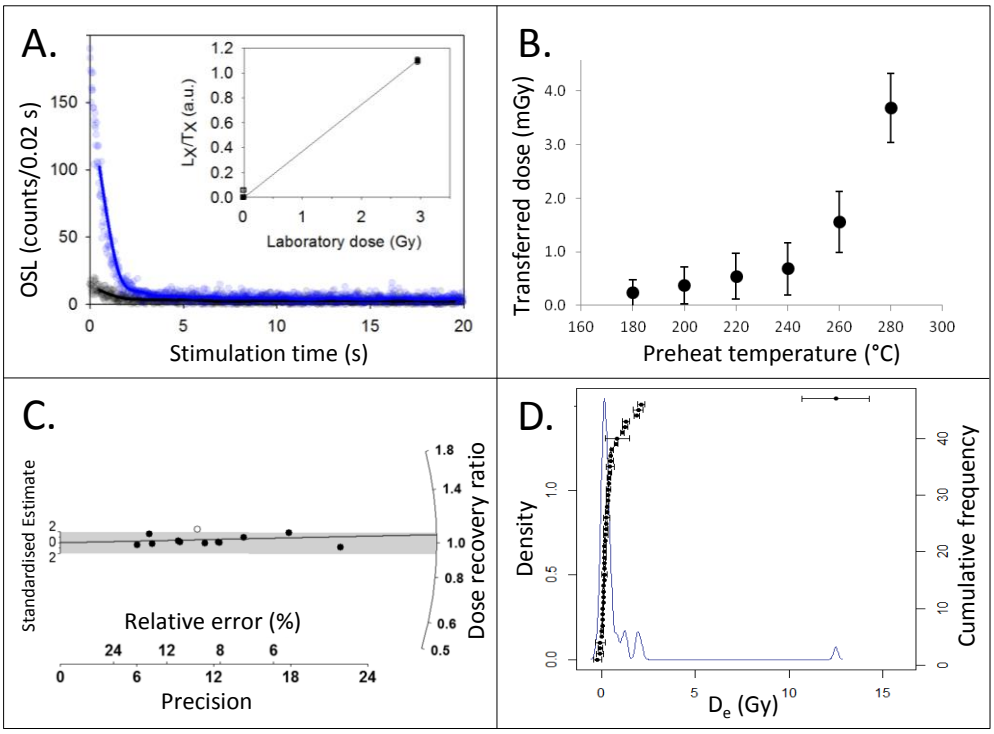

Fig. 5.4. *Results for suitable 180-250 µm quartz sand from the Meghna catchment, sample NCL-1116004, including (A) dose response and decay curves showing the natural and 2.95 Gy regenerated signals for a 3 mm aliquot, (B) thermal transfer tests, (C) radial plot of dose recovery for a 2.95 Gy given beta dose, and (D) D_e frequency distribution for 3 mm aliquots (n = 47).*

curve shape to assess the age range, were measured for these two samples using 8 mm aliquots (~ 1,000 to 4,800 grains).

Equivalent doses were obtained from these two samples using a SAR protocol (Murray and Wintle, 2000, 2003) with 180 °C preheat, 180°C cutheat, and 190°C hot bleach at the end of each SAR cycle (Murray and Wintle, 2003; Ballarini et al., 2007). This employed one regeneration point at 2.58 Gy, a recuperation point, and recycling points to check for sensitivity correction and IR depletion. Dose response curves were fit with a linear regression forced through the origin (Ballarini et al., 2007). The use of one regeneration point is associated with a very minimal systematic error due to curve fitting (Ballarini et al., 2007; Shen and Mauz, 2012); assuming a typical D_0 of 50 Gy (see 'Dating the silt fraction'), this error is +1.6% at 1 Gy, approaches zero at the regeneration point (2.58 Gy) and origin (0 Gy) for fine silt, and produces a relative error that is largest for lowest doses. All measurements were normalized using OSL responses to a 2.58 Gy test dose.

A small aliquot diameter was initially selected to allow detection of incomplete bleaching. Only one of 48 (2%) 1 mm NCL-1116004 quartz sand aliquots (~ 15 grains) produced a measureable signal, so aliquot size for SAR measurement was subsequently increased to 3 mm. We estimate that 3 mm aliquots of 180-250 μm sand each contained ~150 grains and 3 mm aliquots of 75-125 μm sand contained ~700 grains. Forty nine percent of the 3 mm, 180-250 μm NCL-1116004 quartz aliquots met the acceptance criteria; these produced an age of 9 ± 13 a using the unlogged minimum age model (MAMul; Arnold et al., 2009) which was combined with a bootstrap approach (Cunningham and Wallinga, 2012) assuming 20 ± 10 % overdispersion (sigma_b) (e.g.,

Olley et al., 2004; Arnold and Roberts, 2009). This model was selected because the samples exhibited high inter-aliquot scatter (high overdispersion) in equivalent doses (Table 5.3) suggesting incomplete bleaching, and some aliquots produced negative equivalent doses ($D_e s$). High uncertainty was assigned to the sigma_b value because little is known about overdispersion for well-bleached samples in this setting. The unlogged central age model (CAMul; Arnold et al., 2009) and a mean and standard error approach yielded ages for this sample centuries older than the bootstrap minimum approach (Table 5.3).

Despite the smaller grain size and higher number of grains per disk, only 19% of the 3 mm, 75-125 μm NCL-1116012 quartz met the acceptance criteria, so age calculations were less reliable due to the low number of accepted aliquots (Table 5.3). We use these data to discuss luminescence characteristics by grain size and provenance, but exclude quartz BSL sand ages from further analyses because NCL-1116004 does not represent braided river sediment and NCL-1116012 produced too few aliquots (n = 9) for reliable statistics.

5.6.2 Degree of bleaching; a multiple-signal approach

Bleaching of fine sediments was assessed with a multiple signal single aliquot regenerative dose (MS-SAR) approach adapted from the bleaching ratio presented by Reimann et al. (2015). The MS-SAR employed a 250 °C preheat, 250 °C cut-heat, 280 °C hot bleach, and a 5.15 Gy test dose. Feldspar measurements included IRSL at room temperature (IR-25), and subsequent post IRIR at elevated temperatures (pIRIR-90, pIRIR-155, and pIRIR-225) with two regenerative doses of 5.15 Gy and 10.30 Gy. A

BSL signal, thought to arise primarily from the quartz component of the polymineral silt, was measured at 125 °C following depletion of the feldspar signal by the IR and pIRIR measurements. D_{eBSL} was calculated using a linear fit to only the lower regenerative point of 5.15 Gy although a higher 10.30 Gy point was also measured. The higher regenerative point was excluded because 1) an exponential fit was not justified as two points provide too poor constraints and may lead to highly inaccurate dose response curves, and 2) the equivalent doses lie between 0 and the first regeneration point, therefore including the second point with a linear fit may create a systematic overestimation of equivalent dose. To avoid sensitivity changes within SAR cycles, polymineral TL was measured only once every SAR cycle, after IR, pIRIR and OSL measurements of the test dose signal. TL signals were measured up to 300 °C (Appendix D, Table A.D.3).

Where Reimann et al. (2015) used a BSL ratio to infer transport histories of beach deposits following the initial deposition of sand-sized grains that shared a common primary depositional age, we applied the procedure to assess the pre-deposition resetting of polymineral 4-11 and 11-20 µm silts that spanned a range of depositional ages. Thus, changes to the ratio were required to normalize for age, and the bleaching index (BI) used for this study is:

5.1. $$BI_{LS} = \frac{D_{eBSL}\,(D_{eLS} - D_{eBSL})}{D_{eBSL} + 1}$$

where subscript *LS* denotes the luminescence signal of choice (e.g., IR-25, pIRIR-90 etc), and *BSL* is the luminescence measurement obtained with the MS-SAR approach following IR depletion and thought to arise mainly from the quartz component of the polymineral sample (Banerjee et al., 2001; Wallinga et al., 2002). In cases of prolonged bleaching, all signals will be equally reset and the post-depositional D_es obtained from

the different signals will be nearly identical, resulting in very small bleaching index. By contrast, the BI will be elevated for samples that did not experience prolonged bleaching prior to deposition because all feldspar signals bleach slower than the quartz BSL signal and show an increasing trend with stimulation temperature due to reduced bleachability (Thomsen et al., 2008; Reimann et al., 2011; Kars et al., 2014). In practice, feldspar-based D_e*s* are expected to be up to 40% higher even for perfectly bleached samples due to the dose rate contribution of K-40 in the feldspar grains, resulting in slightly elevated BI. On the other hand, anomalous fading of feldspar signals may result in slightly lower BI, especially for IR-25 measurements.

The MS-SAR BSL measurement proved to be mildly imperfect. A 250 °C preheat was selected to allow measurement of pIRIR-225 signals. However, this heating led to an elevated D_{eBSL}, attributed to thermal transfer (Fig. 5.4). In addition, some aliquots exhibited a rising signal during the measurement, resulting in a negative D_{eBSL} (Appendix D, Table A.D.3). Measurements were made for 4-8 aliquots per sample. The BI value for each luminescence signal of each sample was calculated as the mean ± standard error of BI values produced by all aliquots with D_{eBSL} greater than zero. Aliquots with D_{eBSL} less than zero (including one aliquot of NCL-1116010, two aliquots of NCL-1116009, and all aliquots of NCL-1116011, 012, 013, 014) were dismissed from BI calculations because these produced negative and meaningless BI values. This means the bleaching index could not be applied to the youngest samples , which were coincidentally from the most upstream sites and apparently sufficiently bleached based on the near-zero values for D_{eBSL} measured with the MS-SAR sequence.

We observe that all samples show similar trajectories of increasing D_e with more difficult to reset (i.e., higher temperature) pIRIR signals (Fig. 5.5). Bleaching of each luminescence signal was plotted against the expected age to verify that we had, in fact, successfully normalized for age with the bleaching index. Bleaching was also plotted against distance from the coast (a proxy for transport distance) to check if bleaching occurred during transport of the fine grains within the braided river system (Fig. 5.5).

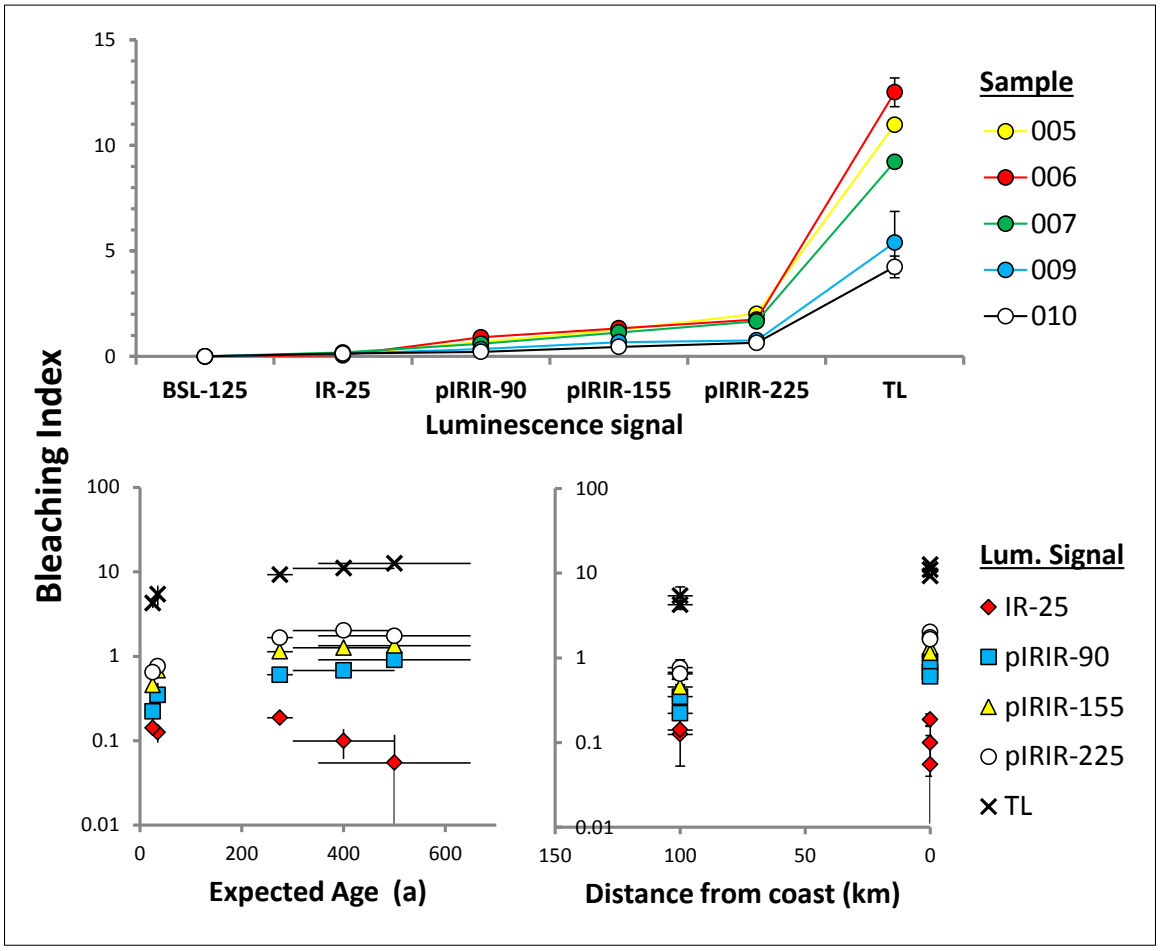

Fig. 5.5. *Results from the MS-SAR bleaching assessment, expressed using the bleaching index (BI) of equation 1. Graphs show, 1) how BI varies with luminescence signal for each sample (upper), and 2) how BI varies with expected age (lower left) and sample location relative to the coast (lower right) for each luminescence signal. The BI is > 0 for samples where feldspar signals were not completely reset upon deposition.*

5.6.3 Dating the silt fraction

The MS-SAR results suggested that the silt fraction of most samples contained quartz with suitable luminescence properties (Appendix D, Table A.D.3). This was further explored with measurements of etched silt using well-established procedures. Thermal transfer (Truelsen and Wallinga, 2003) and dose recovery tests were conducted to inform selection of an appropriate preheat temperature and measurement sequence. A preheat of 180 °C was found to be optimal; above this temperature the samples exhibited thermal transfer (Fig. 5.6). Dose recovery of 2.58 Gy with a sequence employing a 180 °C preheat, 180 °C cut-heat, and 190 °C hot bleach was successful. The recovered dose, calculated as mean ± SE, was 2.65 ± 0.06 Gy, yielding a dose recovery ratio of 1.03 ± 0.02 (Fig. 5.6). The shape of the dose response curve for fine silt was assessed up to ~600 Gy (Fig. 5.6) and was found to be best fit with an exponential plus linear curve. The average D_0 of all samples for which it was measured (n=6) was 50 Gy, with a 5 Gy standard deviation. We estimate that reliable dating of GBMD quartz silt is possible up to about 24 ka, applying the 4.1 Gy/ka dose rate averaged for all 4-11 µm silt samples and the $2D_0$ threshold suggested by Wintle and Murray (2006).

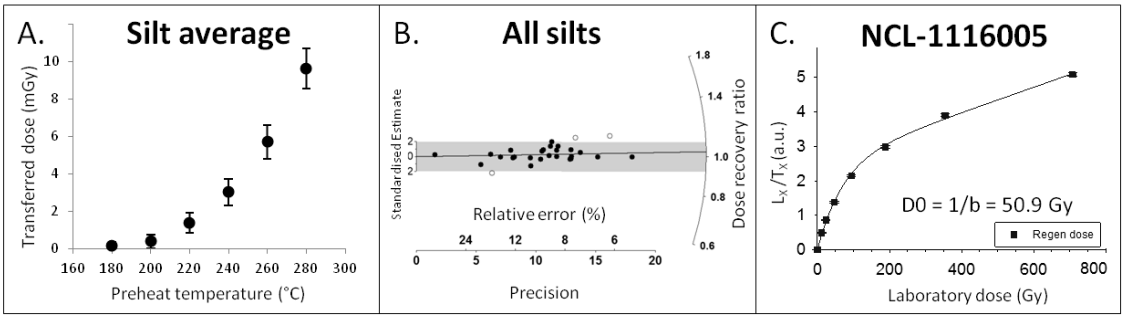

Fig. 5.6. *Average data for all etched quartz silt ~10 µm aliquots showing (A) thermal transfer test, (B) dose recovery for a 2.58 Gy given dose with a dose recovery ratio of: 1.03 ± 0.02, for all quartz silt aliquots (n = 28). (C) shows an example of the dose response curve typical for these silts, fitted with an exponential plus linear regression.*

Equivalent doses were measured from the etched quartz silt aliquots using the SAR protocol outlined above; measurement parameters are identical to those used for etched quartz sand SAR measurements. While the MS-SAR measurement employed for BI assessment showed that silt was generally sufficiently bleached, the standard SAR measurement employed for dating of etched quartz silts yielded more detailed information that indicated that some silt grains may retain relatively minor residual doses. This was suggested by a high degree of scatter in the equivalent doses of etched quartz silt that was relatively largest for the youngest samples (Appendix D, Figs. A.D.2 & A.D.3). The majority of silt aliquots were sufficiently bright (Fig. 5.7) and met the acceptance criteria.

Several models were tested to extract the burial dose from the equivalent dose distribution. These included a mean and standard error, the central and unlogged central

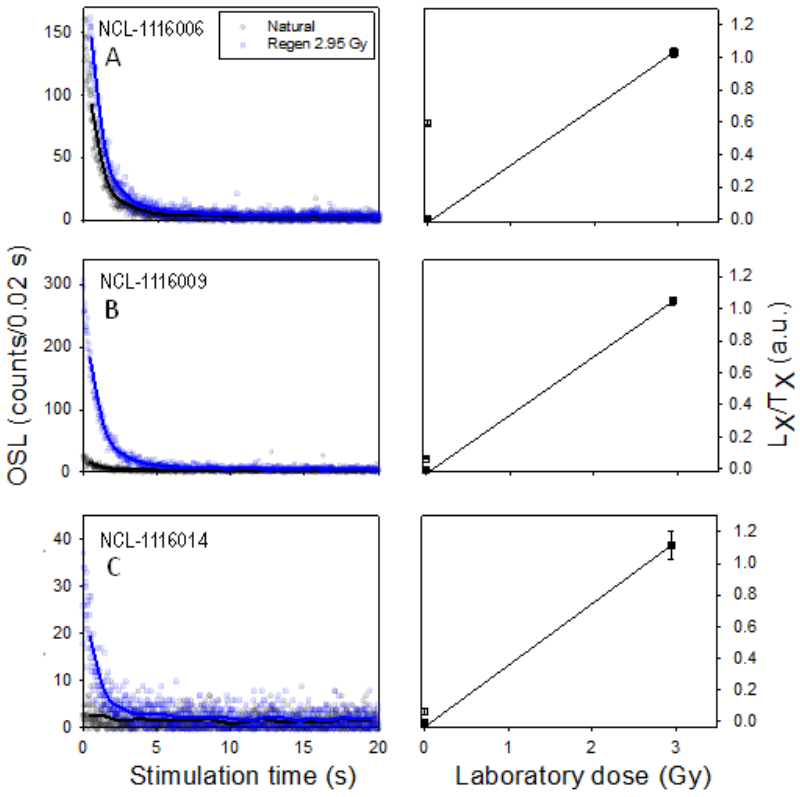

Fig. 5.7. *Examples of typical dose response and decay curves for 4-11 µm etched quartz silts including (a) a relatively old borehole sample, (b) a relatively young borehole sample, (c) a modern cutbank sample.*

age models (Galbraith et al., 1999; Arnold et al., 2009), and the bootstrap unlogged minimum age model (Arnold et al., 2009; Cunningham and Wallinga, 2012) (Table 5.3). The two types of the central age model were rejected because they preferentially weighted high-D_e aliquots due to the lower relative uncertainty on these. However, they yielded valuable information about overdispersion for our samples that guided subsequent age model usage.

Table 5.3. *Quartz sand and quartz silt ages produced with various models including the bootstrap unlogged minimum age model (bootMAM$_{ul}$), mean and standard error (Mean ± SE), and unlogged central age model (CAM$_{ul}$). Overdispersion (OD) obtained with CAM$_{ul}$, and numbers of measured (meas.) and accepted (accpt.) aliquots for each sample are presented. The two sand samples were selected for measurement because the initial quartz sand screening indicated they may contain dateable quartz.*

NCL sample code	**Grain size (μm)**	**n meas.**	**n accpt.**	**bootMAM$_{ul}$ age (a)**	**Mean ± SE age (a)**	**CAM$_{ul}$ age (a)**	**CAM$_{ul}$ OD (%)**
NCL-1116004	180-250	96	47 (49%)	9 ± 13	203 ± 83	253 ± 43	91 ± 12
NCL-1116012	75-125	48	9 (19%)	62 ± 40	166 ± 32	185 ± 44	59 ± 18
NCL-1116002	11-20	20	16 (80%)	10 ± 6	23 ± 7	44 ± 12	55 ± 24
NCL-1116005	4-11	24	22 (92%)	346 ± 19	353 ± 20	352 ± 19	-1 ± 17
NCL-1116006	4-11	30	29 (97%)	361 ± 20	367 ± 20	368 ± 20	4 ± 2
NCL-1116007	4-11	24	24 (100%)	238 ± 15	241 ± 15	240 ± 15	0 ± 14
NCL-1116009	4-11	28	28 (96%)	39 ± 3	54 ± 7	55 ± 4	20 ± 4
NCL-1116010	4-11	28	28 (100%)	28 ± 3	34 ± 3	35 ± 2	16 ± 4
NCL-1116011	4-11	7	5 (71%)	16 ± 10	23 ± 7	32 ± 10	35 ± 33
NCL-1116012	4-11	7	6 (86%)	177 ± 17	257 ± 51	267 ± 41	30 ± 12
NCL-1116014	4-11	34	22 (65%)	22 ± 7	36 ± 5	47 ± 6	34 ± 12

Typically 6-10 aliquots are sufficient for quartz BSL silt dating (Shen et al., 2015); this study aimed for at least 20 accepted aliquots per silt sample because of the scatter observed in equivalent doses. Some samples have fewer accepted aliquots because material was limited. Variability in the brightness of aliquots was tested using sensitivity distributions of natural signal test dose responses (T_N). This showed a wide distribution of brightnesses for each sample, with values for overdispersion around 30% (Appendix D, Table A.D.4). These results suggest that the measurement of up to millions (Duller, 2008) of silt grains per aliquot did not, in fact, produce sufficient signal averaging to yield homogenously bright aliquots for each sample. While we were not able to directly test the number of grains per disk contributing luminescence, we reason that the quartz silt BSL signal was dominated by a few grains, indicated by observations of 1) relatively high overdispersion of silt equivalent doses, in combination with 2) high variability of test dose brightnesses. Future research could explore this using spatially resolved luminescence detection (e.g., Bailiff and Mikhailik, 2003; Kook et al., 2015), but such equipment was not available for this study. We observed that mean T_N brightness increases and the percent of accepted aliquots generally improves coastward, although it is not possible to assign sensitization to sample age, provenance, or transport processes, given the limited number of samples measured for this study (Fig. 5.8).

Ultimately, the bootstrap unlogged minimum age model was selected over the mean and standard error approach for equivalent dose determination because: 1) the single-aliquot silt signals appeared to be dominated by a few grains; 2) overdispersion decreased with age suggesting that heterogeneous bleaching is a major component of this overdispersion; 3) for older samples, the bootstrap unlogged minimum age model yielded

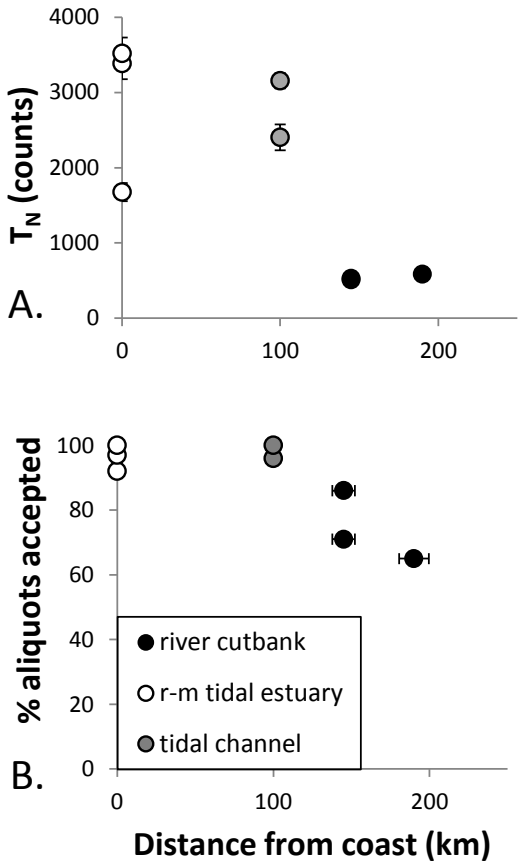

Fig. 5.8. *Test dose sensitivity (A) and percent of aliquots accepted (B) with distance, for etched quartz silt isolated from river cutbank, river-mouth (r-m) tidal estuary, and tidal channel deposits.*

identical results to the mean and central age models, suggesting that there is no bias in the age obtained through the applied MAM, provided that the input parameters are justified; and 4) for younger samples the bootstrap unlogged minimum age model performed best relative to expected ages (Fig. 5.9, Tables 5.2 and 5.3). Further, the bootstrap approach has the advantage of incorporating an error term on overdispersion (Cunningham and Wallinga, 2012), a parameter that is not currently well-constrained in this setting. An overdispersion of 3.6 ± 1.8 % was applied with the bootstrap unlogged minimum age model; this was derived from central age model results on the oldest samples (NCL-1116005, 006, 007). The unlogged version of the minimum age model (Arnold et al., 2009) was necessary for these young samples because some aliquots produced negative D_e*s*.

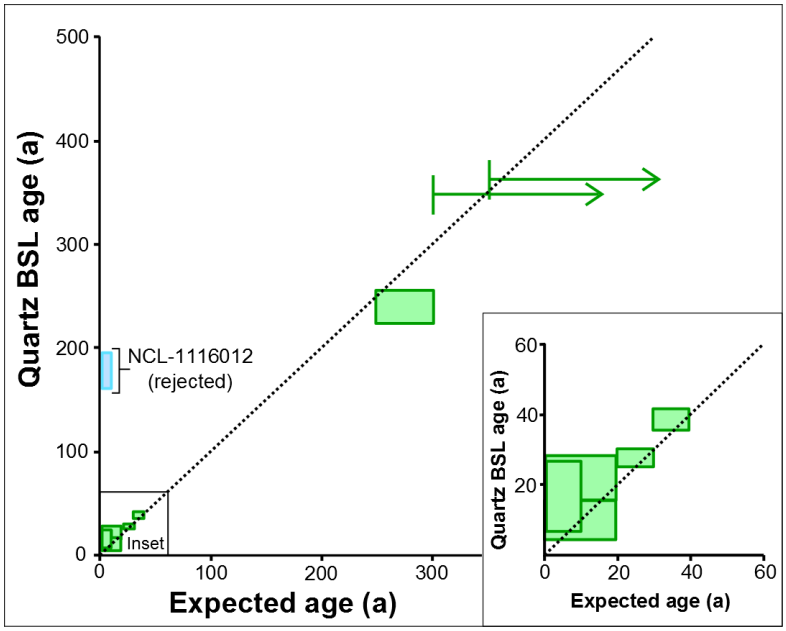

Fig. 5.9. *Comparison of expected ages versus quartz BSL ages obtained for etched quartz silt using the unlogged bootstrap minimum age model. The insert focuses on the youngest samples. Uncertainty on the upper limit of the expected ages for samples NCL-1116005 and 006 is indicated by the green arrows.*

Dose rate details and equivalent dose results obtained with the bootstrap MAM_{ul} for etched quartz silt are provided in Appendix D (Table A.D.1). OSL ages were obtained by dividing the bootstrapped MAM_{ul} $D_e s$ obtained on the quartz silt fraction by the calculated dose rates for this fraction. The thus obtained OSL ages agreed with the expected ages for all but one of the samples (Fig. 5.9). Borehole samples from the Katka-A coastal archeological site (NCL-1116-005, 006, and 007), which were expected to be at least 250 a, indeed yielded the oldest ages. Of this subset, the upper sample (NCL-1116007) produced an age of 238 ± 15 a, which agrees with radiocarbon and thermally reset OSL ages for this horizon (Hanebuth et al., 2013). Deeper samples from this borehole (NCL-1116005, and 006) at 2.48 and 4.18 m depths yielded ages of 346 ± 19 and 361 ± 20 a respectively. These are stratigraphically consistent (no inversions) and suggest rapid sedimentation of this river mouth estuary-tidal flat at rates of 2.5 to 4.5 cm/a sustained for roughly a century (Fig. 5.10).

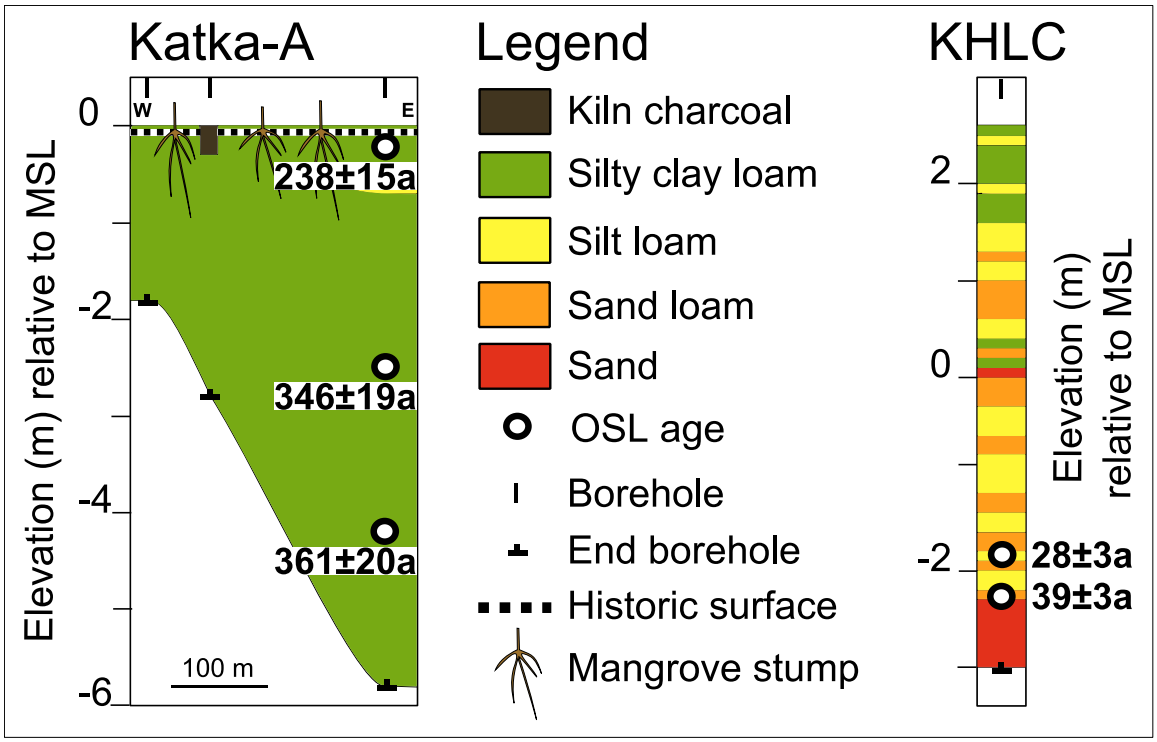

Fig. 5.10. *Katka-A archaeological site cross section and KHLC tidal channel borehole data, showing sediment texture, OSL ages, and other features. Locations are shown in Figure 1. See Hanebuth et al. (2013) for historic and stratigraphic details of this archaeological site. The Katka-A historic surface is an erosional unconformity lined with shell hash, which separates a thin veneer (~1-4 cm) of modern unconsolidated mud above from older consolidated mud below. Mangrove roots are not to horizontal scale.*

Borehole samples from the infilled tidal channel at KHLC (NCL-1116009, and 010) produced ages of 28 ± 3 and 39 ± 3 a at 4.44 and 4.99 m depth respectively (Fig. 5.10). These ages are stratigraphically consistent and agree with anticipated ages for channel infilling at this site, corroborating observations that tidal channel infilling can occur at rates up 20 cm/a over decadal timescales (Wilson et al., in review).

Modern cutbank samples (NCL-1116002, 011, 014) yielded slightly positive, yet near-zero ages of 10 ± 6, 16 ± 10, and 22 ± 7 a. One exception is NCL-1116012 which yielded an age of 177 ± 17 a, significantly older than the 5 ± 5 a expected age based on Google Earth imagery for land emergence at this site. The MS-SAR approach produced a

near-zero BSL age for this sample, and provided no other evidence of insufficient light exposure. We conclude that the anomalous result on this sample is not related to poor resetting, but more likely to experimental problems. There was very little material after etching for this sample (estimated <0.01 g). Only 6 NCL-1116012 aliquots were accepted for age calculation, and the sediment:acetone concentration of these aliquots was poorly controlled due to high relative measurement error and non-standard preparation (pipetting directly from the etching beaker). Based on the discrepancy of the BSL age obtained on etched quartz silt and the MS-SAR BSL obtained on the polymineral silt, in combination with the problems encountered in preparation of this quartz silt, we exclude the results obtained on this sample for further analysis and discussion.

5.7 Discussion

5.7.1 Luminescence sensitivity by provenance and grain size

We find that sands within the delta sourced to both the Ganges and Brahmaputra catchments exhibited poor luminescence sensitivity that precluded quartz OSL dating (Fig. 5.3; Appendix D, Table A.D.2), while sands sourced to the Meghna catchment proved useful for quartz OSL dating (Fig. 5.4, Table 5.3; Appendix D, Table A.D.2). Meghna catchment sand is likely a mixture of both freshly eroded Himalaya sediment with likely poorly sensitized quartz (similar to Ganges and Brahmaputra), and locally-sourced sands eroded from sedimentary rocks by the Kushyara and Surma Rivers which are more likely to have a sensitized quartz BSL signal. The Lower Meghna, which is hydrologically connected to the Meghna catchment, also had a minor population of

acceptable sand grains. Yet, these appear to be highly diluted with unsuitable Ganges- and Brahmaputra-sourced sand by the time they reach the delta front.

Etched quartz silt exhibited suitable luminescence sensitivity for all samples from which sufficient silt was isolated, with no dependency on the provenance of the sediment. We therefore confirm the hypothesis that sand suitability varies by distributary in the GBMD, but reject this hypothesis for quartz silt. We also reject the hypothesis that sand and silt-sized quartz are both poorly sensitized in the GBMD.

Previously reported successes with dating poorly sensitized hinterland sand relied on measurement of large (~7 mm) aliquots (e.g., Mukul et al., 2007, NE Himalaya terrace deposits; Jaiswal et al., 2008, High Himalayan Crystalline sediment; Ray and Srivastava, 2010, Ganges catchment sediment). Our study finds that a similar approach requiring relatively large aliquots and measurement of many disks is necessary to produce sufficient numbers of acceptable sand aliquots for samples that included some suitable sand grains. We note that dating GBMD sand, where possible, is quite expensive in terms of machine time and that measurements on the silt fraction provide a good alternative.

Strontium measured on bulk sediment is a valuable indicator of sand provenance of GBMD sediments, because sandy units tend to be homogenous and well-sorted, so the strontium content of the bulk is representative of individual grains. However, bulk strontium cannot reveal the source of fine silt, which only comprised a small fraction of the bulk sediment (<10%) for most of our samples. Hence, the provenance of the ubiquitous, well-sensitized 4-11 μm silt is a source of speculation; it may be exotic wind-delivered dust, it may be native sediment sourced to the same units as the coarse fractions, or to mudstones within the Meghna catchment.

5.7.2 Luminescence sensitivity upstream to downstream

Research on fluvial sediments from Australia indicates that quartz BSL sensitivity increases during fluvial sediment transport (Pietsch et al., 2008). This sensitization is attributed to ‘maturing’ during repeated cycles of burial during which trapped charge accumulates and exposure during which luminescence is bleached. However, the mechanism is unclear and the timescales of quartz sensitization in fluvial systems are unknown. Our data provide no evidence for sensitization of the quartz BSL signal in sand grains during fluvial transport within the delta. Rather, the best-sensitized quartz sand was sampled in the northeast corner of the delta, as discussed above. This indicates that the timescale for sand transport through this system is less than the timescale for sensitization of quartz here, and suggests a minimum lower limit for quartz BSL sensitization of millennia for GBMD sands.

Quartz silt BSL was found to be sufficiently sensitized throughout the areas where it was sampled, including sites proximal and distal to the coast. However, we observed that mean T_N brightness increased and percent acceptability of silt aliquots improved coastward (Fig. 5.8). These preliminary findings hint that sensitization of silts may occur during transport within the delta.

5.7.3 Degree of bleaching

To obtain accurate depositional ages with luminescence dating, at least a portion of grains must be bleached prior to deposition. Sufficient bleaching of quartz sand has been previously demonstrated for large river systems with long transport distances on the order of 100's of kilometers (Stokes et al., 2001). Bleaching of sands in large rivers is

attributed to storage in bars which affords sediment the opportunity for light exposure (Stokes et al., 2001); this model for bleaching suggests that silts will be less likely to be completely bleached because they may be more rapidly routed through the sediment conduit. Transport within the GBMD should offer many opportunities for bleaching. The transport distance within the delta channel network is on the order of many 100's of kilometers and short-term sequestration of sediment within the braided river system is common via storage in river islands (chars) and bars (Sarker et al., 2003). The majority of these sustain for less than 6 years and 98% have a lifespan less than 26 years in the Brahmaputra (Jamuna) river (Sarker et al., 2003).

The silt measured for this study contained a population of grains that were sufficiently bleached prior to deposition based on near-zero yet positive quartz BSL ages for modern river cutbank samples obtained with the bootstrap unlogged minimum age model. Multi-grain average residual ages of young silt deposits, obtained from the mean and standard error of equivalent dose distributions, were on the order of a few decades. Such offsets are relatively large for these modern deposits, yet can be accommodated with statistical approaches. Our work has shown that ages obtained through different models for analyzing the equivalent dose distribution merge for sediments deposited a few hundred years ago, indicating that any offsets related to heterogeneous bleaching become insignificant at this age range.

We find that sediments that received sufficient bleaching for reliable BSL dating are characterized by BI values of < 2 for pIRIR signals and < 15 for TL signals. This is demonstrated by samples NCL-1116005, 006, 007, 009, and 010 (Fig. 5.5). The application of the BI to samples with unknown depositional ages can provide

confirmation of the well-bleached nature of silt for Holocene sediments, thereby improving confidence in luminescence ages obtained from quartz silt. Further measurements of insufficiently bleached samples are needed to determine the upper threshold of BI values for sufficiently bleached silt.

Tidally reworked samples (NCL-1116009 and 010) do appear to have slightly lower residual doses of pIRIR-155, pIRIR-225, and TL signals than river mouth tidal estuary samples. While the tidally reworked samples are deposited further inland, their total transport distance through the delta may be greater than that of the coastal deposits because they have presumably exited a river-mouth and been redelivered ~100 km inland to the delta plain by tidal processes (Fig. 5.1). Most likely, the transport path of these grains was even much longer due to entrainment by tidal currents, and additional light exposure may have occurred during storage on tidal flats. The dataset in this study has too few data points to make strong conclusions about transport-dependent bleaching using the MS-SAR bleaching analysis; however, this is a promising line of research that we hope can be developed in the future.

Bleaching of sands was difficult to quantify because of the paucity of measurable quartz sand within samples taken from the braided river and tidal region of the delta.

The MS-SAR protocol provides a quick screening of the luminescence sensitivity and bleaching of unetched sediment. This can inform the selection of suitable mineral and grainsize, thereby saving sample preparation and machine time. The bleaching index developed here provides a metric to assess whether resetting of the quartz BSL signal for silt samples could be insufficient. To the best of our knowledge, this is the first tool of its kind that can be used on samples with a wide range of depositional ages. The metric is

designed for Holocene sediments; although it is normalized for age, minute age offsets of a few decades cannot be identified. Hence the BI cannot be applied to modern deposits, where such offsets may be significant relative to the depositional age. For modern deposits, we advocate the use of the BSL ratio presented by Reimann et al. (2015).

5.7.4 Application of luminescence dating to GBMD deposits

Our results indicate that quartz silt is likely to yield accurate OSL ages for GBMD sediments at the majority of locations in the delta. The potential of these findings is highlighted by the results at KHCL, which are consistent with satellite records of land change (Wilson et al., in review) and at Katka-A, which provide the first direct measurements of multi-century-scale accretion rates in the GBMD that reach beyond the ideal decadal scale of ^{210}Pb and avoid the complications of ^{14}C dating (Suckow et al., 2001). Accretion rates based on historical observations and short-lived radioisotopes have been previously reported on the order of cm/yr in the relatively natural forested tidal delta (Rogers et al., 2013) and tens of cm/yr in a breached polder system in the human-modified tidal delta (Auerbach et al., 2015b). However, it was unknown whether high rates of accretion may occur in other settings of the delta at longer timescales and under natural depositional regimes. Further dating is needed to assess if the sedimentation rate documented in the Katka-A borehole represents a discrete phase of aggradation, perhaps driven by local shoreface progradation, which occurs regularly near the active river-mouth (Allison, 1998). Nevertheless, our study establishes the tools and protocol that can be used to test this and other questions about the decadal to millennial scale processes controlling local landscape dynamics and delta evolution. Developing this knowledge

through the application of luminescence dating will be valuable in assessing how the GBDM may fare under future sea level rise scenarios.

5.8 Conclusions

We conclude that GBMD quartz silt has suitable luminescence characteristics including acceptable sensitivity, sufficient bleaching of the quartz OSL signal prior to deposition, and an age range of applicability from a few years up to 24 ka. This finding demonstrates that quartz silt can be used to date the entire Holocene GBMD, where silt is preserved. This is promising for future geochronology research in this delta system, which can help to parse out rates and processes of GBMD evolution and thereby guide delta management for the 21st century and beyond.

The broader implication of this work is that measurement of silt can be used to extend luminescence dating to settings in which it has been historically underused, including other clastics-rich deltas located on active tectonic margins. We encourage others working in regions with questionable or difficult quartz to consider the utility of fine silt, to assess mineral and grain size suitability using a multiple signal approach that screens bleaching and sensitivity, and to validate luminescence protocols through comparison of measured ages to known ages.

5.9 Acknowledgements

Erna Voskuilen and Benny Guralnik of the Netherlands Centre for Luminescence dating assisted with sample preparations and provided insights. We thank Torbjörn Törnqvist of Tulane University for travel support through the Vokes Geology Fund and

comments on an early draft of this manuscript. Field work in Bangladesh and participation of M.S. Steckler was supported through the BanglaPIRE project and Field School (NSF Award IIA 09-68354) and through a CUAHSI Pathfinder Fellowship awarded to E.L. Chamberlain. We acknowledge field contributions and enjoyable discussions with Kazi Matin Ahmed, Syed Humayun Akhter, and students in the Department of Geology at Dhaka University, and Carol Wilson of Louisiana State University. This manuscript benefitted from the comments of two anonymous reviewers.

Appendix A: Anatomy of Mississippi Delta growth and its implications for coastal restoration

A.1. Stratigraphy

Cross sections illustrating the stratigraphy and chronology at all study sites are provided in Fig. A.A.1.

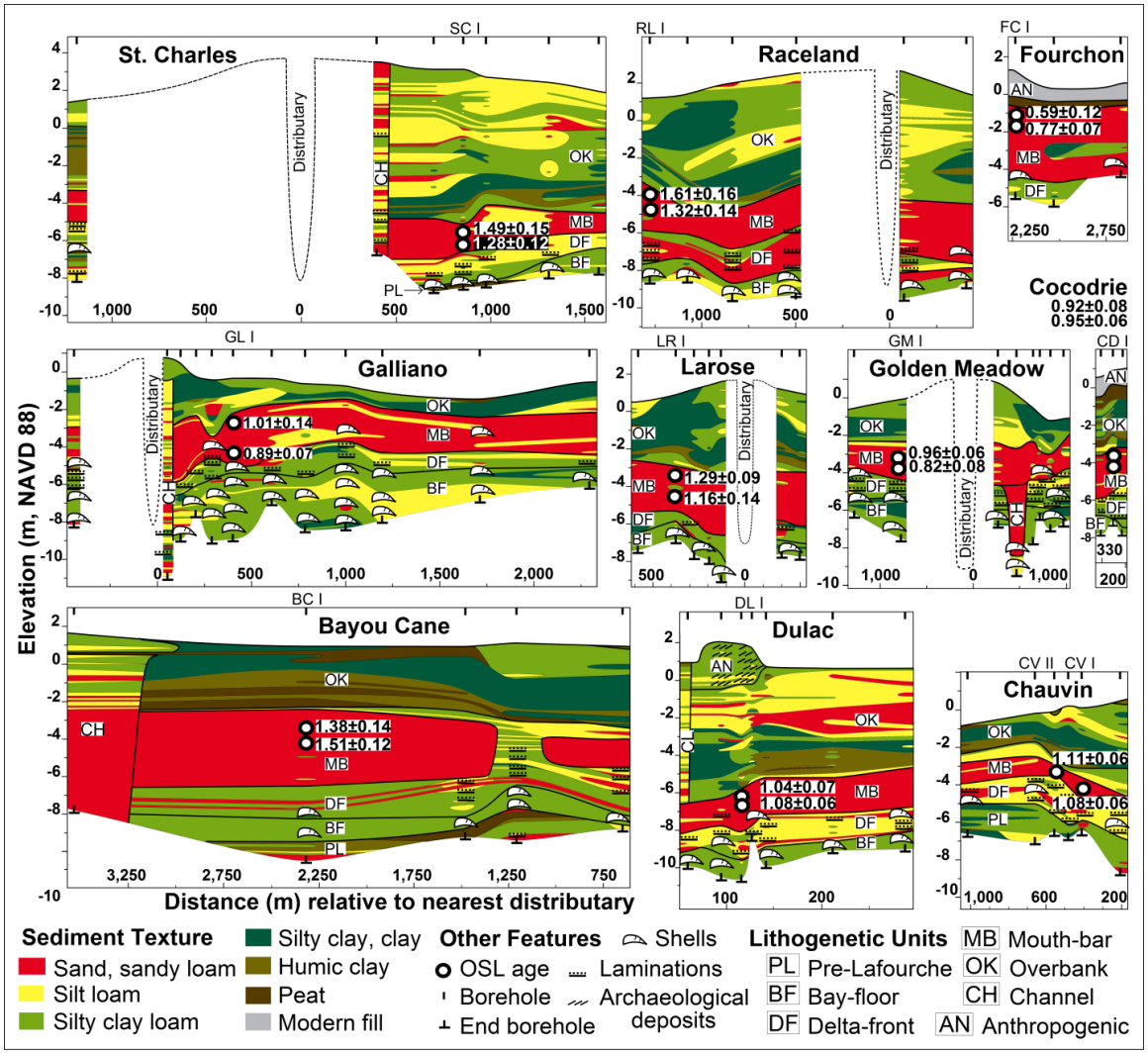

Fig. A.A.1. *Cross sections illustrating the stratigraphy and OSL ages (ka prior to AD 2010) for all study sites. Location and orientation of cross sections are shown in Fig. 1b; the western side is on the left. Distance (in m) is relative to the nearest distributary channel. Deposits underlying the Lafourche bayhead delta that formed in a subaerial setting are referred to as "Pre-Lafourche". One rejected OSL age is shown in white font on a black background.*

A.1.1. Lithogenic unit thicknesses

The thickness of lithogenetic units was calculated as the average thickness obtained for all the boreholes in each cross section, based on the upper and lower limits of stratigraphic features that define the overbank, mouth-bar, and delta-front deposits. Lithogenetic unit definitions are provided in Table A.A.1. The bayhead-delta deposits include the overbank, mouth-bar, and delta-front deposits. The foundation deposits include the mouth-bar plus delta-front deposits.

The boundaries between lithogenetic units are generally very clear, and boreholes were excluded from the analysis if boundaries were unclear or anomalous (e.g., unconformities due to channel scour). Boreholes from the Bayou Cane (n=1) and the Galliano (n=2) cross sections were excluded from average lithogenetic unit thickness calculations for these reasons. The average thickness and associated standard deviation of lithogenetic units was determined for each cross section (Fig. 2.4, Fig. A.A.2), with 2% uncertainty added for non-vertical drilling. Non-vertical drilling can only increase the observed depth (i.e., it is an asymmetric error). This was addressed by reporting 99% of the measured depth and adding 1% of this depth to the uncertainty. Delta-front, mouth-bar, and foundation deposits of the main and lesser distributary cross sections were found to have comparable thicknesses (Fig. A.A.2). Thicknesses of overbank deposits at the Fourchon and Dulac cross sections were corrected to remove the contributions from anthropogenic fill.

Table A.A.1. *Characterization of lithogenetic units. Lithogenetic units were recognized on the basis of sediment texture, sedimentary structures and other features identified in the cores.*

Lithogenetic unit	**Dominant sediment texture**	**Sedimentary structures and other features**
Channel deposits	Sand, sandy loam	Sandier toward center of channel belt, clay laminations
Overbank deposits (natural-levee, crevasse-splay, and flood-basin deposits)	Silty clay loam, silt loam, silty clay, clay, humic clay, peat	Highly variable, may contain wood and herbaceous material
Mouth-bar deposits	Sand (very fine to medium)	Homogenous
Delta-front deposits	Clay, silty clay, silty clay loam, silt loam	Laminations, reworked organics, coarsening-upward
Bay-floor deposits	Clay, silty clay, silty clay loam	*Rangia cuneata*, storm-reworked layers of shell hash
Anthropogenic fill	Highly variable	Gravel, shells, unconsolidated dredge spoil, modern garbage (glass, plastic)
Pre-Lafourche subaerial deposits	Humic clay, peat, silty clay, silty clay loam, silt loam, sand	Relatively consolidated clastic or organic deposits, wood and herbaceous material, stratigraphically below delta-front or bay-floor deposits

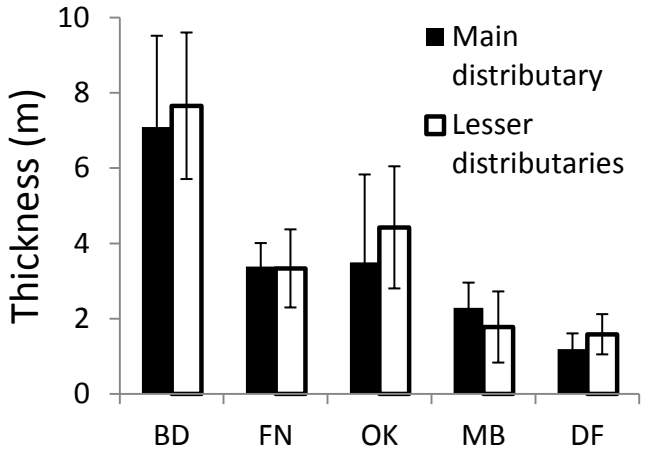

Fig. A.A.2. *Thickness of lithogenetic units at main and lesser distributary cross sections. Comparison of the thickness of overbank (OK), mouth-bar (MB), and delta-front (DF) as well as the interpreted bayhead-delta (BD) and foundation (FN) deposits. Also see Table A.A.3 for more detailed data.*

Table A.A.2. *Borehole information. Location, depth, elevation, and sample depth for all boreholes included in this study.*

Cross section	Borehole number	x UTM (NAD 83)	y UTM (NAD 83)	UTM Zone	Borehole depth (m)	Surface elevation (m, NAVD 88)	OSL samples
St. Charles	601493.028	717560	3293120	15 N	9.5	1.4	
St. Charles	601493.022	717410	3294740	15 N	10.1	3.5	
St. Charles	601493.026	717560	3295010	15 N	11.8	3.1	
St. Charles	601493.027	717630	3295150	15 N	11.6	3.1	SC I-1 (890-895 cm), SC I-2 (920-925 cm)
St. Charles	601493.025	717690	3295260	15 N	11.1	2.7	
St. Charles	601493.024	717840	3295560	15 N	10.3	2.4	
St. Charles	601492.023	717970	3295800	15 N	9.6	1.9	
Raceland	601393.014	732550	3289450	15 N	9.8	1.2	RL I-1 (530-543 cm), RL I-2 (563-574 cm)
Raceland	601393.013	732680	3289620	15 N	9.9	1.4	
Raceland	601393.012	732830	3289810	15 N	11.5	2.0	
Raceland	601393.011	733040	3290070	15 N	11.8	2.5	
Raceland	601393.015	733300	3290590	15 N	12.1	2.6	
Raceland	601393.016	733570	3290810	15 N	10.2	1.4	
Larose	601493.013	748960	3274950	15 N	7.9	0.5	
Larose	601493.012	749020	3275160	15 N	7.7	0.9	LR I-1 (420-435 cm), LR I-2 (535-540 cm)
Larose	601493.011	749050	3275250	15 N	8.8	1.2	
Larose	601493.010	749070	3275330	15 N	9.3	1.4	
Larose	601493.009	749090	3275390	15 N	10.6	1.6	
Larose	601493.014	749990	3275550	15 N	8.8	1.2	
Larose	601494.015	750010	3275640	15 N	8.7	1.0	
Galliano	601393.018	761070	3260970	15 N	7.8	-0.3	
Galliano	601393.017	761570	3260960	15 N	11.7	0.8	
Galliano	601393.007	761640	3260990	15 N	9.4	0.5	
Galliano	601393.006	761710	3261010	15 N	7.3	-0.2	

Table A.A.2. *Continued.*

Galliano	601393.005	761790	3261040	15 N	8.6	-0.4	
Galliano	601393.001	761900	3261070	15 N	8.6	-0.3	GL I-1 (315-320 cm), GL I-2 (380-385 cm)
Galliano	601393.004	762090	3261150	15 N	6.6	-0.3	
Galliano	601393.002	762260	3261210	15 N	7.8	-0.6	
Galliano	601393.003	762460	3261290	15 N	7.6	-0.7	
Galliano	601393.008	762640	3261370	15 N	6.8	-1.1	
Galliano	601393.009	763130	3261560	15 N	5.4	-1.4	
Galliano	601393.010	763680	3261770	15 N	5.6	-0.5	
Golden Meadow	601493.002	763700	3256590	15 N	5.5	-0.6	
Golden Meadow	601493.001	763180	3256650	15 N	7.4	-0.1	GM I-1 (345-355 cm), GM I-2 (352-358 cm)
Golden Meadow	601493.008	764210	3256820	15 N	7.6	0.8	
Golden Meadow	601493.007	764350	3256960	15 N	9.6	0.2	
Golden Meadow	601493.003	764480	3257070	15 N	7.2	-0.5	
Golden Meadow	601493.005	764520	3257120	15 N	5.4	-0.8	
Golden Meadow	601493.004	764610	3257200	15 N	5.8	-1.2	
Golden Meadow	601493.006	764720	3257310	15 N	5.5	-1.1	
Fourchon	601493.016	772510	3227620	15 N	6.7	1.3	FC I-1 (240-258 cm), FC I-2 (266-281 cm)
Fourchon	601493.017	772730	3227670	15 N	6.2	0.3	
Fourchon	601493.018	773090	3227810	15 N	4.9	0.6	
Bayou Cane	601593.002	713950	3278720	15 N	9.4	1.6	
Bayou Cane	601593.001	714880	3279540	15 N	11.4	0.9	BC I-1 (450-455 cm), BC I-2 (475-480 cm)

Table A.A.2. *Continued.*

Bayou Cane	601493.021	715530	3280080	15 N	10.1	0.9	
Bayou Cane	601493.019	715730	3280270	15 N	10.5	2.5	
Bayou Cane	601493.020	716300	3280310	15 N	9.7	0.9	
Dulac	601593.010	723165	3257425	15 N	10.8	0.9	
Dulac	601593.008	723205	3257425	15 N	12.5	2.0	
Dulac	601593.007	723225	3257430	15 N	12.5	1.9	DL I-1 (840-848 cm), DL I-2 (863-868 cm)
Dulac	601593.003	723235	3257425	15 N	10.0	1.7	
Dulac	601593.006	723250	3257420	15 N	10.6	0.7	
Dulac	601593.004	723320	3257430	15 N	9.7	0.6	
Dulac	601593.009	723400	3257430	15 N	9.6	0.6	
Chauvin	601593.013	732580	3260770	15 N	5.8	-0.8	
Chauvin	601593.012	732940	3260670	15 N	6.8	-0.2	
Chauvin	601593.016	733030	3260630	15 N	6.4	-0.1	CV II-1 (317-323 cm)
Chauvin	601593.015	733110	3260610	15 N	7.0	0.2	
Chauvin	601593.014	733170	3260590	15 N	6.5	0.1	CV I-1 (440-445 cm)
Chauvin	601593.011	733370	3260520	15 N	9.2	0.5	
Cocodrie	601593.018	727240	3238530	15 N	8.4	0.0	
Cocodrie	601593.019	727300	3238520	15 N	8.0	0.9	CD I-1 (470-477 cm), CD I-2 (488-498 cm)
Cocodrie	601593.023	727350	3238520	15 N	8.8	1.0	

Table A.A.3. *Lithogenetic unit thickness. Average thickness (uncertainty represents one standard deviation) of the bayhead-delta, foundation, overbank, mouth-bar, and delta-front deposits for each cross section. Distances from the polyfurcation point (PP) are shown in river kilometers.*

Transect	**Distance from PP (river km)**	**Bore-holes (n)**	**Bayhead-delta deposits (m)**	**Foundation deposits (m)**	**Overbank deposits (m)**	**Mouth-bar deposits (m)**	**Delta-front deposits (m)**
Main Dist-ributary	**n.a.**	**42**	**7.1 ± 2.4**	**3.4 ± 0.6**	**3.5 ± 2.3**	**2.3 ± 0.7**	**1.2 ± 0.4**
St. Charles	9	7	9.6 ± 1.9	2.9 ± 0.8	6.7 ± 1.4	1.7 ± 0.5	1.2 ± 0.4
Raceland	26	6	9.8 ± 1.2	3.8 ± 0.7	5.9 ± 0.9	2.2 ± 0.5	1.6 ± 0.5
Larose	51	7	7.8 ± 0.6	3.6 ± 0.3	4.2 ± 0.7	2.7 ± 0.2	0.8 ± 0.1
Galliano	72	11	5.1 ± 1.1	3.4 ± 0.5	1.7 ± 0.8	2.4 ± 0.8	1.1 ± 0.3
Golden Meadow	77	8	5.2 ± 0.8	3.2 ± 0.4	2.1 ± 0.7	1.8 ± 0.4	1.4 ± 0.4
Fourchon	110	3	n.a.	n.a.	0.5 ± 0.2	3.8 ± 0.2	n.a.
Lesser Dist-ributaries	**n.a.**	**20**	**7.7 ± 1.9**	**3.3 ± 1.0**	**4.4 ± 1.6**	**1.8 ± 0.9**	**1.6 ± 0.5**
Bayou Cane	20	4	8.6 ± 0.9	4.9 ± 1.1	4.0 ± 0.9	2.9 ± 1.3	2.0 ± 0.4
Dulac	48	7	9.5 ± 0.8	3.3 ± 0.5	6.1 ± 0.7	2.1 ± 0.3	1.3 ± 0.4
Chauvin	51	6	5.6 ± 1.2	2.4 ± 0.3	3.2 ± 1.1	0.8 ± 0.4	1.7 ± 0.5
Cocodrie	75	3	6.9 ± 0.6	3.6 ± 0.5	3.3 ± 0.2	2.0 ± 0.1	1.5 ± 0.4
All boreholes	**n.a.**	**62**	**7.3 ± 2.3**	**3.4 ± 0.8**	**3.8 ± 2.2**	**2.1 ± 0.8**	**1.3 ± 0.5**

A.2. OSL dating

The measurement protocol (Table A.A.4), values for overdispersion (Table A.A.5) obtained with the central age model (CAM) (Galbraith et al., 1999), and dose rate details and paleodoses (Table A.A.6) are provided here. Details of the OSL analyses, and comparison of ages with those produced using different methods are also discussed. While samples for this project were collected between 2013-2016, OSL ages are reported relative to 2010, to be consistent with previous, closely related work (Shen et al., 2015; Hijma et al., 2017).

A.2.1. Sample exclusions and additions to analyses

Of the 20 samples measured for this project, one (Galliano I-2) was excluded from the overdispersion analysis (Table A.A.5) because of inconsistent mask size. Two grain size fractions of St. Charles I-2 were included in the overdispersion analysis. Three samples of 75-125 μm quartz sand sampled at the Dulac cross section and measured for a separate project (Dulac I-3, Dulac I-4, Dulac I-5) were included in the overdispersion analysis to increase the data available for this grain size fraction.

A.2.2. Cleaning of outlying aliquots

Cleaning of D_e datasets was tested to remove outlying aliquots beyond 4, 3, and 2 standard deviations from the sample mean (Fig. A.A.3). Samples Galliano I-1 and Galliano I-2 were excluded from the cleaning analysis because of variable aliquot sizes. We found that a 4 standard deviation cleaning was optimal for treatment of the D_e datasets prior to input into CAM for overdispersion quantification, because this removed 1% of aliquots which were exclusively high-D_e outliers. Prior to input into the bootstrap minimum age model (BootMAM) (Galbraith et al., 1999; Cunningham and Wallinga, 2012) for paleodose estimation, a 3 standard deviation cleaning was applied. This removed 6% of the total aliquots. Of the aliquots removed by a 3 standard deviation cleaning, 99% were high-D_e aliquots which likely do not represent the depositional age of the sediments, and 1% were low-D_e aliquots. We found that a 2 standard deviation cleaning removed 24% of aliquots comprised of 82% high-D_e and 18% low-D_e aliquots. This was deemed to be too much lost information.

A.2.3. Sample rejection

The D_es of two grain size fractions (75-125 and 125-180 μm) of St. Charles I-2 were measured because the coarser (125-180 μm) fraction of sediment was found, after measurements, to have too little material to produce a sufficient number of D_es for reliable age model statistics. Both fractions of St. Charles I-2 produced ages that agreed with the age of another sample from the same unit (St. Charles I-1) within 2σ unshared uncertainty. Yet, St. Charles I-2 ages were younger than expected given their stratigraphic context, regardless of the burial dose estimation approach. Therefore, we rejected St. Charles I-2 and used only one sample (St. Charles I-1) to define the timing of land emergence at this cross section.

A.2.4. Comparison with a previous approach

This study employed OSL dating methods based on the newest insights (Cunningham and Wallinga, 2010, 2012) with regard to dating young fluvial sediments. As such, the methods used in this study differ from methods used previously to date late Holocene Mississippi Delta deposits (Shen et al., 2015; Hijma et al., 2017) in terms of background integration interval, aliquot acceptance criteria, cleaning of aliquots, age model usage, and radionuclide conversion factors applied to dose rate calculations (Table A.A.7). To facilitate comparisons of mouth-bar sand ages produced by this study with previously published ages for Mississippi Delta deposits, we also analyzed the mouth-bar samples using methods applied by previous work (Shen et al., 2015; Hijma et al., 2017). Mouth-bar sand ages produced with both approaches agreed within 1σ unshared uncertainty (see Methods), with the exception of Cocodrie I-2 (Fig. A.A.4; Table A.A.8).

Similarly, all weighted mean ages agreed between the two approaches, with the exception of the Cocodrie cross section (river km 75). However, the ages produced with the present approach were systematically lower than those calculated using the previous approach, for the majority (18 out of 21) of the grain size fractions measured for this study. Weighted mean ages produced with the present approach were lower than those produced with the previous approach for all cross sections except for the Fourchon cross section, where the weighted means obtained with both approaches were nearly identical (Fig. A.A.4; Table A.A.8). The average age offset between the two approaches was 70 ± 20 years, calculated as the mean and standard error of the previous approach ages minus the present approach ages. This offset is largely related to improved sampling of the fast OSL component through the early background approach, which avoids age overestimation due to incorporation of other, lesser bleached, OSL components (Cunningham and Wallinga, 2010). Ages produced for this study using the present approach were also characterized by larger uncertainties for samples with limited numbers or irregularly dispersed D_es at the aliquot level. The increased uncertainty proved to be a major advantage in calculating ages for each cross section using a weighted mean of paired ages, because it awards greater representation to the high precision ages, which are also the ages most likely to be correct due to robust D_e datasets.

Table A.A.4. *Details of the SAR protocol.*

Step	Treatment	Details
1	Dose	Natural, 3-4 regenerative doses (2.5 to 15 Gy)*, recuperation (0 Gy), recycling (2.5 to 5 Gy)*, recycling (2.5 to 5 Gy)*
2	Preheat	200 or 220 °C for 10 s*
3	OSL	125 °C for 40 s
4	Test dose	4-5 Gy*
5	Cutheat	180 °C for 0 s
6	OSL	125 °C for 40 s
*the protocol evolved with this project, and so a range of values are provided		

Table A.A.5. *Overdispersion details, lab codes, and sample collection years, and name abbreviations as used in Fig. A.A.3. LV = University of Liverpool lab code.*

Sample name	**LV code**	**Sample collection year**	**OD (%)**
75 - 125 µm			
Saint Charles (SC) I-2	LV772	2015	23.0 ± 2.1
Dulac (DL) I-5	LV802	2015	20.0 ± 2.2
Dulac (DL) I-4	LV803	2015	17.5 ± 2.2
Golden Meadow (GM) I-2	LV729	2014	15.5 ± 2.6
Chauvin (CV) I-1	LV778	2015	10.5 ± 1.2
Dulac (DL) I-3	LV804	2015	9.6 ± 1.6
Chauvin (CV) II-1	LV780	2015	9.6 ± 1.1
125-180 µm			
Larose (LR) I-2	LV731	2014	75.1 ± 7.8
St. Charles (SC) I-1	LV771	2015	54.2 ± 6.9
Larose (LR) I-1	LV730	2014	53.0 ± 5.3
Bayou Cane (BC) I-2	LV773	2015	44.2 ± 4.2
Galliano (GL) I-1	LV658	2013	43.6 ± 7.5
Saint Charles (SC) I-2	LV772	2015	42.1 ± 6.8
Raceland (RL) I-1	LV724	2013	40.1 ± 4.4
Raceland (RL) I-2	LV725	2013	40.0 ± 4.5
Bayou Cane (BC) I-1	LV774	2015	35.5 ± 3.3
Fourchon (FC) I-1	LV727	2014	32.1 ± 4.5
Golden Meadow (GM) I-1	LV728	2014	29.1 ± 4.4
Fourchon (FC) I-2	LV726	2014	25.9 ± 4.7
Cocodrie (CD) I-2	LV776	2015	18.1 ± 2.3
Cocodrie (CD) I-1	LV777	2015	16.7 ± 1.8
Dulac (DL) I-1	LV801	2015	10.1 ± 1.2
Dulac (DL) I-2	LV800	2015	7.7 ± 1.3

Table A.A.6. *Dose rate details and paleodose. Dose rate parameters include water content, grain size, activities of isotopes derived from the uranium (U) and thorium (Th) chain, and from potassium (40K), the internal dose rate of quartz (Q internal), and the cosmogenic dose rate (D cosm.). The calculated dose rate (D) is given here.*

Sample name	Water content (%)	Grain size (µm)	U (Bq/kg)	Th (Bq/kg)	K (Bq/kg)	Q internal (Gy/ka)	D cosm. (Gy/ka)	D (Gy/ka)	Paleo-dose (Gy)
Bayou Cane I-1	23 ± 5	125-180	30.14 ± 0.60	27.46 ± 0.38	536.46 ± 13.91	0.03 ± 0.02	0.11 ± 0.01	2.18 ± 0.11	3.00 ± 0.26
Bayou Cane I-2	21 ± 5	125-180	32.28 ± 0.65	29.15 ± 0.43	497.93 ± 13.12	0.03 ± 0.02	0.10 ± 0.01	2.22 ± 0.11	3.34 ± 0.20
Cocodrie I-1	21 ± 5	125-180	28.83 ± 0.58	26.74 ± 0.40	444.58 ± 11.78	0.03 ± 0.02	0.10 ± 0.01	2.00 ± 0.08	1.83 ± 0.14
Cocodrie I-2	24 ± 5	125-180	33.89 ± 0.68	29.75 ± 0.45	502.08 ± 13.27	0.03 ± 0.02	0.10 ± 0.01	2.17 ± 0.10	2.05 ± 0.06
Chauvin I-1	22 ± 5	75-125	47.51 ± 0.91	41.82 ± 0.53	499.35 ± 13.04	0.03 ± 0.02	0.11 ± 0.01	2.59 ± 0.14	2.79 ± 0.06
Chauvin II-1	27 ± 5	75-125	41.12 ± 0.81	36.03 ± 0.51	542.01 ± 14.26	0.03 ± 0.02	0.13 ± 0.01	2.39 ± 0.12	2.64 ± 0.06
Dulac I-1	22 ± 5	125-180	36.78 ± 0.72	31.75 ± 0.45	523.33 ± 13.73	0.03 ± 0.02	0.05 ± 0.01	2.29 ± 0.12	2.37 ± 0.09
Dulac I-2	22 ± 5	125-180	33.60 ± 0.67	29.48 ± 0.42	507.03 ± 13.28	0.03 ± 0.02	0.05 ± 0.01	2.18 ± 0.10	2.34 ± 0.07
Fourchon I-1	20 ± 5	125-180	18.56 ± 0.41	17.01 ± 0.32	471.00 ± 12.49	0.03 ± 0.02	0.15 ± 0.02	1.82 ± 0.07	1.09 ± 0.21
Fourchon I-2	21 ± 5	125-180	17.65 ± 0.40	16.30 ± 0.34	466.52 ± 12.58	0.03 ± 0.02	0.14 ± 0.01	1.77 ± 0.07	1.39 ± 0.10

Table A.A.6. *Continued.*

Galliano I-1	19 ± 5	125-180	23.65 ± 0.57	21.24± 0.54	484.02 ± 13.13	0.03 ± 0.02	0.10 ± 0.01	1.98 ± 0.09	2.00 ± 0.25
Galliano I-2	19 ± 5	125-180	34.02 ± 0.76	34.68 ± 0.84	468.42 ± 12.78	0.03 ± 0.02	0.12 ± 0.01	2.29 ± 0.11	2.06 ± 0.14
Golden Meadow I-1	22 ± 5	125-180	27.37 ± 0.57	25.78 ± 0.41	504.74 ± 13.37	0.03 ± 0.02	0.13 ± 0.01	2.06 ± 0.09	2.01 ± 0.09
Golden Meadow I-2	24 ± 5	75-125	36.24 ± 0.75	31.88 ± 0.52	550.30 ± 14.76	0.03 ± 0.02	0.13± 0.01	2.34 ± 0.12	1.93 ± 0.16
Larose I-1	23 ± 5	125-180	23.76 ± 0.50	22.26 ± 0.38	511.85 ± 13.56	0.03 ± 0.02	0.11 ± 0.01	1.96 ± 0.08	2.55 ± 0.14
Larose I-2	27 ± 5	125-180	36.68 ± 0.77	34.07 ± 0.58	579.71 ± 15.68	0.03 ± 0.02	0.09 ± 0.01	2.29 ± 0.11	2.69 ± 0.30
Raceland I-1	18 ± 5	125-180	18.21 ± 0.40	18.61 ± 0.34	419.67 ± 11.25	0.03 ± 0.02	0.09 ± 0.01	1.72 ± 0.07	2.79 ± 0.25
Raceland I-2	20 ± 5	125-180	32.37 ± 0.65	31.08 ± 0.45	478.01 ± 12.59	0.03 ± 0.02	0.09 ± 0.01	2.17 ± 0.10	2.90 ± 0.27
St. Charles I-1	21 ± 5	125-180	37.89 ± 0.75	38.28 ± 0.56	476.81 ± 12.65	0.03 ± 0.02	0.05 ± 0.01	2.29 ± 0.11	3.42 ± 0.30
St. Charles I-2	23 ± 5	75-125	41.75 ± 0.83	39.06 ± 0.60	540.39 ± 14.40	0.03 ± 0.02	0.05 ± 0.01	2.50 ± 0.14	2.79 ± 0.20
St. Charles I-2	23 ± 5	125-180	41.75 ± 0.83	39.06 ± 0.60	540.39 ± 14.40	0.03 ± 0.02	0.05 ± 0.01	2.46 ± 0.13	3.15 ± 0.22

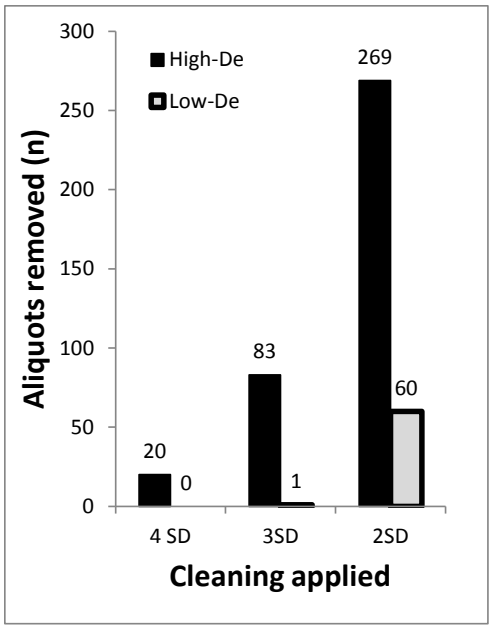

Fig. A.A.3. *Number of aliquots removed by cleaning with 4, 3, and 2 standard deviations (SD).*

Table A.A.7. *Experimental details of the approach used in the present study versus the approach used by previous studies (Shen et al., 2015; Hijma et al., 2017) that applied OSL dating to Holocene Mississippi Delta deposits.*

Aliquot equivalent doses	**This study**	**Previous studies**
Signal (s)	first 0.48	first 0.48
Background (s)	0.48-1.76	32-40
Use recycled points for fitting	no	yes
Force curve through origin	yes	no
Measurement error (%)	1.7	1.7
Monte Carlo uncertainty[a]	yes, x1000	no
Use errors when applying criteria	yes	no
IR depletion test	10%	10%
Maximum test dose error	20%	no
Maximum paleodose error	no	no
Maximum recuperation	5% (% largest R)	5% (% N)
Tn >3sigma above BG	no	no
Age model usage		
Cleaning of aliquot datasets	3 standard deviations	applied 'as needed'
Age model	bootMAM	MAM or CAM
Overdispersion input to age model	11 ± 4% (128-180 µm), 11 ± 3% (75-125 µm)	10% for all sand grain sizes
Include error on overdispersion	yes	no
Dose rate calculations		
Radionuclide conversion factors	Guérin et al. (2011)	Adamiec and Aitken (1998)
[a] (Duller, 2016)		

Fig. A.A.4. *Comparison of mouth-bar sand ages estimated using the present OSL dating approach versus ages estimated for the same samples using previously published methods. Weighted mean ages with their unshared uncertainties for each cross section are shown versus distance from the polyfurcation point. The ages at Fourchon (river km 110) are nearly identical, although the uncertainty is higher with the present approach.*

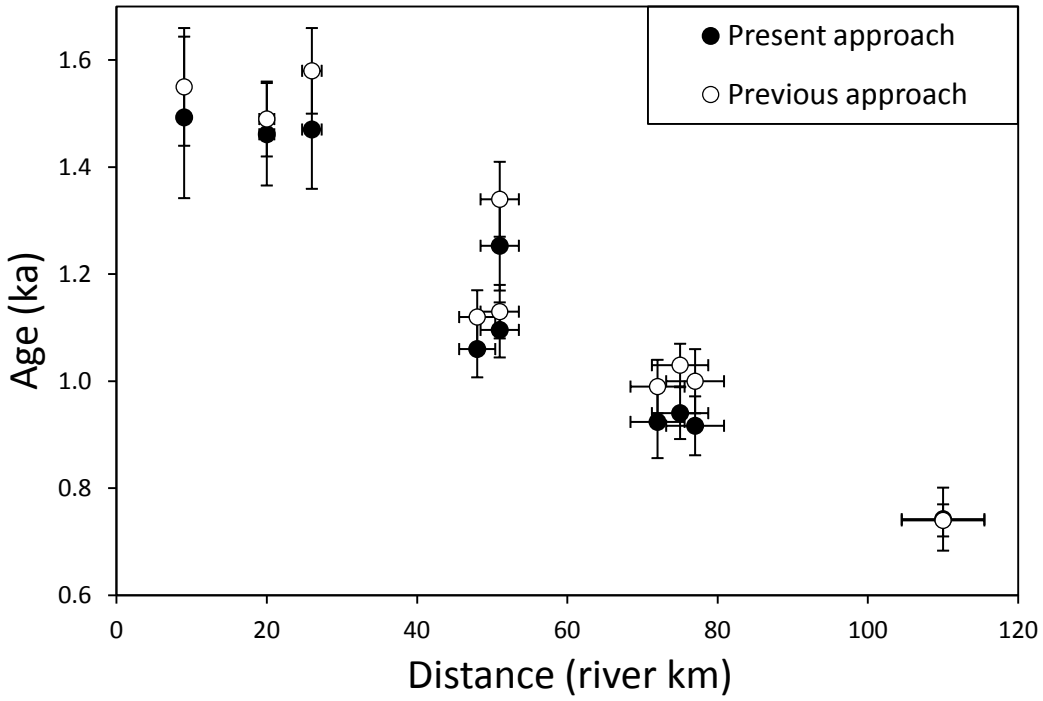

Table A.A.8. *Comparison of OSL ages and uncertainty produced with the present approach versus the previously used approach. Red numbers indicate rejected ages.*

Transect	**River Km**	**Sample name**	**Present approach**		**Previous approach**		**Age,$_{Previous}$ - Age,$_{Present}$**
			Age (ka)	**Weighted mean (ka)**	**Age (ka)**	**Weighted mean (ka)**	**Age difference (ka)**
St. Charles	9	SC I-1	1.49 ± 0.15	1.49 ± 0.15	1.55 ± 0.11	1.55 ± 0.11	0.06 ± 0.19
		SC I-2[a]	1.12 ± 0.10		1.24 ± 0.08		0.13 ± 0.08
		SC I-2[b]	1.28 ± 0.12		1.14 ± 0.10		-0.14 ± 0.10
Bayou Cane	20	BC I-2	1.51 ± 0.12	1.46 ± 0.10	1.44 ± 0.09	1.49 ± 0.07	-0.07 ± 0.13
		BC I-1	1.38 ± 0.14		1.52 ± 0.09		0.14 ± 0.09
Raceland	26	RL I-1	1.61 ± 0.16	1.47 ± 0.11	1.62 ± 0.11	1.58 ± 0.08	0.01 ± 0.16
		RL I-2	1.32 ± 0.14		1.54 ± 0.11		0.22 ± 0.11
Dulac	48	DL I-2	1.08 ± 0.06	1.06 ± 0.05	1.12 ± 0.06	1.12 ± 0.05	0.04 ± 0.08
		DL I-1	1.04 ± 0.07		1.11 ± 0.06		0.07 ± 0.06
Larose	51	LR I-1	1.29 ± 0.09	1.25 ± 0.08	1.38 ± 0.08	1.34 ± 0.07	0.10 ± 0.12
		LR I-2	1.16 ± 0.14		1.29 ± 0.09		0.13 ± 0.09
Chauvin	51	CV I-1	1.08 ± 0.06	1.10 ± 0.05	1.11 ± 0.06	1.13 ± 0.05	0.03 ± 0.08
		CV II-1	1.11 ± 0.06		1.14 ± 0.06		0.03 ± 0.06
Galliano	72	GL I-2	0.89 ± 0.07	0.92 ± 0.07	0.96 ± 0.07	0.99 ± 0.05	0.07 ± 0.10
		GL I-1	1.01 ± 0.14		1.02 ± 0.07		0.01 ± 0.07
Cocodrie	75	CD I-2	0.95 ± 0.06	0.94 ± 0.05	1.05 ± 0.06	1.03 ± 0.04	0.10 ± 0.08
		CD I-1	0.92 ± 0.08		1.02 ± 0.05		0.10 ± 0.05
Golden Meadow	77	GM I-1	0.96 ± 0.06	0.92 ± 0.06	1.07 ± 0.06	1.00 ± 0.06	0.11 ± 0.08
		GM I-2	0.82 ± 0.08		0.93 ± 0.06		0.12 ± 0.06
Fourchon	110	FC I-2	0.77 ± 0.07	0.74 ± 0.06	0.75 ± 0.04	0.74 ± 0.03	-0.02 ± 0.07
		FC I-1	0.59 ± 0.12		0.73 ± 0.03		0.14 ± 0.03
[a]75-125 µm, [b]125-180 µm							

Appendix B: The inconvenient truth of fresh sediment: Insights from a new method for quantifying subsidence in the Mississippi Delta

Table A.B.1. *Stratigraphic, location, and chronologic data for St. Charles (SC), Raceland (RL), Larose (LR) Galliano (GL), Golden Meadow (GM), Fourchon (FC), Bayou Cane (BC), Dulac (DL), Chauvin (CV), Cocodrie (CD) and Paincourtville (PV) localities.*

Cross section	**SC**	**RL**	**LR**	**GL**	**GM**	**FC**	**BC**	**DL**	**CV**	**CD**	**PV[a]**
Boreholes (n, total)	7	6	7	12	8	3	5	7	6	3	103
Boreholes (n, accepted)	6	6	7	10	8	3	3	7	6	3	103
Distance from Donaldsonville (river km)	64	82	106	127	132	165	75	103	106	130	17
Holocene thickness (m)	43	46	37	40	40	49	38	58	58	61	44
Age (ka)	1.49 ± 0.15	1.47 ± 0.11	1.25 ± 0.08	0.92 ± 0.07	0.92 ± 0.06	0.74 ± 0.06	1.46 ± 0.10	1.06 ± 0.05	1.10 ± 0.05	0.94 ± 0.05	1.50 ± 0.05
Sedimentation time (ka)	0.89 ± 0.15	0.87 ± 0.11	0.65 ± 0.08	0.32 ± 0.07	0.32 ± 0.06	0.14 ± 0.06	0.86 ± 0.10	0.46 ± 0.05	0.50 ± 0.05	0.34 ± 0.05	0.90 ± 0.05
Cumulative subsidence (m)	2.89 ± 0.78	2.75 ± 0.71	1.88 ± 0.49	1.13 ± 0.53	1.46 ± 0.47	-0.18 ± 0.40	1.76 ± 0.91	4.34 ± 0.71	2.11 ± 0.83	2.50 ± 0.35	1.66 ± 1.33
Subsidence rate (mm/yr)	1.93 ± 0.54	1.87 ± 0.49	1.50 ± 0.41	1.22 ± 0.59	1.59 ± 0.52	-0.25 ± 0.54	1.21 ± 0.63	4.10 ± 0.70	1.93 ± 0.77	2.66 ± 0.37	2.75 ± 2.25
Overbank thickness (m)	6.73 ± 1.36	5.92 ± 0.91	4.20 ± 0.73	1.66 ± 0.77	2.07 ± 0.71	0.46 ± 0.16	3.99 ± 0.87	6.63 ± 1.15	3.18 ± 1.14	3.33 ± 0.21	7.00 ± 5.00
[a]Törnqvist et al. (2008)											

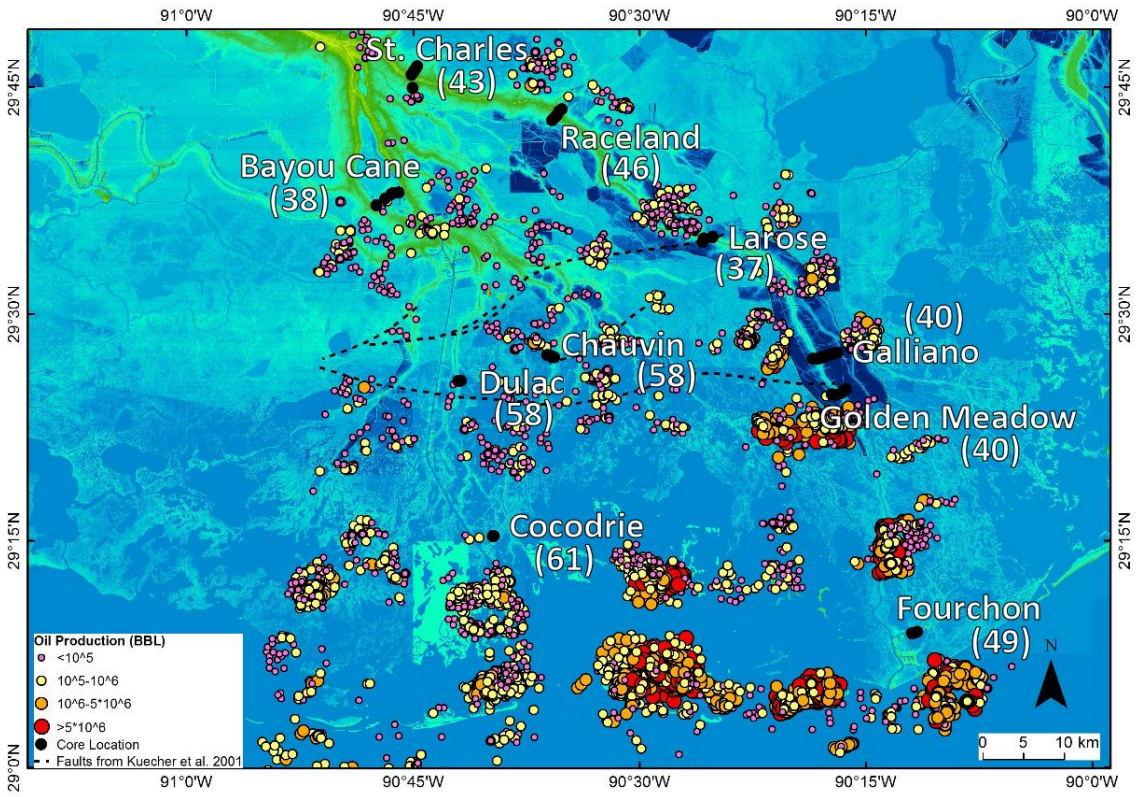

Fig. A.B.1. *Location relative to study sites and values for oil (billions of barrels) extracted from 1977-2015 in the Lafourche subdelta.*

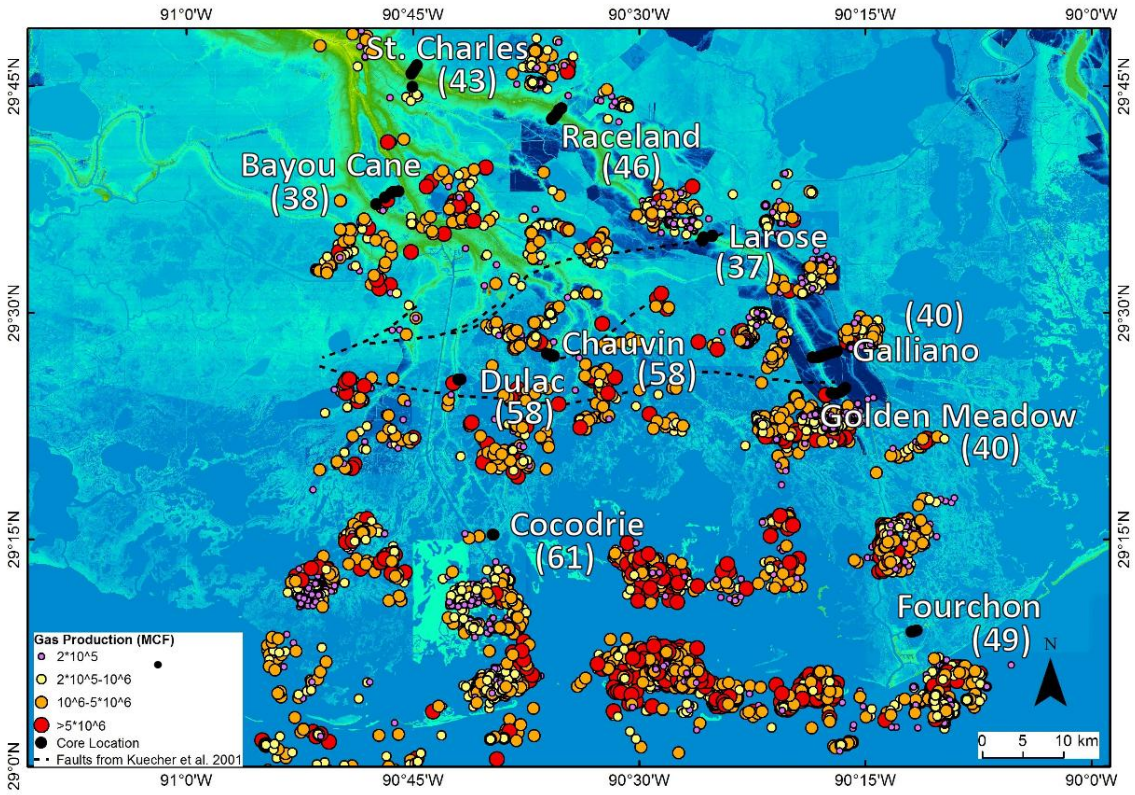

Fig. A.B.2. *Locations relative to study sites and values for gas (million cubic feet) extracted from 1977-2015 in the Lafourche subdelta.*

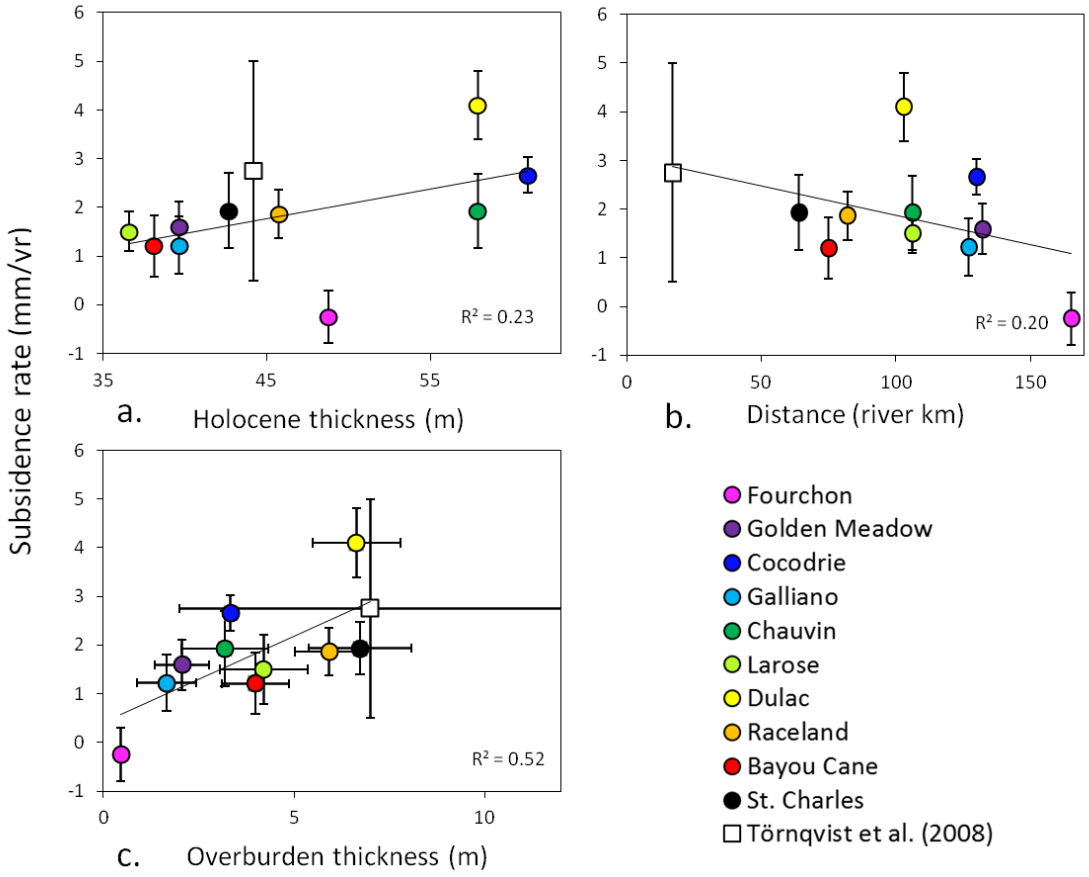

Fig. A.B.3. *Subsidence rates and their relationship to (a) thickness of Holocene deposits, (b) distance, and (c) overburden thickness.*

Appendix C: OSL bleaching of sediments in a major meandering river and its delta: The Mississippi system, USA

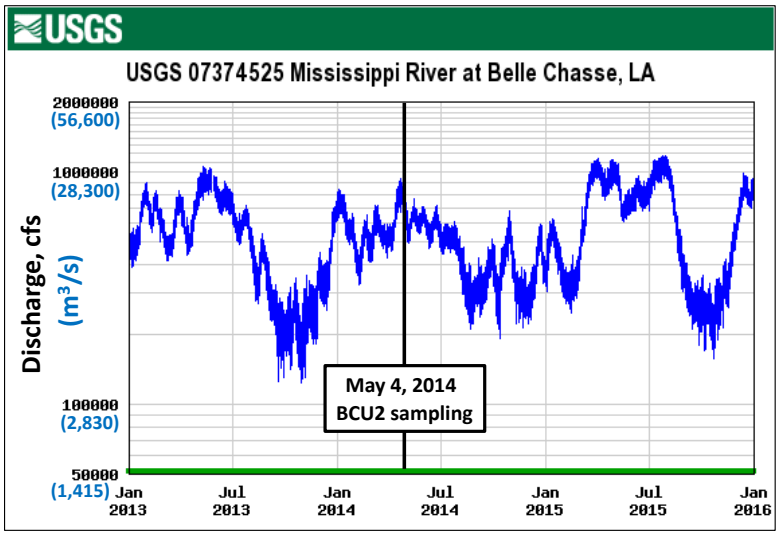

Fig. A.C.1. *Mississippi River water discharge at Bell Chasse (river km 121), a monitoring station that generally represents discharge conditions at sample site BCU2, for a 3 year interval including the collection date of modern river OSL samples.*

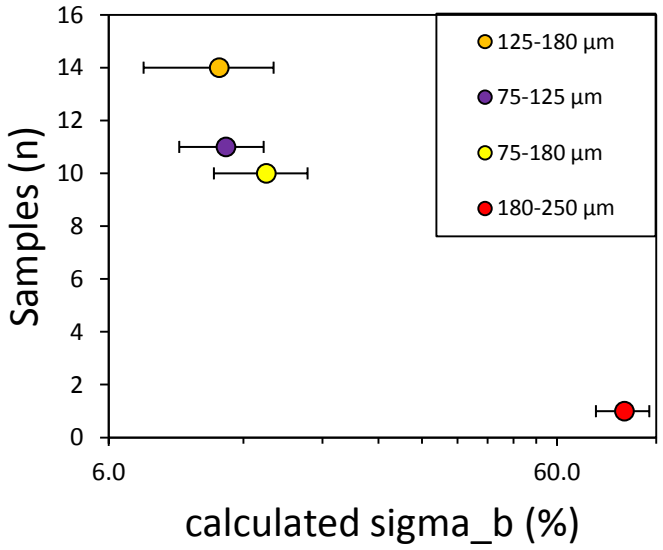

Fig. A.C.2. *Effect of sample number on calculated sigma_b.*

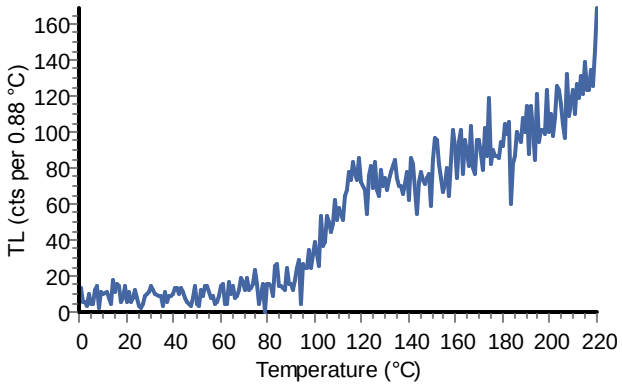

Fig. A.C.3. *Typical TL response for PV I-4 silt.*

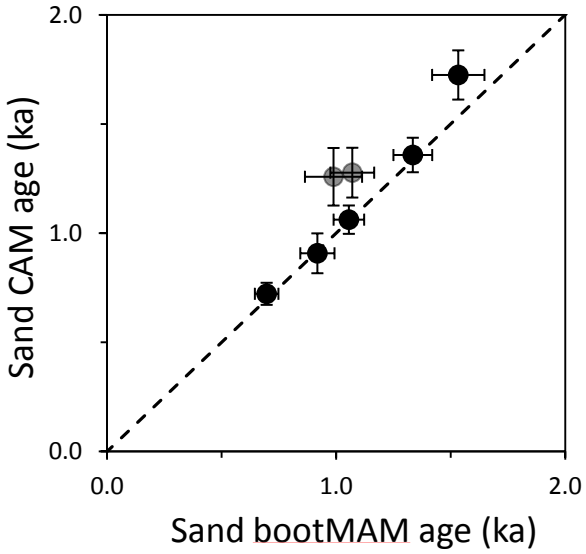

Fig. A.C.4. *Comparison of sand ages obtained with CAM and bootMAM for 7 samples used in the paired sand/silt analysis.*

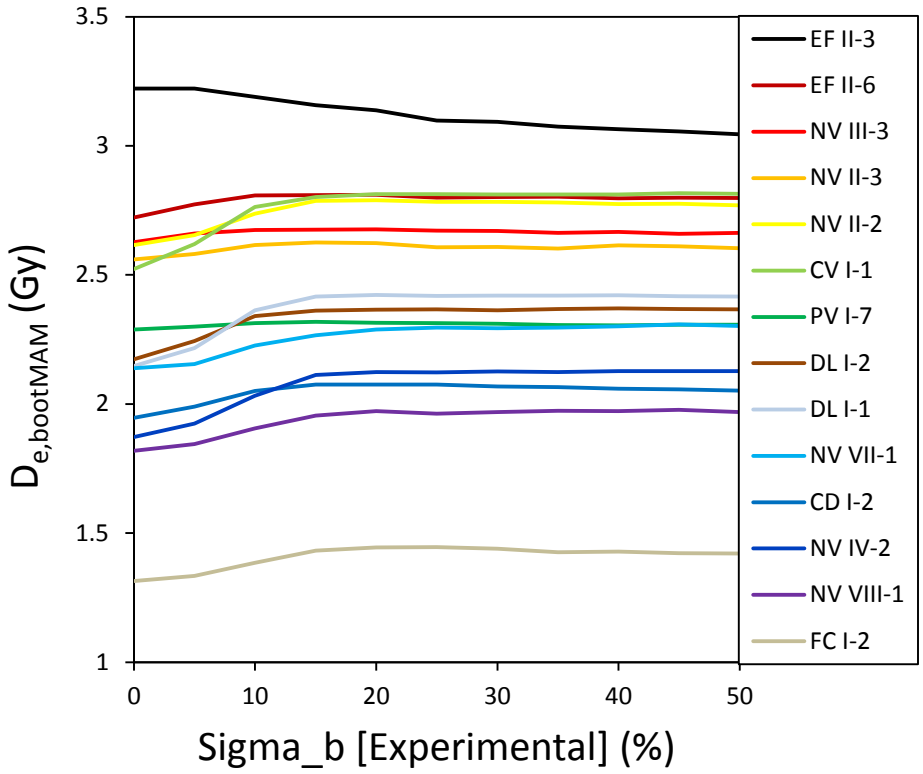

Fig. A.C.5. *Response of D_es estimated with bootMAM to experimental sigma_b values, for well bleached samples. EF II-2 and EF II-1 are not shown because these samples had less than 20 aliquots and therefore less robust statistics, however, they showed the same trend.*

Table A.C.1. *Inventory of samples used in this study.*

Sample name*	**LV lab code**	**Primary study**	**Locality**	**Environment**	**Grain size (μm)**	**aliquots (n)**
BCU2 I-1		This study	Mississippi River	suspended load	4-20	4
BCU2 I-2		This study	Mississippi River	suspended load	4-20	2
BCU2 I-3		This study	Mississippi River	suspended load	4-20	3
BCU2 I-3		This study	Mississippi River	suspended load	45-75	1
BCU2 I-4		This study	Mississippi River	suspended load	4-20	2
BCU2 I-5		This study	Mississippi River	suspended load	4-20	2
BCU2 I-5		This study	Mississippi River	suspended load	45-75	4
BCU2 I-6		This study	Mississippi River	bedload	125-180	39
BCU2 I-6		This study	Mississippi River	bedload	180-250	30
RL I-1	LV724	Chapter 2	Lafourche bayhead delta	mouth-bar deposits	125-180	56
RL I-2	LV725	Chapter 2	Lafourche bayhead delta	mouth-bar deposits	125-180	63
FC I-2	LV726	Chapter 2	Lafourche bayhead delta	mouth-bar deposits	125-180	31
FC I-1	LV727	Chapter 2	Lafourche bayhead delta	mouth-bar deposits	125-180	49
GM I-1	LV728	Chapter 2	Lafourche bayhead delta	mouth-bar deposits	125-180	41
GM I-2	LV729	Chapter 2	Lafourche bayhead delta	mouth-bar deposits	75-125	67
LR I-1	LV730	Chapter 2	Lafourche bayhead delta	mouth-bar deposits	125-180	61
LR I-2	LV731	Chapter 2	Lafourche bayhead delta	mouth-bar deposits	125-180	50
SC I-1	LV771	Chapter 2	Lafourche bayhead delta	mouth-bar deposits	125-180	40
BC I-2	LV773	Chapter 2	Lafourche bayhead delta	mouth-bar deposits	125-180	65
BC I-1	LV774	Chapter 2	Lafourche bayhead delta	mouth-bar deposits	75-125	72
CD I-2	LV776	Chapter 2	Lafourche bayhead delta	mouth-bar deposits	125-180	63

Table A.C.1. *Continued.*

CD I-1	LV777	Chapter 2	Lafourche bayhead delta	mouth-bar deposits	125-180	73
CV I-1	LV778	Chapter 2	Lafourche bayhead delta	mouth-bar deposits	75-125	87
CV II-1	LV780	Chapter 2	Lafourche bayhead delta	mouth-bar deposits	75-125	84
DL I-2	LV800	Chapter 2	Lafourche bayhead delta	mouth-bar deposits	125-180	72
DL I-1	LV801	Chapter 2	Lafourche bayhead delta	mouth-bar deposits	125-180	75
PV I-4	LV287	Shen et al. (2015)	Lafourche subdelta	overbank deposits	100-200, 4-11	31, 33
PV I-5	LV288	Shen et al. (2015)	Lafourche subdelta	overbank deposits	100-200, 4-11	51, 17
NV II-2	LV641	Shen et al. (2015)	Lafourche subdelta	overbank deposits	90-180, 4-11	52, 3
NV II-3	LV642	Shen et al. (2015)	Lafourche subdelta	overbank deposits	90-180, 4-11	52, 23
NV X-1	LV419	Shen et al. (2015)	Lafourche subdelta	overbank deposits	75-180, 4-11	60, 22
EF II-2	LV598	Shen et al. (2015)	Lafourche subdelta	overbank deposits	75-125, 4-11	12
EF II-3	LV599	Shen et al. (2015)	Lafourche subdelta	overbank deposits	75-125, 4-11	26, 6
NV VIII-1	LV416	Shen et al. (2015)	Lafourche subdelta	overbank deposits	75-180	53
PV I-7	LV587	Shen et al. (2015)	Lafourche subdelta	overbank deposits	90-180	34
PV I-8	LV646	Shen et al. (2015)	Lafourche subdelta	overbank deposits	90-180	32
NV II-4a	LV653	Shen et al. (2015)	Lafourche subdelta	overbank deposits	75-125	37
NV III-1	LV432	Shen et al. (2015)	Lafourche subdelta	overbank deposits	75-180	49
NV III-3	LV433	Shen et al. (2015)	Lafourche subdelta	overbank deposits	75-180	60
NV IV-1	LV427	Shen et al. (2015)	Lafourche subdelta	overbank deposits	75-180	32
NV-IV-2	LV428	Shen et al. (2015)	Lafourche subdelta	overbank deposits	75-180	61
NV V-1	LV435	Shen et al. (2015)	Lafourche subdelta	overbank deposits	75-180	49
NV V-2	LV436	Shen et al. (2015)	Lafourche subdelta	overbank deposits	75-180	48
NV VII-1	LV415	Shen et al. (2015)	Lafourche subdelta	overbank deposits	75-180	54

Table A.C.1. *Continued.*

NV IX-1	LV418	Shen et al. (2015)	Lafourche subdelta	overbank deposits	75-180	68
NV X-3	LV471	Shen et al. (2015)	Lafourche subdelta	overbank deposits	75-125	29
EF II-1	LV596	Shen et al. (2015)	Lafourche subdelta	overbank deposits	75-125	14
EF II-6	LV721	Shen et al. (2015)	Lafourche subdelta	overbank deposits	75-125	35
EF III-1a	LV654	Shen et al. (2015)	Lafourche subdelta	overbank deposits	75-125	55
*BCU2 = Bonnet Carre Upper 2, RL = Raceland, FC = Fourchon, GM = Golden Meadow, LR = Larose, SC = St. Charles, BC = Bayou Cane, CD = Cocodrie, CV = Chauvin, DL = Dulac, PV = Paincourtville, NV = Napoleonville, EF = Elmfield						

Table A.C.2. *Details of the luminescence analyses used by this study and by previous studies.*

Aliquot equivalent doses	**This study**	**Chapter 2**	**Shen et al. (2015)**
Signal (s)	first 0.48	first 0.48	first 0.48
Background (s)	0.48-1.76	0.48-1.76	32-40
Use recycled points for fitting	no	no	yes
Force curve through origin	yes	yes	yes
Measurement error (%)	1.7	1.7	1.7
Monte Carlo uncertainty[a]	yes, x1000	yes, x1000	no
Use errors when applying criteria	yes	yes	no
IR depletion test	10%	10%	10%
Maximum test dose error	20%	20%	no
Maximum paleodose error	no	no	no
Maximum recuperation	5% (% largest R)	5% (% largest R)	5% (% N)
Tn >3sigma above BG	no	no	no
Age model usage			
Cleaning of aliquot datasets	3 standard deviations	3 standard deviations	applied 'as needed'
Age models	bootMAM (sand deposits), bootMAMul (modern river sands) mean ± standard error (modern river silts) CAM (silt deposits)	bootMAM	MAM or CAM
Overdispersion input to age model	Theoretically derived from a benchmark (see Table 4.2)	11 ± 4% (128-180 µm), 11 ± 3% (75-125 µm)	10% for all sand grain sizes
Include error on overdispersion	yes	yes	no
[a]Duller, G.A.T. (2016)			

Table A.C.3. *Overdispersion of each sample quantified with the central age model, following a 4 standard deviation cleaning of the aliquot D_e datasets to remove outliers.*

Sample name	**Grain size (µm)**	**Aliquots (n)**	**Overdispersion (%)**
PV I-7	90-180	34	3 ± 6
EF II-1	75-125	14	22 ± 9
EF II-2	75-125	12	22 ± 11
EF II-3	75-125	26	19 ± 5
NV II-4a	75-125	37	22 ± 4
EF III-1a	75-125	54	36 ± 4
EF II-6	75-125	35	7 ± 3
RL I-1	125-180	55	40 ± 4
RL I-2	125-180	60	40 ± 4
FC I-2	125-180	31	26 ± 5
FC I-1	125-180	49	32 ± 4
GM I-1	125-180	41	29 ± 4
GM I-2	75-125	64	15 ± 3
LR I-1	125-180	61	53 ± 5
LR I-2	125-180	50	75 ± 8
BCU2 I-6	125-180	38	94 ± 3
BCU2 I-6	180-250	29	85 ± 12
SC I-1	125-180	40	54 ± 7
BC I-2	125-180	64	44 ± 4
BC I-1	75-125	70	35 ± 3
CD I-2	125-180	63	18 ± 2
CD I-1	125-180	72	17 ± 2
CV I-1	75-125	86	11 ± 1
CV II-1	75-125	83	10 ± 1
NV II-2	90-180	52	13 ± 3
DL I-2	125-180	71	8 ± 1
DL I-1	125-180	73	10 ± 1
NV II-3	90-180	52	8 ± 4
NV IV-1	75-180	31	23 ± 4
NV IV-2	75-180	61	11 ± 2
NV III-1	75-180	49	23 ± 4
NV III-3	75-180	57	4 ± 4
NV V-1	75-180	49	40 ± 5
NV V-2	75-180	47	41 ± 5
NV VII-1	75-180	54	22 ± 3

Table A.C.3. *Continued.*

NV VIII-1	75-180	52	13 ± 3
NV IX-1	75-180	68	14 ± 3
PV I-8	90-180	31	36 ± 5
NV X-1	75-180	60	36 ± 4
NV X-3	75-125	29	47 ± 7
PV I-4	100-200	31	23 ± 4
PV I-5	100-200	49	31 ± 3

Table A.C.4. *Equivalent dose and age results for sand/silt pairs extracted from the same sample.*

Sample name	**Silt $D_{e,CAM}$ (Gy)**	**Silt dose rate (Gy/ka)**	**Silt age (ka)**	**Sand $D_{e,bootMAM}$ (Gy)**	**Sand $D_{e,CAM}$ (Gy)**	**Sand dose rate (Gy/ka)**	**Sand bootMAM age (ka)**	**Sand CAM age (ka)**
PV I-4	4.013 ± 0.223	2.784 ± 0.130	1.441 ± 0.104	2.470 ± 0.249	3.145 ± 0.146	2.498 ± 0.219	0.989 ± 0.132	1.259 ± 0.125
PV I-5	5.144 ± 0.132	3.110 ± 0.156	1.654 ± 0.093	2.947 ± 0.245	3.517 ± 0.120	2.753 ± 0.183	1.071 ± 0.114	1.278 ± 0.096
NV II-3	3.108 ± 0.028	2.804 ± 0.125	1.109 ± 0.051	2.626 ± 0.079	2.642 ± 0.067	2.488 ± 0.138	1.056 ± 0.067	1.062 ± 0.065
NV VIII-1	1.952 ± 0.025	3.053 ± 0.143	0.640 ± 0.031	1.897 ± 0.068	1.967 ± 0.054	2.723 ± 0.176	0.697 ± 0.051	0.722 ± 0.051
NV X-1	3.729 ± 0.052	2.796 ± 0.119	1.334 ± 0.060	3.821 ± 0.185	4.299 ± 0.140	2.492 ± 0.141	1.533 ± 0.114	1.725 ± 0.113
EF II-2	2.500 ± 0.049	3.411 ± 0.153	0.733 ± 0.036	2.759 ± 0.140	2.729 ± 0.213	3.005 ± 0.191	0.918 ± 0.075	0.908 ± 0.091
EF II-3	3.712 ± 0.061	2.720 ± 0.109	1.365 ± 0.059	3.222 ± 0.115	3.279 ± 0.082	2.414 ± 0.127	1.335 ± 0.085	1.359 ± 0.079

Appendix D: Luminescence dating of delta sediments: Novel approaches explored in the Ganges-Brahmaputra-Meghna Delta

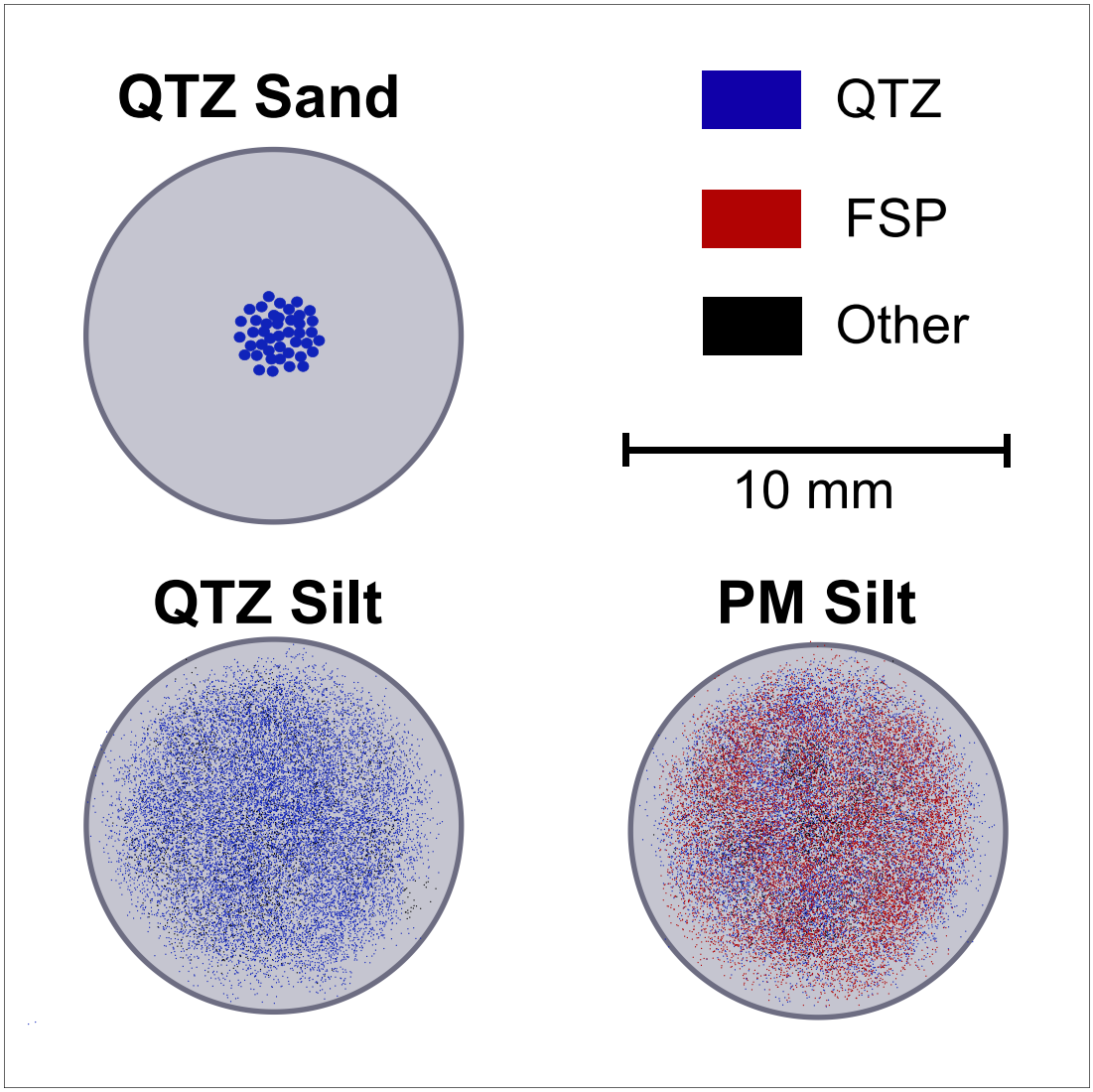

Fig. A.D.1. *Cartoon showing grain-size and mineralogy of aliquots used in this study including sand and silt quartz (QTZ) and polymineral (PM) aliquots that may contain QTZ, feldspar (FSP), or other minerals. QTZ sand is prepared for single-aliquot measurement in this example.*

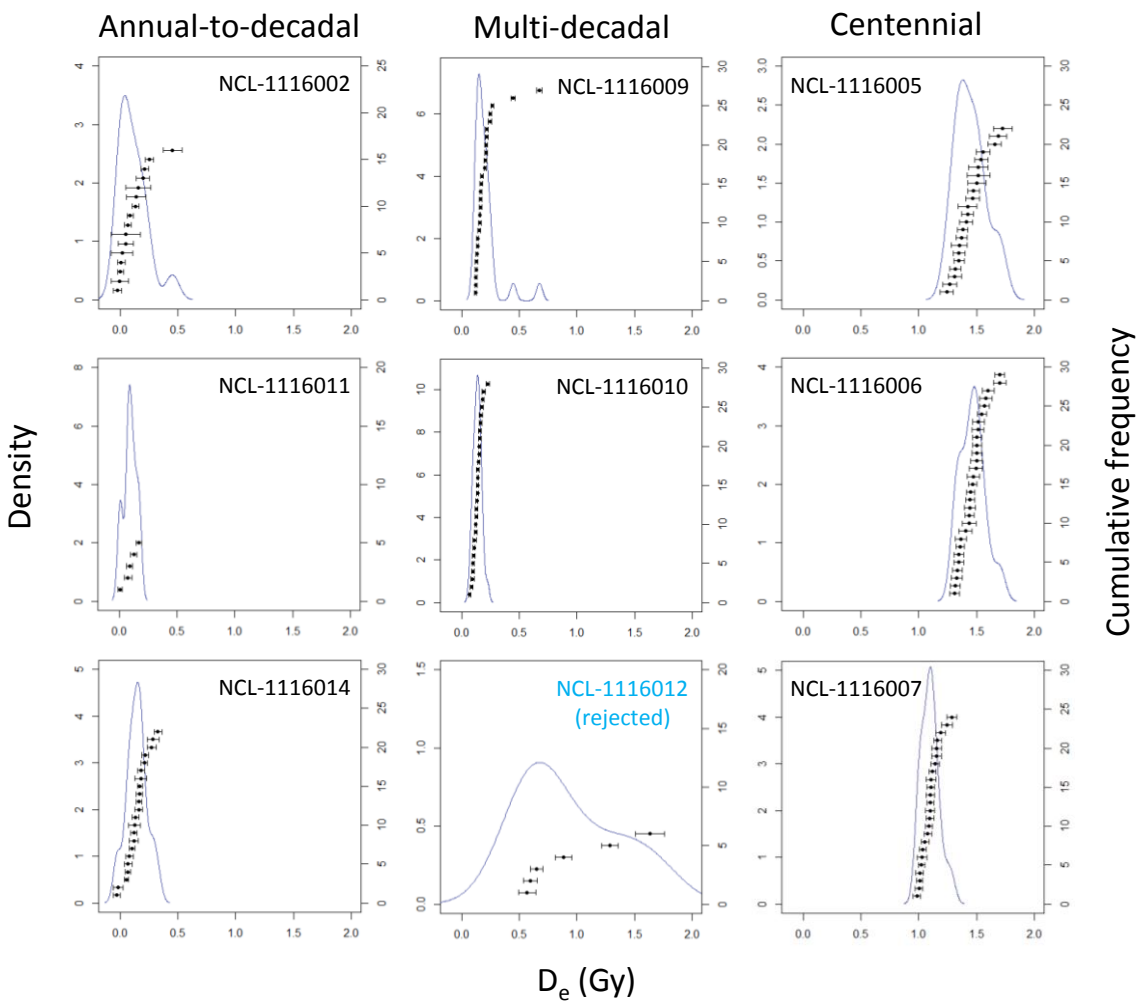

Fig. A.D.2. *Frequency distributions of equivalent doses obtained from etched quartz silt. The columns are grouped by timescale of depositional ages. NCL-1116012 had an expected age of 5 ± 5 a and was rejected for reasons outlined in the main text (see "Dating the silt fraction").*

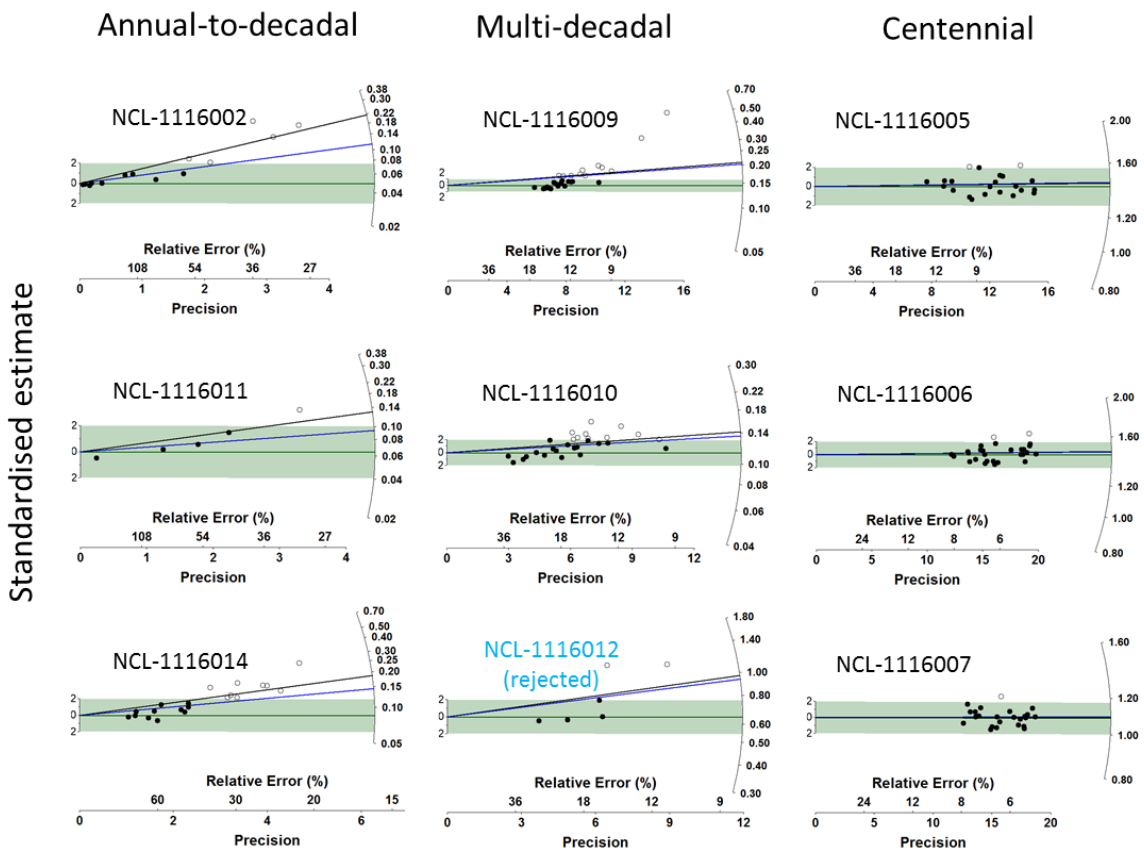

Fig. A.D.3. *Radial plots showing equivalent doses obtained from etched quartz silt. The columns are grouped by timescale of depositional ages. The equivalent dose estimates obtained with the bootstrap unlogged minimum age model (green line) is shaded to 2δ. Equivalent dose estimates obtained with a mean ± standard error (blue line) and the unlogged central age model (black line) are also presented. NCL-1116012 had an expected age of 5 ± 5 a and was rejected due for reasons outlined in the main text (see "Dating the silt fraction"). Annual-to-decadal aged samples NCL-1116002 and NCL-1116014 each had two aliquots with* D_e *< 0 Gy. These aliquots are not shown in these radial plots, but are included in the equivalent dose estimations.*

Table A.D.1. *Details for dose rates of quartz sand and silt, including percent water, grain size, activities of uranium (U), thorium (Th) and potassium (K), the internal dose rate of quartz (Qi), the cosmogenic dose rate (D cosm.) and the calculated dose rate (D). Equivalent doses (D_e) obtained with the bootstrap unlogged minimum age model are also presented here.*

NCL sample code	**water (%)**	**grain size (μm)**	**U (Bq/kg)**	**Th (Bq/kg)**	**K (Bq/kg)**	**Qi (Gy/ka)**	**D cosm. (Gy/ka)**	**D (Gy/ka)**	**D_e (Gy)**
NCL-1116004	5 ± 5	180-250	35.64 ± 0.72	74.94 ± 0.88	398.01 ± 10.69	0.03 ± 0.02	0.21 ± 0.02	3.28 ± 0.21	0.03 ± 0.04
NCL-1116012	22 ± 5	75-125	42.71 ± 0.86	58.77± 0.78	667.69 ± 17.69	0.03 ± 0.02	0.17 ± 0.02	3.26 ± 0.24	0.20 ± 0.13
NCL-1116002	17 ± 5	11-20	59.94 ± 1.19	86.30 ± 1.08	778.39 ± 20.62	n/a	0.18 ± 0.02	4.93 ± 0.40	0.05 ± 0.03
NCL-1116005	34 ± 5	4-11	56.86 ± 1.12	88.67 ± 1.08	904.07 ± 23.66	n/a	0.14 ± 0.01	4.09 ± 0.21	1.42 ± 0.02
NCL-1116006	33 ± 5	4-11	56.60 ± 1.10	83.68 ± 0.97	871.61 ± 22.58	n/a	0.11 ± 0.01	3.99 ± 0.21	1.44 ± 0.03
NCL-1116007	27 ± 5	4-11	61.64 ± 1.22	84.82 ± 1.09	849.22 ± 22.50	n/a	0.21 ± 0.02	4.55 ± 0.28	1.08 ± 0.01
NCL-1116009	28 ± 5	4-11	55.56 ± 1.10	74.89 ± 0.95	690.37 ± 18.33	n/a	0.09 ± 0.01	3.75 ± 0.19	0.15 ± 0.01
NCL-1116010	28 ± 5	4-11	62.54 ± 1.23	79.02 ± 1.01	745.61 ± 19.77	n/a	0.10 ± 0.01	4.04 ± 0.22	0.11 ± 0.01
NCL-1116011	26 ±5	4-11	56.52 ± 1.10	72.18 ± 0.88	743.38 ± 19.45	n/a	0.19 ± 0.02	4.08 ± 0.23	0.07 ± 0.04
NCL-1116012	22 ± 5	4-11	42.71 ± 0.86	58.77± 0.78	667.69 ± 17.69	n/a	0.17 ± 0.02	3.64 ± 0.20	0.65 ± 0.05
NCL-1116014	30 ± 5	4-11	58.16 ± 1.16	80.50 ± 1.04	747.55 ± 19.90	n/a	0.18 ± 0.02	3.99 ± 0.21	0.09 ± 0.03

Table A.D.2. *Results of the initial screening of etched quartz sand with standard SAR measurement of (n) 3 mm aliquots of etched quartz.*

NCL sample code	**Grain size (µm)**	**n measured**	**n accepted**
NCL-1116003	180-250	5	0 (0%)
NCL-1116004	180-250	5	3 (60%)
NCL-1116008	125-180	5	1 (20%)
NCL-1116008	180-250	5	0 (0%)
NCL-1116011	75-125	5	0 (0%)
NCL-1116012	75-125	5	3 (60%)
NCL-1116012	125-180	5	2 (40%)
NCL-1116013	75-125	5	0 (0%)
NCL-1116013	125-180	5	1 (20%)
TOTAL		45	10 (22%)

Table A.D.3. *MS-SAR equivalent dose results, calculated as the mean ± standard error of all aliquots measured (n) for each sample. Results are organized left to right by signal measurement order. BI values calculated using these average D_es may vary slightly from BI values calculated as the average of aliquot-level BI values, due to the dismissal of aliquots with negative BSL equivalent doses.*

NCL sample code	**Grain size (μm)**	**n**	**IR-25 (Gy)**	**pIRIR-90 (Gy)**	**pIRIR-155 (Gy)**	**pIRIR-225 (Gy)**	**BSL (Gy)**	**TL (Gy)**
NCL-1116002	11-20	5	2.23 ± 0.03	4.92 ± 0.13	7.23 ± 0.11	9.35 ± 0.22	n/a	45.1 ± 0.5
NCL-1116005	4-11	5	1.80 ± 0.01	2.74 ± 0.07	3.66 ± 0.13	4.91 ± 0.19	1.63 ± 0.06	19.4 ± 0.2
NCL-1116006	4-11	4	1.88 ± 0.03	3.21 ± 0.12	3.89 ± 0.08	4.54 ± 0.18	1.79 ± 0.13	21.3 ± 0.7
NCL-1116007	4-11	7	1.56 ± 0.02	2.32 ± 0.04	3.31 ± 0.33	4.26 ± 0.09	1.21 ± 0.04	18.1 ± 0.2
NCL-1116009	4-11	6	0.98 ± 0.02	2.44 ± 0.09	3.54 ± 0.33	4.65 ± 0.22	0.14 ± 0.08	29.5 ± 0.3
NCL-1116009	11-20	6	1.05 ± 0.03	2.61 ± 0.22	3.81 ± 0.08	4.79 ± 0.28	-0.29 ± 0.06	32.6 ± 0.9
NCL-1116009	4-20	4	1.09 ± 0.04	2.33 ± 0.11	3.89 ± 0.28	4.78 ± 0.27	-0.07 ± 0.05	30.2 ± 0.6
NCL-1116010	4-11	7	1.12 ± 0.03	2.84 ± 0.31	3.49 ± 0.38	5.04 ± 0.24	0.12 ± 0.07	27.3 ± 0.6
NCL-1116011	4-11	4	1.67 ± 0.02	3.86 ± 0.33	5.83 ± 0.07	7.02 ± 0.55	-0.75 ± 0.17	43.4 ± 3.2
NCL-1116012	4-11	7	2.03 ± 0.04	4.80 ± 0.39	7.33 ± 0.70	8.64 ± 0.76	n/a*	35.6 ± 0.9
NCL-1116012	11-20	8	1.97 ± 0.04	4.51 ± 0.08	7.09 ± 0.35	8.40 ± 0.21	n/a*	59.2 ± 3.5
NCL-1116012	4-20	4	2.39 ± 0.12	5.48 ± 0.54	7.55 ± 0.67	8.77 ± 1.14	-0.82 ± 0.62	42.5 ± 1.3
NCL-1116013	4-11	6	1.65 ± 0.02	3.51 ± 0.20	5.52 ± 0.36	7.19 ± 0.57	-0.28 ± 0.13	34.4 ± 0.2
NCL-1116013	11-20	6	1.46 ± 0.03	3.66 ± 0.15	5.00 ± 0.19	6.61 ± 0.24	-1.98 ± 0.47	35.1 ± 1.2
NCL-1116013	4-20	4	1.52 ± 0.11	3.15 ± 0.12	5.05 ± 0.48	5.55 ± 0.83	-0.62 ± 0.63	35.0 ± 2.3
NCL-1116014	4-11	4	1.44 ± 0.05	3.37 ± 0.49	5.32 ± 0.38	6.48 ± 0.67	-0.14 ± 0.16	34.7 ± 1.0
* No acceptable results due to poor quality signals.								

Table A.D.4. *Weighted mean brightness and overdispersion (OD) of natural signal test dose responses (T_N) calculated with the central age model, for 4-11 µm etched quartz silts.*

NCL sample code	**T_N brightness (counts)**	**T_N OD (%)**
NCL-1116005	1584 ± 117	35 ± 5
NCL-1116006	3216 ± 190	32 ± 4
NCL-1116007	3365 ± 210	31 ± 4
NCL-1116009	3117 ± 95	16 ± 2
NCL-1116010	2273 ± 138	32 ± 4
NCL-1116011	489 ± 64	29 ± 9
NCL-1116012	503 ± 65	31 ± 9
NCL-1116014	566 ± 39	32 ± 5

Bibliography

Aitken, M. J., 1985, Thermoluminescence dating, Academic press.

Allison, M., Yuill, B., Törnqvist, T., Amelung, F., Dixon, T. H., Erkens, G., Stuurman, R., Jones, C., Milne, G., Steckler, M., Syvitski, J., and Teatini, P., 2016, Global risks and research priorities for coastal subsidence: Eos, v. 97, no. 19, p. 22-27.

Allison, M. A., 1998, Historical changes in the Ganges-Brahmaputra delta front: Journal of Coastal Research, v. 14, no. 4, p. 1269-1275.

Allison, M. A., Demas, C. R., Ebersole, B. A., Kleiss, B. A., Little, C. D., Meselhe, E. A., Powell, N. J., Pratt, T. C., and Vosburg, B. M., 2012, A water and sediment budget for the lower Mississippi-Atchafalaya River in flood years 2008-2010: Implications for sediment discharge to the oceans and coastal restoration in Louisiana: Journal of Hydrology, v. 432-433, p. 84-97.

Allison, M. A., Khan, S. R., Goodbred, S. L., and Kuehl, S. A., 2003, Stratigraphic evolution of the late Holocene Ganges-Brahmaputra lower delta plain: Sedimentary Geology, v. 155, p. 317-342.

Allison, M. A., Ramirez, M. T., and Meselhe, E. A., 2014, Diversion of Mississippi River Water Downstream of New Orleans, Louisiana, USA to Maximize Sediment Capture and Ameliorate Coastal Land Loss: Water Resources Management, v. 28, no. 12, p. 4113-4126.

Allison, M. A., Vosburg, B. M., Ramirez, M. T., and Meselhe, E. A., 2013, Mississippi River channel response to the Bonnet Carre Spillway opening in the 2011 flood and its implications for the design and operation of river diversions: Journal of Hydrology, v. 477, p. 104-118.

Arnold, L. J., and Roberts, R. G., 2009, Stochastic modelling of multi-grain equivalent dose (D-e) distributions: Implications for OSL dating of sediment mixtures: Quaternary Geochronology, v. 4, no. 3, p. 204-230.

Arnold, L. J., Roberts, R. G., Galbraith, R. F., and DeLong, S. B., 2009, A revised burial dose estimation procedure for optical dating of young and modern-age sediments: Quaternary Geochronology, v. 4, no. 4, p. 306-325.

Aslan, A., Autin, W. J., and Blum, M. D., 2005, Causes of river avulsion: insights from the late Holocene avulsion history of the Mississippi River, U.S.A: Journal of Sedimentary Research, v. 75, p. 650-664.

Auerbach, L. W., Goodbred, S. L., Jr., Mondal, D. R., Wilson, C. A., Ahmed, K. R., Roy, K., Steckler, M. S., Small, C., Gilligan, J. M., and Ackerly, B. A., 2015a, Flood risk of natural and embanked landscapes on the Ganges-Brahmaputra tidal delta plain: Nature Climate Change, v. 5, no. 2, p. 153-157.

Auerbach, L. W., Goodbred, S. L., Mondal, D. R., Wilson, C. A., Ahmed, K. R., Roy, K., Steckler, M. S., Small, C., Gilligan, J. M., and Ackerly, B. A., 2015b, Flood risk of natural and embanked landscapes on the Ganges-Brahmaputra tidal delta plain: Nature Climate Change, v. 5, no. 2, p. 153-157.

Bailey, R. M., 2000, The interpretation of quartz optically stimulated luminescence equivalent dose versus time plots: Radiation Measurements, v. 32, no. 2, p. 129-140.

Bailiff, I. K., and Mikhailik, V. B., 2003, Spatially-resolved measurement of optically stimulated luminescence and time-resolved luminescence: Radiation Measurements, v. 37, no. 2, p. 151-159.

Ballarini, M., Wallinga, J., Wintle, A. G., and Bos, A. J. J., 2007, A modified SAR protocol for optical dating of individual grains from young quartz samples: Radiation Measurements, v. 42, no. 3, p. 360-369.

Banerjee, D., Murray, A. S., Botter-Jensen, L., and Lang, A., 2001, Equivalent dose estimation using a single aliquot of polymineral fine grains: Radiation Measurements, v. 33, no. 1, p. 73-94.

Berendsen, H. J. A., and Stouthamer, E., 2000, Late Weichselian and Holocene palaeogeography of the Rhine-Meuse delta, The Netherlands: Palaeogeography, Palaeoclimatology, Palaeoecology, v. 161, p. 311-335.

Berger, G. W., Luternauer, J. L., and Clague, J. J., 1990, Zeroing Tests and Application of Thermoluminescence Dating to Fraser-River Delta Sediments: Canadian Journal of Earth Sciences, v. 27, no. 12, p. 1737-1745.

Best, J. L., Ashworth, P. J., Sarker, M. H., and Roden, J. E., 2007, The Brahmaputra-Jamuna River, Bangladesh: Large rivers: geomorphology and management, p. 395-430.

Blum, M. D., and Roberts, H. H., 2009, Drowning of the Mississippi Delta due to insufficient sediment supply and global sea-level rise: Nature Geoscience, v. 2, no. 7, p. 488-491.

Blum, M. D., and Roberts, H. H., 2012, The Mississippi Delta Region: Past, Present, and Future: Annual Review of Earth and Planetary Sciences, Vol 40, v. 40, p. 655-683.

Blum, M. D., and Roberts, H. H., 2014, Is sand in the Mississippi River delta a sustainable resource?: Nature Geoscience, v. 7, no. 12, p. 851-852.

Brammer, H., 2014, Bangladesh's dynamic coastal regions and sea-level rise: Climate Risk Management, v. 1, p. 51-62.

Chamberlain, E. L., Wallinga, J., Reimann, T., Goodbred, S. L., Steckler, M., Shen, Z., and Sincavage, R., 2017, Luminescence dating of delta sediments: novel approaches explored for the Ganges-Brahmaputra-Meghna Delta: Quaternary Geochronology, v. 41, p. 97-111.

Chatanantavet, P., Lamb, M. P., and Nittrouer, J. A., 2012, Backwater controls of avulsion location on deltas: Geophysical Research Letters, v. 39, p. L01402.

Church, J. A., Clark, P. U., Cazenave, A., Gregory, J. M., Jevrejeva, S., Levermann, A., Merrifield, M. A., Milne, G. A., Nerem, R. S., Nunn, P. D., Payne, A. J., Pfeffer, W. T., Stammer, D., and Unnikrishnan, A. S., 2013, Sea level change, *in* Stocker, T. F., Qin, D., Plattner, G.-K., Tignor, M. M. B., Allen, S. K., Boschung, J., Nauels, A., Xia, Y., Bex, V., and Midgley, P. M., eds., Climate Change 2013. The Physical Science Basis: Cambridge, Cambridge University Press, p. 1137-1216.

Couvillion, B. R., Beck, H. J., Schoolmaster, D., and Fischer, M., 2017, Land Area Chane in Coastal Louisiana (1932 to 2016): U.S. Geological Survey.

CPRA, 2017, Louisiana's Comprehensive Master Plan for a Susutainable Coast: Baton Rouge, LA, Coastal Protection and Restoration Authority of Louisiana.

Cunningham, A. C., and Wallinga, J., 2010, Selection of integration time intervals for quartz OSL decay curves: Quaternary Geochronology, v. 5, no. 6, p. 657-666.

Cunningham, A. C., and Wallinga, J., 2012, Realizing the potential of fluvial archives using robust OSL chronologies: Quaternary Geochronology, v. 12, p. 98-106.

Cunningham, A. C., Wallinga, J., and Minderhoud, P. S. J., 2011, Expectations of Scatter in Equivalent-Dose Distributions When Using Multi-Grain Aliquots for Osl Dating: Geochronometria, v. 38, no. 4, p. 424-431.

DeWolf, S., Nooner, S. L., Steckler, M. S., Zumberge, M. A., and Akhter, S. H., Optical Fiber Borehole Strainmeter Arrays for Measuring Sediment Compaction in Bangladesh, *in* Proceedings AGU Fall Meeting Abstracts2013.

Dokka, R. K., Sella, G. F., and Dixon, T. H., 2006, Tectonic control of subsidence and southward displacement of southeast Louisiana with respect to stable North America: Geophysical Research Letters, v. 33, p. L23308.

Duller, G. A. T., 2003, Distinguishing quartz and feldspar in single grain luminescence measurements: Radiation Measurements, v. 37, no. 2, p. 161-165.

Duller, G. A. T., 2008, Single-grain optical dating of Quaternary sediments: why aliquot size matters in luminescence dating: Boreas, v. 37, no. 4, p. 589-612.

Duller, G. A. T., 2016, Analyst v4.31.9 user manual, p. 83 pp.

Durcan, J. A., King, G. E., and Duller, G. A., 2015, DRAC: Dose Rate and Age Calculator for trapped charge dating: Quaternary Geochronology, v. 28, p. 54-61.

Edmonds, D., and Slingerland, R., 2007, Mechanics of river mouth bar formation: Implications for the morphodynamics of delta distributary networks: Journal of Geophysical Research: Earth Surface, v. 112, no. F2.

Edmonds, D. A., Hoyal, D. C. J. D., Sheets, B. A., and Slingerland, R. L., 2009, Predicting delta avulsions: Implications for coastal wetland restoration: Geology, v. 37, no. 8, p. 759-762.

Ellet, C., 1853, The Mississippi and Ohio Rivers: Containing Plans for the Protection of the Delta from Inundation; and Investigations of the Practicability and Cost of Improving the Navigation of the Ohio and Other Rivers by Means of Reservoirs, Etc, Philadelphia, PA, Lippincott, Grambo, & Co.

Ericson, J. P., Vorosmarty, C. J., Dingman, S. L., Ward, L. G., and Meybeck, M., 2006, Effective sea-level rise and deltas: Causes of change and human dimension implications: Global and Planetary Change, v. 50, no. 1-2, p. 63-82.

Erkens, G., 2009, Sediment dynamics in the Rhine catchment: quantification of fluvial response to climate change and human impact, Utrecht University.

Esposito, C. R., Shen, Z., Törnqvist, T. E., Marshak, J., and White, C., 2017, Efficient retention of mud drives land building on the Mississippi Delta plain: Earth Surface Dynamics, v. 5, no. 3, p. 387.

Fernandes, A. M., Törnqvist, T. E., Straub, K. M., and Mohrig, D., 2016, Connecting the backwater hydraulics of coastal rivers to fluvio-deltaic sedimentology and stratigraphy: Geology, v. 44, no. 12, p. 979-982.

Fisk, H. N., 1944, Geological Investigation of the Alluvial Valley of the Lower Mississippi River, Vicksburg, Mississippi River Commission, 78 p.:

Fisk, H. N., 1952, Geological Investigation of the Atchafalaya Basin and the Problem of Mississippi River Diversion, Vicksburg, Waterways Experiment Station, 145 p.:

Fisk, H. N., McFarlan, E., Jr., Kolb, C. R., and Wilbert, L. J., Jr., 1954, Sedimentary framework of the modern Mississippi delta: Journal of Sedimentary Petrology, v. 24, p. 76-99.

Frazier, D. E., 1967, Recent deltaic deposits of the Mississippi River: their development and chronology: Gulf Coast Association of Geological Societies Transactions, v. 17, p. 287-311.

Fuller, I. C., Macklin, M. G., Lewin, J., Passmore, D. G., and Wintle, A. G., 1998, River response to high-frequency climate oscillations in southern Europe over the past 200 ky: Geology, v. 26, no. 3, p. 275-278.

Gagliano, S. M., 1999, Faulting, subsidence and land loss in coastal Louisiana, Baton Rouge, Coastal Environments, Inc.

Gagliano, S. M., Kemp III, E. B., Wicker, K. M., Wiltenmuth, K. S., and Sabate, R. W., 2003, Neo-tectonic framework of southeast Louisiana and applications to coastal restoration.

Galbraith, R. F., Roberts, R. G., Laslett, G. M., Yoshida, H., and Olley, J. M., 1999, Optical dating of single and multiple grains of quartz from Jinmium rock shelter, northern Australia: Part I, experimental design and statistical models: Archaeometry, v. 41, no. 2, p. 339-364.

Galler, J. J., and Allison, M. A., 2008, Estuarine controls on fine-grained sediment storage in the Lower Mississippi and Atchafalaya Rivers: Geological Society of America Bulletin, v. 120, no. 3-4, p. 386-398.

Ganti, V., Chadwick, A. J., Hassenruck-Gudipati, H. J., Fuller, B. M., and Lamb, M. P., 2016, Experimental river delta size set by multiple floods and backwater hydrodynamics: Science Advances, v. 2, no. 5, p. e1501768.

Ganti, V., Chu, Z., Lamb, M. P., Nittrouer, J. A., and Parker, G., 2014, Testing morphodynamic controls on the location and frequency of river avulsions on fans

versus deltas: Huanghe (Yellow River), China: Geophysical Research Letters, v. 41, no. 22, p. 7882-7890.

Gilbert, G. K., 1885, The topographic features of lake shores, US Government Printing Office.

Gilbert, G. K., and Murphy, E. C., 1914, The transportation of debris by running water, US Government Printing Office, v. 86.

Giosan, L., Donnelly, J. P., Constantinescu, S., Filip, F., Ovejanu, I., Vespremeanu-Stroe, A., Vespremeanu, E., and Duller, G. A. T., 2006, Young Danube delta documents stable Black Sea level since the middle Holocene: Morphodynamic, paleogeographic, and archaeological implications: Geology, v. 34, no. 9, p. 757-760.

Godfrey-Smith, D. I., Huntley, D. J., and Chen, W. H., 1988, Optical Dating Studies of Quartz and Feldspar Sediment Extracts: Quaternary Science Reviews, v. 7, no. 3-4, p. 373-380.

González, J. L., and Törnqvist, T. E., 2009, A new Late Holocene sea-level record from the Mississippi Delta: evidence for a climate/sea level connection?: Quaternary Science Reviews, v. 28, no. 17-18, p. 1737-1749.

Goodbred, S. L., 2003, Response of the Ganges dispersal system to climate change: a source-to-sink view since the last interstade: Sedimentary Geology, v. 162, p. 83-104.

Goodbred, S. L., and Kuehl, S. A., 1999, Holocene and modern sediment budgets for the Ganges-Brahmaputra river system: Evidence for highstand dispersal to flood-plain, shelf, and deep-sea depocenters: Geology, v. 27, p. 559-562.

Goodbred, S. L., Paolo, P. M., Ullah, M. S., Pate, R. D., Khan, S. R., Kuehl, S. A., Singh, S. K., and Rahaman, W., 2014, Piecing together the Ganges-Brahmaputra-Meghna River delta: Use of sediment provenance to reconstruct the history and interaction of multiple fluvial systems during Holocene delta evolution: Geological Society of America Bulletin, v. 126, no. 11-12, p. 1495-1510.

Guérin, G., Mercier, N., and Adamiec, G., 2011, Dose-rate conversion factors: update: Ancient TL, v. 29, no. 1, p. 5-8.

Guralnik, B., Ankjaergaard, C., Jain, M., Murray, A. S., Muller, A., Walle, M., Lowick, S. E., Preusser, F., Rhodes, E. J., Wu, T. S., Mathew, G., and Herman, F., 2015, OSL-thermochronometry using bedrock quartz: A note of caution: Quaternary Geochronology, v. 25, p. 37-48.

Hampson, G. J., 2010, Sediment dispersal and quantitative stratigraphic architecture across an ancient shelf: Sedimentology, v. 57, no. 1.

Hanebuth, T. J. J., Kudrass, H. R., Linstädter, J., Islam, B., and Zander, A. M., 2013, Rapid coastal subsidence in the central Ganges-Brahmaputra Delta (Bangladesh) since the 17th century deduced from submerged salt-producing kilns: Geology, v. 41, no. 9, p. 987-990.

Harrison, S., Glasser, N. F., Winchester, V., Haresign, E., Warren, C., Duller, G. A. T., Bailey, R., Ivy-Ochs, S., Jansson, K., and Kubik, P., 2008, Glaciar Leon, Chilean Patagonia: late-Holocene chronology and geomorphology: Holocene, v. 18, no. 4, p. 643-652.

Heinrich, P., Paulsell, R., Milner, R., Snead, J., and Peele, H., 2015, Investigation and GIS development of the buried Holocene-Pleistocene surface in the Louisiana coastal plain, Louisiana State University, Louisiana Geological Survey.

Higgins, S., Overeem, I., Tanaka, A., and Syvitski, J. P. M., 2013, Land subsidence at aquaculture facilities in the Yellow River delta, China: Geophysical Research Letters, v. 40, no. 15, p. 3898-3902.

Hijma, M. P., Shen, Z., Törnqvist, T. E., and Mauz, B., 2017, Late Holocene evolution of a coupled, mud-dominated delta plain–chenier plain system, coastal Louisiana, USA: Earth Surface Dynamics Discussions.

Hill, D. F., Griffiths, S. D., Peltier, W. R., Horton, B. P., and Törnqvist, T. E., 2011, High-resolution numerical modeling of tides in the western Atlantic, Gulf of Mexico, and Caribbean Sea during the Holocene: Journal of Geophysical Research, v. 116, p. C10014.

Hjulstrom, F., 1935, Studies of the morphological activity of rivers as illustrated by the River Fyris, Bulletin: Geological Institute Upsalsa, v. 25, p. 221-527.

Hobo, N., 2015, The sedimentary dynamics in natural and human-influenced delta channel belts, Utrecht University.

Holtz, R. D., and Kovacs, W. D., 1981, An introduction to geotechnical engineering, v. Monograph.

Hooijer, A., Page, S., Jauhiainen, J., Lee, W., Lu, X., Idris, A., and Anshari, G., 2012, Subsidence and carbon loss in drained tropical peatlands: Biogeosciences, v. 9, no. 3, p. 1053.

Hori, K., Tanabe, S., Saito, Y., Haruyama, S., Nguyen, V., and Kitamura, A., 2004, Delta initiation and Holocene sea-level change: example from the Song Hong (Red River) delta, Vietnam: Sedimentary Geology, v. 164, p. 237-249.

Islam, M. R., Begum, S. F., Yamaguchi, Y., and Ogawa, K., 1999, The Ganges and Brahmaputra rivers in Bangladesh: basin denudation and sedimentation: Hydrological Processes, v. 13, no. 17, p. 2907-2923.

Jain, M., and Ankjærgaard, C., 2011, Towards a non-fading signal in feldspar: Insight into charge transport and tunnelling from time-resolved optically stimulated luminescence: Radiation Measurements, v. 46, no. 3, p. 292-309.

Jain, M., Murray, A., and Botter-Jensen, L., 2004, Optically stimulated luminescence dating: how significant is incomplete light exposure in fluvial environments?[Datation par luminescence stimulée optiquement: quelle signification en cas de blanchiment incomplet des sédiments fluviatiles?]: Quaternaire, v. 15, no. 1, p. 143-157.

Jaiswal, M. K., Srivastava, P., Tripathi, J. K., and Islam, R., 2008, Feasibility of the SAR technique on quartz sand of terraces of NW Himalaya: A case study from Devprayag: Geochronometria, v. 31, p. 45-52.

Jankowski, K. L., Törnqvist, T. E., and Fernandes, A. M., 2017, Vulnerability of Louisiana's coastal wetlands to present-day rates of relative sea-level rise: Nature Communications, v. 8, p. 14792.

Jerolmack, D. J., and Swenson, J. B., 2007, Scaling relationships and evolution of distributary networks on wave-influenced deltas: Geophysical Research Letters, v. 34, no. 23, p. L23402.

Jones, H. P., Hole, D. G., and Zavaleta, E. S., 2012, Harnessing nature to help people adapt to climate change: Nature Climate Change, v. 2, no. 7, p. 504-509.

Karegar, M. A., Dixon, T. H., and Malservisi, R., 2015, A three-dimensional surface velocity field for the Mississippi Delta: Implications for coastal restoration and flood potential: Geology, v. 43, no. 6, p. 519-522.

Kars, R. H., Reimann, T., Ankjaergaard, C., and Wallinga, J., 2014, Bleaching of the post-IR IRSL signal: new insights for feldspar luminescence dating: Boreas, v. 43, no. 4, p. 780-791.

Kesel, R. H., 2003, Human modifications to the sediment regime of the Lower Mississippi River flood plain: Geomorphology, v. 56, p. 325-334.

Kim, W., Mohrig, D., Twilley, R., Paola, C., and Parker, G., 2009, Is it feasible to build new land in the Mississippi River delta?: Eos, v. 90, p. 373-374.

Kolker, A. S., Allison, M. A., and Hameed, S., 2011, An evaluation of subsidence rates and sea-level variability in the northern Gulf of Mexico: Geophysical Research Letters, v. 38, p. L21404.

Kook, M., Lapp, T., Murray, A., Thomsen, K. J., and Jain, M., 2015, A luminescence imaging system for the routine measurement of single-grain OSL dose distributions: Radiation Measurements, v. 81, p. 171-177.

Kortekaas, M., and Murray, A. S., 2005, A method for the removal of mica from quartz separates: Ancient TL, v. 23, no. 2, p. 43-46.

Kosters, E. C., and Suter, J. R., 1993, Facies relationships and systems tracts in the late Holocene Mississippi Delta plain: Journal of Sedimentary Petrology, v. 63, p. 727-733.

Kuecher, G., Roberts, H., Thompson, M., and Matthews, I., 2001, Evidence for active growth faulting in the Terrebonne delta plain, south Louisiana: Implications for wetland loss and the vertical migration of petroleum: Environmental Geosciences, v. 8, no. 2, p. 77-94.

Lawson, M. J., Roder, B. J., Stang, D. M., and Rhodes, E. J., 2012, OSL and IRSL characteristics of quartz and feldspar from southern California, USA: Radiation Measurements, v. 47, no. 9, p. 830-836.

Lukas, S., Spencer, J. Q. G., Robinson, R. A. J., and Benn, D. I., 2007, Problems associated with luminescence dating of Late Quaternary glacial sediments in the NW Scottish Highlands: Quaternary Geochronology, v. 2, no. 1-4, p. 243-248.

Madsen, A. T., Buylaert, J. P., and Murray, A. S., 2011, Luminescence dating of young coastal deposits from New Zealand using feldspar: Geochronometria, v. 38, no. 4, p. 379-390.

Mallinson, D., 2008, A brief description of optically stimulated luminescence dating, Volume 2016.

Marriner, N., Flaux, C., Morhange, C., and Kaniewski, D., 2012, Nile Delta's sinking past: Quantifiable links with Holocene compaction and climate-driven changes in sediment supply?: Geology, v. 40, no. 12, p. 1083-1086.

Maselli, V., and Trincardi, F., 2013, Man made deltas: Scientific Reports, v. 3.

Mauz, B., Bode, T., Mainz, E., Blanchard, H., Hilger, W., Dikau, R., and Zöller, L., 2002, The luminescence dating laboratory at the University of Bonn: equipment and procedures: Ancient TL, v. 20, no. 2, p. 53-61.

Mauz, B., and Lang, A., 2004, Removal of the feldspar-derived luminescence component from polymineral fine silt samples for optical dating applications: evaluation of chemical treatment protocols and quality control procedures: Ancient TL, v. 22, no. 1, p. 1-8.

Mauz, B., Packman, S., and Lang, A., 2006, The alpha effectiveness in silt-sized quartz: new data obtained by single and multiple aliquot protocols: Ancient TL, v. 24, no. 2, p. 47-52.

Mayya, Y. S., Morthekai, P., Murari, M. K., and Singhvi, A. K., 2006, Towards quantifying beta microdosimetric effects in single-grain quartz dose distribution: Radiation Measurements, v. 41, no. 7-8, p. 1032-1039.

Mazzotti, S., Lambert, A., Van der Kooij, M., and Mainville, A., 2009, Impact of anthropogenic subsidence on relative sea-level rise in the Fraser River delta: Geology, v. 37, no. 9, p. 771-774.

McArthur, J. M., Ravenscroft, P., Banerjee, D. M., Milsom, J., Hudson-Edwards, K. A., Sengupta, S., Bristow, C., Sarkar, A., Tonkin, S., and Purohit, R., 2008, How paleosols influence groundwater flow and arsenic pollution: A model from the Bengal Basin and its worldwide implication: Water Resources Research, v. 44, no. 11.

McGuire, C., and Rhodes, E. J., 2015, Downstream MET-IRSL single-grain distributions in the Mojave River, southern California: Testing assumptions of a virtual velocity model: Quaternary Geochronology, v. 30, p. 239-244.

Meckel, T. A., 2008, An attempt to reconcile subsidence rates determined from various techniques in southern Louisiana: Quaternary Science Reviews, v. 27, no. 15-16, p. 1517-1522.

Meckel, T. A., Ten Brink, U. S., and Williams, S. J., 2006, Current subsidence rates due to compaction of Holocene sediments in southern Louisiana: Geophysical Research Letters, v. 33, p. L11403.

Mejdahl, V., 1979, Thermoluminescence Dating - Beta-Dose Attenuation in Quartz Grains: Archaeometry, v. 21, no. Feb, p. 61-72.

Milliman, J., and Haq, B. U., 1996, Sea-level rise and coastal subsidence. Causes, consequences, and strategies, Dordrecht, Kluwer.

Milliman, J. D., and Farnsworth, K. L., 2013, River discharge to the coastal ocean: a global synthesis, Cambridge University Press.

Milliman, J. D., and Meade, R. H., 1983, World-wide delivery of river sediment to the oceans: Journal of Geology, v. 91, p. 1-21.

Milliman, J. D., and Syvitski, J. P. M., 1992, Geomorphic Tectonic Control of Sediment Discharge to the Ocean - the Importance of Small Mountainous Rivers: Journal of Geology, v. 100, no. 5, p. 525-544.

Morton, R. A., Bernier, J. C., and Barras, J. A., 2006, Evidence of regional subsidence and associated interior wetland loss induced by hydrocarbon production, Gulf Coast region, USA: Environmental Geology, v. 50, p. 261-274.

Mukul, M., Jaiswal, M., and Singhvi, A. K., 2007, Timing of recent out-of-sequence active deformation in the frontal Himalayan wedge: Insights from the Darjiling sub-Himalaya, India: Geology, v. 35, no. 11, p. 999-1002.

Murray, A. S., Olley, J. M., and Caitcheon, G. G., 1995, Measurement of Equivalent Doses in Quartz from Contemporary Water-Lain Sediments Using Optically Stimulated Luminescence: Quaternary Science Reviews, v. 14, no. 4, p. 365-371.

Murray, A. S., Thomsen, K. J., Masuda, N., Buylaert, J. P., and Jain, M., 2012, Identifying well-bleached quartz using the different bleaching rates of quartz and feldspar luminescence signals: Radiation Measurements, v. 47, no. 9, p. 688-695.

Murray, A. S., and Wintle, A. G., 2000, Luminescence dating of quartz using an improved single-aliquot regenerative-dose protocol: Radiation Measurements, v. 32, no. 1, p. 57-73.

Murray, A. S., and Wintle, A. G., 2003, The single aliquot regenerative dose protocol: potential for improvements in reliability: Radiation Measurements, v. 37, no. 4-5, p. 377-381.

Muto, T., 2001, Shoreline autoretreat substantiated in flume experiments: Journal of Sedimentary Research, v. 71, p. 246-254.

Muto, T., and Steel, R. J., 1992, Retreat of the front in a prograding delta: Geology, v. 20, p. 967-970.

Neill, C. F., and Allison, M. A., 2005, Subaqueous deltaic formation on the Atchafalaya Shelf, Louisiana: Marine Geology, v. 214, no. 4, p. 411-430.

Nelson, B. W., 1970, Hydrography, sediment dispersal, and recent historical development of the Po River delta, Italy, *in* Morgan, J. P., ed., Society of Economic Paleontologists and Mineralogists Special Publication, Volume 15, p. 152-184.

Nienhuis, J. H., Törnqvist, T. E., Jankowski, K. L., Fernandes, A. M., and Keogh, M. E., 2017, A New Subsidence Map for Coastal Louisiana: GSA Today, v. 27.

Nittrouer, J. A., and Viparelli, E., 2014, Sand as a stable and sustainable resource for nourishing the Mississippi River delta: Nature Geoscience, v. 7, no. 5, p. 350-354.

Olley, J., Caitcheon, G., and Murray, A., 1998, The distribution of apparent dose as determined by optically stimulated luminescence in small aliquots of fluvial quartz: Implications for dating young sediments: Quaternary Science Reviews, v. 17, no. 11, p. 1033-1040.

Olley, J. M., Caitcheon, G. G., and Roberts, R. G., 1999, The origin of dose distributions in fluvial sediments, and the prospect of dating single grains from fluvial deposits using optically stimulated luminescence: Radiation Measurements, v. 30, no. 2, p. 207-217.

Olley, J. M., Pietsch, T., and Roberts, R. G., 2004, Optical dating of Holocene sediments from a variety of geomorphic settings using single grains of quartz: Geomorphology, v. 60, no. 3-4, p. 337-358.

Paola, C., Twilley, R. R., Edmonds, D. A., Kim, W., Mohrig, D., Parker, G., Viparelli, E., and Voller, V. R., 2011, Natural Processes in Delta Restoration: Application to the Mississippi Delta: Annual Review of Marine Science, Vol 3, v. 3, p. 67-91.

Parker, G., Muto, T., Akamatsu, Y., Dietrich, W. E., and Lauer, J. W., 2008, Unravelling the conundrum of river response to rising sea-level from laboratory to field. Part I: Laboratory experiments: Sedimentology, v. 55, no. 6, p. 1643-1655.

Parker, G., Paola, C., Whipple, K. X., and Mohrig, D., 1998, Alluvial fans formed by channelized fluvial and sheet flow. I: Theory: Journal of Hydraulic Engineering-Asce, v. 124, no. 10, p. 985-995.

Penland, S., Boyd, R., and Suter, J. R., 1988, Transgressive depositional systems of the Mississippi delta plain: a model for barrier shoreline and shelf sand development: Journal of Sedimentary Petrology, v. 58, p. 932-949.

Pietsch, T. J., Olleya, J. M., and Nanson, G. C., 2008, Fluvial transport as a natural luminescence sensitiser of quartz: Quaternary Geochronology, v. 3, no. 4, p. 365-376.

Poolton, N. R. J., Ozanyan, K. B., Wallinga, J., Murray, A. S., and Botter-Jensen, L., 2002, Electrons in feldspar II: a consideration of the influence of conduction band-tail states on luminescence processes: Physics and Chemistry of Minerals, v. 29, no. 3, p. 217-225.

Poolton, N. R. J., Smith, G. M., Riedi, P. C., Bulur, E., Botter-Jensen, L., Murray, A. S., and Adrian, M., 2000, Luminescence sensitivity changes in natural quartz induced by high temperature annealing: a high frequency EPR and OSL study: Journal of Physics D-Applied Physics, v. 33, no. 8, p. 1007-1017.

Prescott, J. R., and Hutton, J. T., 1994, Cosmic-Ray Contributions to Dose-Rates for Luminescence and Esr Dating - Large Depths and Long-Term Time Variations: Radiation Measurements, v. 23, no. 2-3, p. 497-500.

Preusser, F., Ramseyer, K., and Schluchter, C., 2006, Characterisation of low OSL intensity quartz from the New Zealand Alps: Radiation Measurements, v. 41, no. 7-8, p. 871-877.

Ramirez, M. T., and Allison, M. A., 2013, Suspension of bed material over sand bars in the Lower Mississippi River and its implications for Mississippi delta

environmental restoration: Journal of Geophysical Research-Earth Surface, v. 118, no. 2, p. 1085-1104.

Ray, Y., and Srivastava, P., 2010, Widespread aggradation in the mountainous catchment of the Alaknanda-Ganga River System: timescales and implications to Hinterland-foreland relationships: Quaternary Science Reviews, v. 29, no. 17-18, p. 2238-2260.

Reimann, T., Notenboom, P. D., De Schipper, M. A., and Wallinga, J., 2015, Testing for sufficient signal resetting during sediment transport using a polymineral multiple-signal luminescence approach: Quaternary Geochronology, v. 25, p. 26-36.

Reimann, T., Thomsen, K. J., Jain, M., Murray, A. S., and Frechen, M., 2012, Single-grain dating of young sediments using the pIRIR signal from feldspar: Quaternary Geochronology, v. 11, p. 28-41.

Reimann, T., Tsukamoto, S., Naumann, M., and Frechen, M., 2011, The potential of using K-rich feldspars for optical dating of young coastal sediments - A test case from Darss-Zingst peninsula (southern Baltic Sea coast): Quaternary Geochronology, v. 6, no. 2, p. 207-222.

Rhodes, E. J., Ramsey, C. B., Outram, Z., Batt, C., Willis, L., Dockrill, S., and Bond, J., 2003, Bayesian methods applied to the interpretation of multiple OSL dates: high precision sediment ages from Old Scatness Broch excavations, Shetland Isles: Quaternary Science Reviews, v. 22, no. 10-13, p. 1231-1244.

Rink, W. J., 2003, Thermoluminescence of quartz and feldspar sand grains as a tracer of nearshore environmental processes in the southeastern Mediterranean Sea: Journal of Coastal Research, v. 19, no. 3, p. 723-730.

Rittenour, T. M., 2008, Luminescence dating of fluvial deposits: applications to geomorphic, palaeoseismic and archaeological research: Boreas, v. 37, no. 4, p. 613-635.

Rittenour, T. M., Blum, M. D., and Goble, R. J., 2007, Fluvial evolution of the lower Mississippi River valley during the last 100 k.y. glacial cycle: Response to glaciation and sea-level change: Geological Society of America Bulletin, v. 119, no. 5-6, p. 586-608.

Rittenour, T. M., Goble, R. J., and Blum, M. D., 2005, Development of an OSL chronology for Late Pleistocene channel belts in the lower Mississippi valley, USA: Quaternary Science Reviews, v. 24, p. 2539-2554.

Roberts, H. H., 1997, Dynamic changes of the Holocene Mississippi River delta plain: The delta cycle: Journal of Coastal Research, v. 13, p. 605-627.

Roberts, H. H., Walker, N., Cunningham, R., Kemp, G. P., and Majersky, S., 1997, Evolution of sedimentary architecture and surface morphology: Atchafalaya and Wax Lake deltas, Louisiana (1973-1994): Gulf Coast Association of Geological Societies Transactions, v. 47, p. 477-484.

Roberts, R. G., Jones, R., Spooner, N. A., Head, M. J., Murray, A. S., and Smith, M. A., 1994, The Human Colonization of Australia - Optical Dates of 53,000 and 60,000 Years Bracket Human Arrival at Deaf-Adder Gorge, Northern-Territory: Quaternary Science Reviews, v. 13, no. 5-7, p. 575-583.

Rogers, K. G., Goodbred, S. L., and Mondal, D. R., 2013, Monsoon sedimentation on the 'abandoned' tide-influenced Ganges-Brahmaputra delta plain: Estuarine Coastal and Shelf Science, v. 131, p. 297-309.

Russell, R. J., Howe, H. V., McGuirt, J. H., Dohm, C. F., Hadley, W., Jr., Kniffen, F. B., and Brown, C. A., 1936, Lower Mississippi River Delta. Reports on the geology of Plaquemines and St. Bernard Parishes: Louisiana Geological Survey Geological Bulletin, v. 9, p. 1-454.

Saito, Y., Wei, H. L., Zhou, Y. Q., Nishimura, A., Sato, Y., and Yokota, S., 2000, Delta progradation and chenier formation in the Huanghe (Yellow River) Delta, China: Journal of Asian Earth Sciences, v. 18, no. 4, p. 489-497.

Sarker, M. H., Huque, I., Alam, M., and Koudstaal, R., 2003, Rivers, chars and char dwellers of Bangladesh: International Journal of River Basin Management, v. 1, no. 1, p. 61-80.

Saucier, R. T., 1994, Geomorphology and Quaternary Geologic History of the Lower Mississippi Valley, Vicksburg, Mississippi River Commission, 364 p.:

Shaw, J. B., and Mohrig, D., 2014, The importance of erosion in distributary channel network growth, Wax Lake Delta, Louisiana, USA: Geology, v. 42, no. 1, p. 31-34.

Shen, Z., and Lang, A., 2016, Quartz fast component opticallystimulated luminescence: Towards routine extraction for dating applications: Radiation Measurements, v. 89, p. 27-34.

Shen, Z., Törnqvist, T. E., Autin, W. J., Mateo, Z. R. P., Straub, K. M., and Mauz, B., 2012, Rapid and widespread response of the Lower Mississippi River to eustatic forcing during the last glacial-interglacial cycle: Geological Society of America Bulletin, v. 124, no. 5-6, p. 690-704.

Shen, Z., Tornqvist, T. E., Mauz, B., Chamberlain, E. L., Nijhuis, A. G., and Sandoval, L., 2015, Episodic overbank deposition as a dominant mechanism of floodplain and delta-plain aggradation: Geology, v. 43, no. 10, p. 875-878.

Shen, Z. X., and Mauz, B., 2012, Optical dating of young deltaic deposits on a decadal time scale: Quaternary Geochronology, v. 10, p. 110-116.

Shields, M. R., Bianchi, T. S., Mohrig, D., Hutchings, J. A., Kenney, W. F., Kolker, A. S., and Curtis, J. H., 2017, Carbon storage in the Mississippi River delta enhanced by environmental engineering.

Shu, L., and Finlayson, B., 1993, Flood Management on the Lower Yellow-River - Hydrological and Geomorphological Perspectives: Sedimentary Geology, v. 85, no. 1-4, p. 285-296.

Singarayer, J. S., Bailey, R. M., Ward, S., and Stokes, S., 2005, Assessing the completeness of optical resetting of quartz OSL in the natural environment: Radiation Measurements, v. 40, no. 1, p. 13-25.

Singh, S. K., and France-Lanord, C., 2002, Tracing the distribution of erosion in the Brahmaputra watershed from isotopic compositions of stream sediments: Earth and Planetary Science Letters, v. 202, no. 3, p. 645-662.

Singhvi, A., and Lang, A., 1998, Improvements in infra-red dating of partially bleached sediments-the'Differential'Partial Bleach Technique: growth, v. 1, p. 2.

Sohbati, R., Murray, A. S., Chapot, M. S., Jain, M., and Pederson, J., 2012, Optically stimulated luminescence (OSL) as a chronometer for surface exposure dating: Journal of Geophysical Research-Solid Earth, v. 117.

Spooner, N. A., 1994, The Anomalous Fading of Infrared-Stimulated Luminescence from Feldspars: Radiation Measurements, v. 23, no. 2-3, p. 625-632.

Steckler, M. S., Akhter, S. H., and Seeber, L., 2008, Collision of the Ganges-Brahmaputra Delta with the Burma Arc: Implications for earthquake hazard: Earth and Planetary Science Letters, v. 273, no. 3-4, p. 367-378.

Stive, M. J. F., de Schipper, M. A., Luijendijk, A. P., Aarninkhof, S. G. J., van Gelder-Maas, C., de Vries, J., de Vries, S., Henriquez, M., Marx, S., and Ranasinghe, R., 2013, A New Alternative to Saving Our Beaches from Sea-Level Rise: The Sand Engine: Journal of Coastal Research, v. 29, no. 5, p. 1001-1008.

Stokes, S., Bray, H. E., and Blum, M. D., 2001, Optical resetting in large drainage basins: tests of zeroing assumptions using single-aliquot procedures: Quaternary Science Reviews, v. 20, no. 5-9, p. 879-885.

Stouthamer, E., and Berendsen, H. J. A., 2000, Factors controlling the Holocene avulsion history of the Rhine-Meused delta (The Netherlands): Journal of Sedimentary Research, v. 70, no. 5, p. 1051-1064.

Suckow, A., Morgenstern, U., and Kudrass, H. R., 2001, Absolute dating of recent sediments in the cyclone-influenced shelf area off Bangladesh: Comparison of gamma spectrometric (Cs-137, Pb-201, Ra-228), radiocarbon, and Si-32 ages: Radiocarbon, v. 43, no. 2B, p. 917-927.

Sugisaki, S., Buylaert, J. P., Murray, A., Tada, R., Zheng, H. B., Ke, W., Saito, K., Chao, L., Li, S. Y., and Irino, T., 2015, OSL dating of fine-grained quartz from Holocene Yangtze delta sediments: Quaternary Geochronology, v. 30, p. 226-232.

Syvitski, J. P. M., Kettner, A. J., Overeem, I., Hutton, E. W. H., Hannon, M. T., Brakenridge, G. R., Day, J., Vörösmarty, C., Saito, Y., Giosan, L., and Nicholls, R. J., 2009, Sinking deltas due to human activities: Nature Geoscience, v. 2, no. 10, p. 681-686.

Syvitski, J. P. M., Vörösmarty, C. J., Kettner, A. J., and Green, P., 2005, Impact of humans on the flux of terrestrial sediment to the global coastal ocean: Science, v. 308, p. 376-380.

Tamura, T., Saito, Y., Bateman, M. D., Nguyen, V. L., Ta, T. K. O., and Matsumoto, D., 2012, Luminescence dating of beach ridges for characterizing multi-decadal to centennial deltaic shoreline changes during Late Holocene, Mekong River delta: Marine Geology, v. 326, p. 140-153.

Terzaghi, K., and Peck, R. B., 1967, Soil mechanics in engineering practice (second edition), New York, John Wiley and Sons Inc.

Thomas, P. J., Reddy, D. V., Kumar, D., Nagabhushanam, P., Sukhija, B. S., and Sahoo, R. N., 2007, Optical dating of liquefaction features to constrain prehistoric earthquakes in Upper Assam, NE India - Some preliminary results: Quaternary Geochronology, v. 2, no. 1-4, p. 278-283.

Thomsen, K. J., Murray, A., and Bøtter-Jensen, L., 2005, Sources of variability in OSL dose measurements using single grains of quartz: Radiation Measurements, v. 39, no. 1, p. 47-61.

Thomsen, K. J., Murray, A. S., Jain, M., and Botter-Jensen, L., 2008, Laboratory fading rates of various luminescence signals from feldspar-rich sediment extracts: Radiation Measurements, v. 43, no. 9-10, p. 1474-1486.

Törnqvist, T. E., González, J. L., Newsom, L. A., Van der Borg, K., De Jong, A. F. M., and Kurnik, C. W., 2004, Deciphering Holocene sea-level history on the U.S. Gulf Coast: A high-resolution record from the Mississippi Delta: Geological Society of America Bulletin, v. 116, p. 1026-1039.

Törnqvist, T. E., Kidder, T. R., Autin, W. J., Van der Borg, K., De Jong, A. F. M., Klerks, C. J. W., Snijders, E. M. A., Storms, J. E. A., Van Dam, R. L., and Wiemann, M. C., 1996, A revised chronology for Mississippi River subdeltas: Science, v. 273, p. 1693-1696.

Törnqvist, T. E., and Van Dijk, G. J., 1993, Optimizing sampling strategy for radiocarbon dating of Holocene fluvial systems in a vertically aggrading setting: Boreas, v. 22, p. 129-145.

Törnqvist, T. E., Wallace, D. J., Storms, J. E. A., Wallinga, J., Van Dam, R. L., Blaauw, M., Derksen, M. S., Klerks, C. J. W., Meijneken, C., and Snijders, E. M. A., 2008, Mississippi Delta subsidence primarily caused by compaction of Holocene strata: Nature Geoscience, v. 1, no. 3, p. 173-176.

Truelsen, J. L., and Wallinga, J., 2003, Zeroing of the OSL signal as a function of grain size: investigating bleaching and thermal transfer for a young fluvial sample: Geochronometria, v. 22, no. 1, p. e8.

van Gorp, W., Veldkamp, A., Temme, A., Maddy, D., Demir, T., van der Schriek, T., Reimann, T., Wallinga, J., Wijbrans, J., and Schoorl, J. M., 2013, Fluvial response to Holocene volcanic damming and breaching in the Gediz and Geren rivers, western Turkey: Geomorphology, v. 201, p. 430-448.

Wallinga, J., 2002a, Optically stimulated luminescence dating of fluvial deposits: a review: Boreas, v. 31, no. 4, p. 303-322.

Wallinga, J., 2002b, On the detection of OSL age overestimation using single-aliquot techniques: Geochronometria, v. 21, p. 17-26.

Wallinga, J., and Bos, I. J., 2010, Optical dating of fluvio-deltaic clastic lake-fill sediments - A feasibility study in the Holocene Rhine delta (western Netherlands): Quaternary Geochronology, v. 5, no. 5, p. 602-610.

Wallinga, J., Murray, A. S., and Botter-Jensen, L., 2002, Measurement of the dose in quartz in the presence of feldspar contamination: Radiation Protection Dosimetry, v. 101, no. 1-4, p. 367-370.

Wang, X. L., Lu, Y. C., and Zhao, H., 2006, On the performances of the single-aliquot regenerative-dose (SAR) protocol for Chinese loess: fine quartz and polymineral grains: Radiation Measurements, v. 41, no. 1, p. 1-8.

Wasson, R. J., 2003, A sediment budget for the Ganga-Brahmaputra catchment: Current Science, v. 84, no. 8, p. 1041-1047.

Webb, E. L., Friess, D. A., Krauss, K. W., Cahoon, D. R., Guntenspergen, G. R., and Phelps, J., 2013, A global standard for monitoring coastal wetland vulnerability to accelerated sea-level rise: Nature Climate Change, v. 3, no. 5, p. 458-465.

Weinman, B., Goodbred, S. L., Zheng, Y., Aziz, Z., Steckler, M., van Geen, A., Singhvi, A. K., and Nagar, Y. C., 2008, Contributions of floodplain stratigraphy and evolution to the spatial patterns of groundwater arsenic in Araihazar, Bangladesh: Geological Society of America Bulletin, v. 120, no. 11-12, p. 1567-1580.

Wellner, R., Beaubouef, R., Van Wagoner, J., Roberts, H., and Sun, T., 2005, Jet-plume depositional bodies – The primary building blocks of Wax Lake Delta: Gulf Coast Association of Geological Societies Transactions, v. 55, p. 867-909.

Wilson, C. A., and Goodbred, S. L., 2015, Construction and maintenance of the Ganges-Brahmaputra Meghna delta: Linking process, morphology, and stratigraphy: Annual Review of Marine Science, v. 7, p. 67-88.

Wilson, C. A., Goodbred, S. L., Small, C., Gilligan, J. M., Sams, S., and Mallick, B., in review, Widespread infilling of tidal channels and navigable waterways in human-modified tidal deltaplain of southwest Bangladesh: Elementa.

Wintle, A. G., and Murray, A. S., 2006, A review of quartz optically stimulated luminescence characteristics and their relevance in single-aliquot regeneration dating protocols: Radiation Measurements, v. 41, no. 4, p. 369-391.

Wolstencroft, M., Shen, Z., Törnqvist, T. E., Milne, G. A., and Kulp, M., 2014, Understanding subsidence in the Mississippi Delta region due to sediment, ice, and ocean loading: Insights from geophysical modeling: Journal of Geophysical Research: Solid Earth, v. 119, no. 4, p. 3838-3856.

Wright, L. D., 1977, Sediment transport and deposition at river mouths: A synthesis: Geological Society of America Bulletin, v. 88, p. 857-868.

Biography

Elizabeth L. Chamberlain is native to southeastern Wisconsin, USA. She graduated in 2002 from Palmyra-Eagle High School, where she was recognized as valedictorian and as a National Merit Scholar. In 2007 she received three concurrent undergraduate degrees from Louisiana State University, a Bachelor of Arts in English-Creative Writing, a Bachelor of Science in Animal Science, and a Bachelor of Arts in Liberal Arts- Studio Art with a concentration in lithography. In 2012, Elizabeth was awarded a Master of Science in Geology from Louisiana State University for her research on the Baton Rouge Aquifer System, under the direction of Professor Jeffery S. Hanor. That year she began a doctoral program in the Department of Earth and Environmental Sciences at Tulane University, advised by Professor Torbjörn E. Törnqvist. As a doctoral student, Elizabeth has conducted internships at the luminescence laboratory of the University of Liverpool, UK, and at the Netherlands Centre for Luminescence Dating at Wageningen University and Research Centre, NL. In addition, she has participated in three field campaigns in the Ganges-Brahmaputra-Meghna Delta, Bangladesh, and led and contributed to numerous field campaigns in the Mississippi Delta and Lower Mississippi River Valley, focused on both geologic and archaeological research. Following completion of the doctoral program, Elizabeth will conduct research on the timing and drivers of distributary channel activity in the Ganges-Brahmaputra-Meghna Delta. This work will be guided by Professors Steven L. Goodbred, Tony Reimann, and Jakob Wallinga, and conducted as part of the National Center for Earth-Surface Dynamics postdoctoral program.